AN APPROACH FOR REMOTE LANDSLIDE MAPPING, SOUTH NAHANNI WATERSHED, NORTHWEST TERRITORIES, CANADA

by

Courtney E. Jermyn

B.Sc., University of Waterloo, 2004

THESIS SUBMITTED IN PARTIAL FULFILLMENT OF
THE REQUIREMENTS FOR THE DEGREE OF
MASTER OF SCIENCE
IN
NATURAL RESOURCES AND ENVIRONMENTAL STUDIES

UNIVERSITY OF NORTHERN BRITISH COLUMBIA

June 2011

Your file Votre référence
ISBN: 978-0-494-87560-5

Our file Notre référence
ISBN: 978-0-494-87560-5

ABSTRACT

This thesis presents two cost-effective techniques for landslide mapping in large, remote regions. The first technique uses ASTER satellite imagery to characterize and determine landslide distribution for part of the South Nahanni watershed. Results obtained from this study confirm that ASTER images are suitable for regional-scale landslide mapping.

The second technique involved the creation of landslide susceptibility models for debris flow and rock/debris slides using logistic regression analysis. Cross validation confirmed the models' success. The debris flow model performed best whereas the rock/debris slide model was only moderately successful.

Taken together, the two methods developed in this thesis provide a means to conduct a preliminary landslide investigation in large, remote regions or in developing countries where data are limited or site investigation is not possible. Maps produced from this analysis can be used to gain information on areas susceptible to landslides and to target key areas remotely before conducting field investigations.

Key words: Landslides, mapping, ASTER satellite imagery, landslide susceptibility, and logistic regression analysis.

TABLE OF CONTENTS

LIST OF TABLES

LIST OF FIGURES

ACKNOWLEDGEMENTS

This project was made possible by grants received from Parks Canada and Northern Studies Training Program (NSTP). I would like to thank David Murray and Steve Catto, from Parks Canada, for making this project possible and allowing me to visit the majestic Nahanni National Park Reserve.

During the duration of my thesis I have had the opportunity to be mentored by numerous outstanding individuals. It is to these individuals that my heartfelt gratitude and thanks go out to. If it was not for them my thesis would not have seen its completion and I would not be who I am today.

I would like to express my gratitude to my supervisory committee, Brian Menounos, Marten Geertsema, Peter Bobrowsky, John Clague, and Roger Wheate, for their ongoing patience, guidance, and support. Brian, thank you for encouraging independent thought and helping me develop my technical writing skills. Your help as significantly impacted the quality of my thesis. Marten, I would like to thank you for all your support and mentorship throughout the course of my thesis and taking the time to help me out in the field. Peter, thank you for giving me my start in my career, initiating this project, and all the ongoing support and opportunities you have provided me over the past six years. It has meant a lot. John, thank you for all the wisdom, advice, and guidance you have given me throughout the years. It has been an honour. Roger, thank you for all the encouragement throughout the years and assistance in answering my GIS questions and helping me trouble shoot some difficult problems.

I owe thanks to Lionel Jackson, Reginald Hermanns, Andree Blais-Stevens, Gordon Mckenna, and Rejean Couture for their mentorship, wisdom, and friendship. Thanks to Marianne Ceh, Oscar Cerritos, Sean Ramsey, Lucy Lee, and Robert Cocking for sharing your knowledge of GIS, and Carolyn Huston, Ian Bercovitz, and Alexander Brenning for taking time to share your knowledge in statistics/geostatistics with me. My thesis would not have been completed if it weren't for your help.

I would also like to thank all my employers and colleagues for their support and patience. Specifically, Catherine Hickson, Mike Ellerbeck from the Geological Survey of Canada, Michael Porter, Matthias Jakob, and Kris Holm from BGC Engineering Inc.; and Heidi Evensen and Bill Eisbrenner from the Ministry of Transportation.

To my family, thank you for all your love, support, and reassurance. Paul van der Zee, your understanding, patience, and support mean the world to me. Thanks for waiting!

I am indebted to so many others for their support and friendship. Some of whom include: Fikre Debela, Saeid Abedi, Bessy Alexopoulos, Marta Soczewinska, Christian Trippen, Heidi Imhoff, the Vancouveramabobamajiggers, Liana Sipelis, Tanya Huang, and Junita Balogh. Thank you for putting up with me over the years. I know I was not there for a lot of things but you were always in my thoughts. Kim MacLean, Nathalie Pilon, Sheila and Doug Armstrong, and Helen Hayward thank you for opening up your homes to me. Your hospitality was greatly appreciated and my doors will always be open to you.

The Dali Lama once said, "Share your knowledge. It's a way to achieve immortality." To everyone; trust you will be remembered always and I will pay the generosity forward. I am eternally grateful for everything!

CHAPTER 1: INTRODUCTION

Landslide maps support land-use planning, engineering design and civil protection programs by identifying locations subject to landslide hazards (Hervás and Bobrowsky 2009). In recent years, population growth and expansion of settlements into hazardous areas have increased landslide risk in industrialized and developing countries (Guzzetti et al. 1999). The high costs involved in conducting landslide research challenges investigators working in remote regions to produce landslide hazard maps. To continue implementing proper landslide mapping programs for the prevention and mitigation of landslides, suitable cost-effective methodologies are required.

With new developments in satellite technology and ready access to satellite imagery, landslide research using sun-synchronous satellites is cost-effective. This thesis presents an effective approach to landslide distribution and susceptibility mapping in a large, remote region in northern Canada - South Nahanni Watershed, NWT.

The thesis is organized as follows: Chapter 2 describes identified landslides in the South Nahanni watershed using Advanced Spaceborne Thermal and Emission Radiometer (ASTER) satellite imagery. The chapter discusses landslide types and summarizes general observations made in the field. It also reviews ASTER satellite imagery as an alternative to small-scale aerial photography for identifying and mapping landslides. Chapter 3 describes the logistic regression models used to construct landslide susceptibility maps and the methods to identify factors favouring debris flows, earth flows, earth slides, and rock/debris slides. Chapter 4 summarizes the major results of this study, identifies the study's major limitations, and provides suggestions for future work. Three appendices are included in this thesis: A - landslide description with figures; B - a landslide type and distribution map, and landslide inventory database; and C - a description of model building and map procedures, including R scripts, results and susceptibility maps of debris flow and rock/debris slides.

CHAPTER 2: LANDSLIDE IDENTIFICATION AND MAPPING USING ASTER SATELLITE IMAGERY

Abstract

The remoteness and vast extent of the Canadian North challenge landslide identification and mapping using traditional methods. The present study uses Advanced Spaceborne Thermal and Emission Radiometer (ASTER) imagery to identify and map landslides in the 24,000 km^2 South Nahanni watershed. Over 4,000 landslides were identified and digitized from 14 epipolar ASTER images acquired between 2000 and 2005. Landslide classes include rock slides, debris flows, earth flows, complex rock slide-debris flows, and earth slide-debris flows. Debris flows represent the most common landslide type. The largest failure is a rock slide with an area of approximately 8 km^2. The landslide with the longest runout (4 km) is a rock slide-earth flow in Devonian shale, south of the South Nahanni River.

Landslides in the South Nahanni watershed, greater than 1 ha are easily detectable with ASTER imagery. Limitations in the use of ASTER imagery for landslide detection include lower spatial resolution (15 m) than high-resolution aerial photos (nominally 1 to 2 m), extensive shadows on north-facing slopes, and cloud cover.

Despite limitations associated with ASTER imagery, the approach taken in this paper provides a cost-effective strategy for landslide identification and mapping, which can be used as a preliminary tool for land-use and project planning decisions. This method can be applied to develop landslide inventories where resources are limited or for preliminary reconnaissance work.

Key words: Landslides, ASTER imagery, Nahanni National Park Reserve, mapping, inventory

Introduction

Landslides are typically identified using a combination of aerial photo interpretation and fieldwork. Landslide investigations conducted in remote regions or developing countries are often difficult because aerial photos and site access are, respectively, limited and expensive (Weirich and Blesius 2006). Yet there is increasing interest in completing landslide assessments in remote and developing regions for natural resource development, infrastructure and urban expansion, and natural hazard assessment.

Here I describe a landslide inventory study in the South Nahanni watershed, Northwest Territories, Canada. The watershed contains many areas of unstable terrain, and landslide research in this basin is limited. Aerial photographs acquired in 1949 exist for the South Nahanni region, but 2,220 images at 1:40,000 scale are required to cover the watershed. The number of photographs precludes a cost-effective inventory. Guzzetti et al. (1999), for example, took fiveperson/years to identify and map landslides on 2,100 air photos at 1:33,000 scale in the Marche Region of Central Italy. Furthermore, although these photographs could be used to identify old landslides, they do not allow identification of recent failures.

Landslides can be mapped from satellite images in several ways. Change detection is one option (Nichol and Wong 2005). This technique uses a series of superimposed images acquired at different dates to detect any changes in the land cover. Change detection is best used for landslide identification following a significant triggering event such as an intense rainstorm or earthquake. Regions with sparse vegetation, steep slopes, bedrock outcrops and alpine regions pose challenges for landslide identification using change detection techniques because it is difficult to discern landslides from other physiographic features. With limited information on landslide activity in the South Nahanni watershed and its sparse land cover, change detection is not a viable option.

Stereo viewing is another method that can be used to identify landslides from satellite imagery. The technique works by draping scenes over a generated DEM, or by using anaglyph images (van Westen et al. 2008). An anaglyph, also known as epipolar pairs, comprises two images with slightly different perspectives and contrasting colours, usually red and blue. The two images are superimposed and can be viewed in stereo using anaglyph glasses. Anaglyphs provide better topographic and morphological detail than non-stereo imagery (Nichol et al. 2006).

Several satellites acquire stereo imagery and include high-resolution scenes such as Quickbird [0.60 cm ground sampling distance (GSD)], GeoEye-1 [0.5 m GSD], and Ikonos [1.0 m GSD], and high resolution SPOT and moderate resolution ASTER imagery [2.5 m and 15 m GDS, respectively]. Nichol et al. (2006) concluded that Ikonos images are comparable in resolution to large-scale, 1:10,000-scale aerial photos, although they are expensive. In their cost estimate, Nichol et al. (2006) found that ASTER scenes were relatively inexpensive compared with other types of satellite imagery such as Ikonos.

The objectives of this study are to identify landslides in the South Nahanni watershed and to review the effectiveness of ASTER imagery to locate and classify landslides in remote areas. Results from the landslide mapping interpretation and field observations are compared with aerial photograph interpretation methods to determine whether ASTER imagery is suitable for landslide detection in Canada's north.

Study Area

The study area comprises 24,000 km^2 of the South Nahanni watershed in the Northwest Territories, Canada (Figure 2.1). The area comprises the Nahanni National Park Reserve boundary of 2005 andselected regions in the east and west of the watershed. We selected the eastern and western portions because of their significantly different terrain conditions.

The watershed heads in the Selwyn Mountains and extends to the confluence of the South Nahanni and Liard rivers. Elevations range from 150 metres above sea level (m asl) in the east to over 2,700 m asl near the watershed's western edge. The area includes rugged mountainsand glaciated terrain in the west, and plateaus, river valleys, and its famous karst landscape (Ford 1980) in the east.

The study area is located in the discontinuous permafrost zone (Brown 1978). Its climate is continental with a mean annual temperature of -4.5°C. Annual precipitation is 566 mm (Parks Canada 1984a, 2003).

The main rock types in the South Nahanni watershed are Devonian shale, limestone, dolostone, and calcareous sandstone (Figure 2.2; Jefferson et al. 2003; Wright et al. 2007). Outcrops of sedimentary rock include carbonate, shale, and interbedded clastic litihologies, for example, sandstone interbedded with shale. Mesozoic granites intrude the sedimentary rocks and form the westernmost mountains in the study area – the Backbone Ranges (Jefferson et al. 2003; Wright et al. 2007). The rockshave been tectonically displaced upward and eastward or folded along thrust faults (Jefferson et al. 2003; Wright et al. 2007). A M6.8 earthquake with an epicenter near North Nahanni River happened in 1985, demonstrating ongoing compression and uplift in the area (Evans et al. 1987; Wetmiller et al. 1988; Jefferson et al. 2003; Wright et al. 2007).

Surficial deposits in the study area include till, glaciofluvial gravel, and glaciolacustrine silt and sand. Some of the glacial deposits have been reworked into Holocene colluvium and fluvial deposits on terraces, floodplains, and fans (Duk-Rodkin et al. 2007). Minor loess and organic deposits are also present in the study area (Sanborn and Smith 2007).

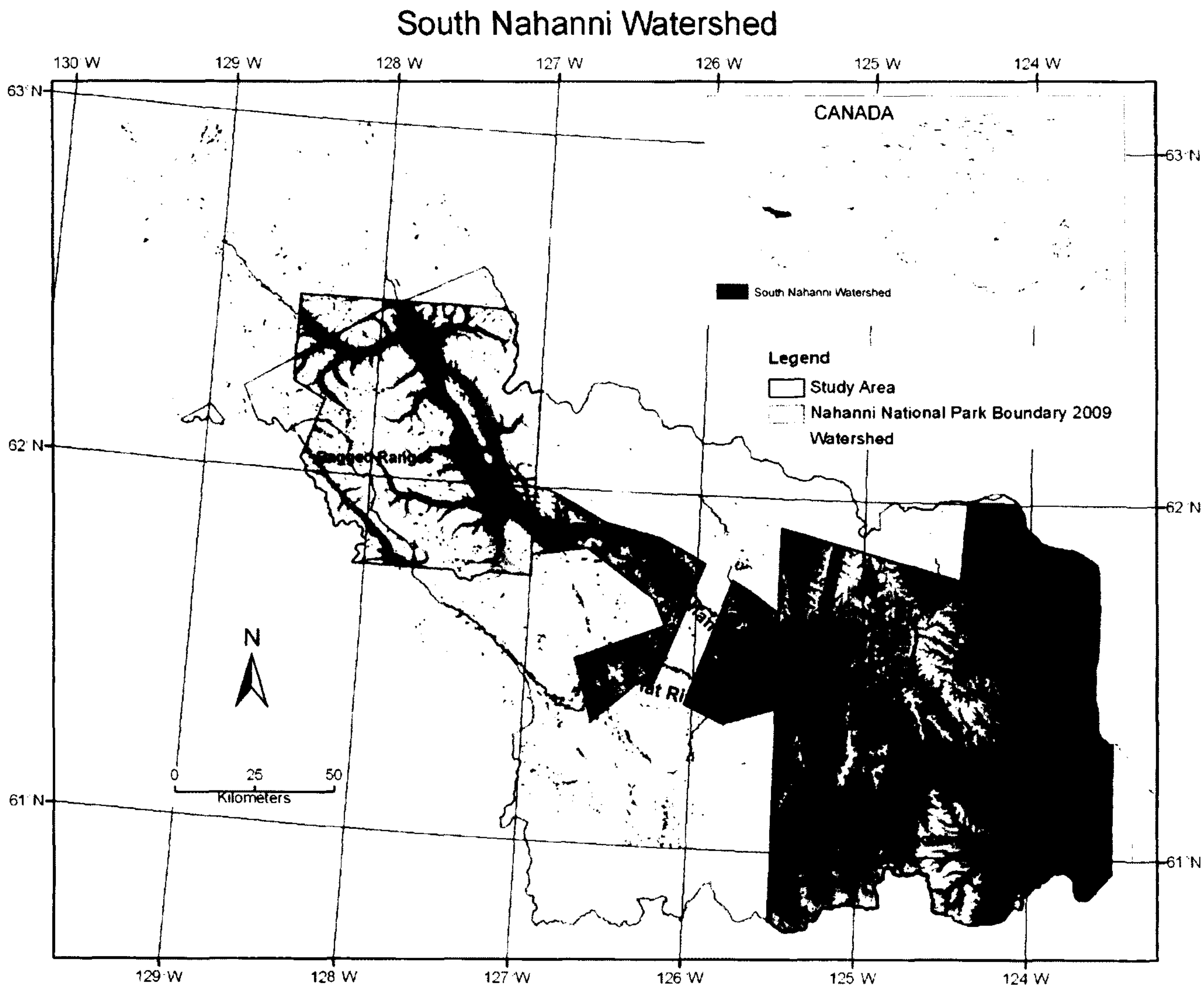

Figure 2.1: South Nahanni Study area.

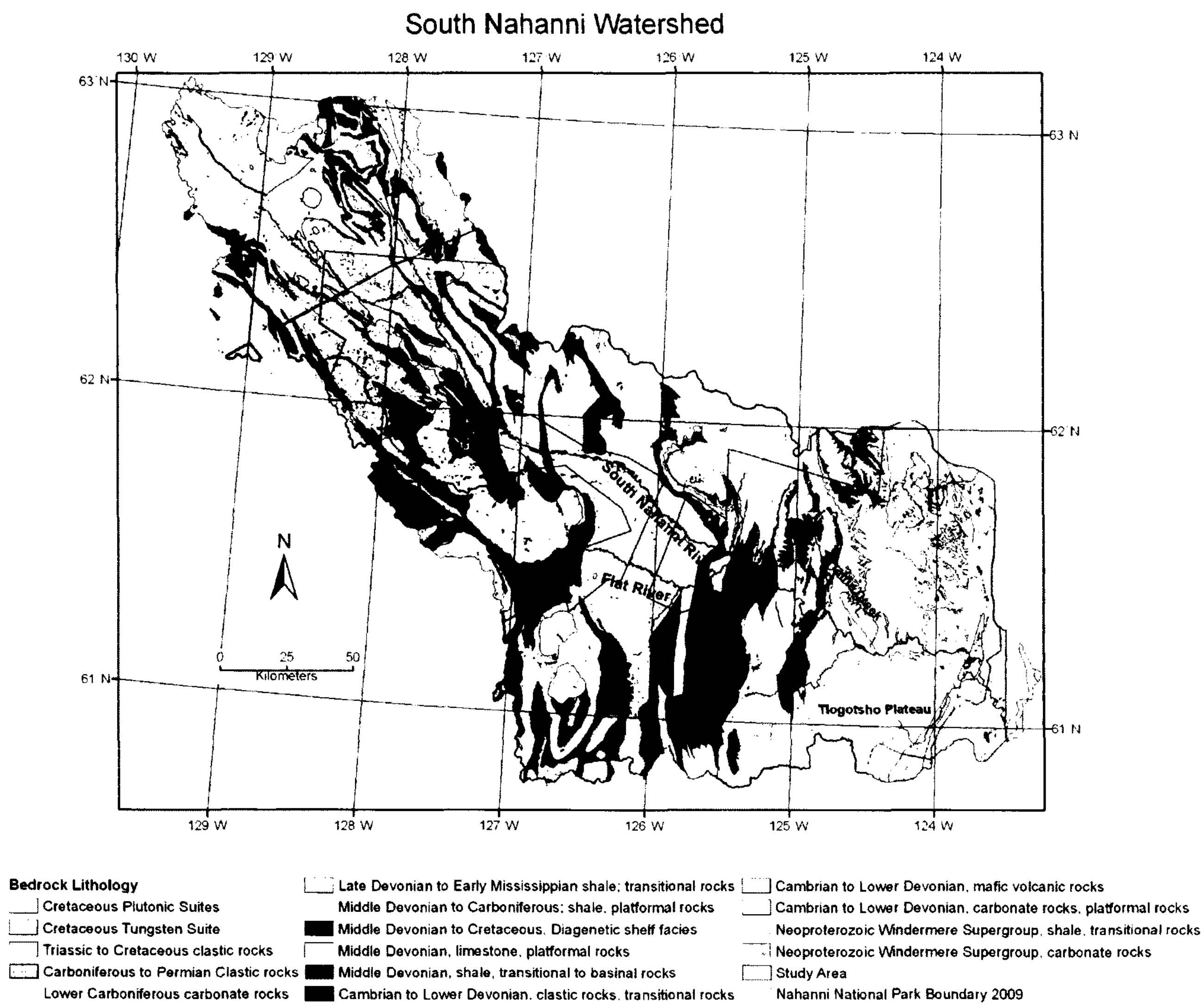

Figure 2.2: Bedrock geology of the South Nahanni watershed (Wright et al. 2007).

Previous Work on Northwest Territories Landslides

Most landslide studies in the Northwest Territories have focused on describing where landslides occur or on individual failures (Code 1973; McRoberts and Morgenstern 1973; Ford 1976; Eisbacher 1977, 1979; Evans et al. 1987; Jackson 1987; Evans and Clague 1989, 1994; Dyke 1990; Clague 1992; Aylsworth et al. 2000; Lyle et al. 2004; Couture and Riopel 2006; Huntley and Duk-Rodkin 2006; Huntley et al. 2006). Only Aylsworth et al. (2000) and Huntley et al. (2006) have mapped landslides on a regional scale. Eisbacher (1977, 1979) restricted his regional study to large rock avalanches in the Mackenzie Mountains.

Previous researchers have described a variety of landslide types involving earth (unconsolidated sediment) and bedrock (see Appendix A for material type definitions). Failures in earthinclude retrogressive thaw flows, active layer detachments, and earth slides. Many of these landslides occur in fine-textured till or glaciolacustrine deposits and commonly involve permafrost. The rock landslides aretopples, falls, rock slides and avalanches. Structure and orientation of bedding play an important role (Eisbacher 1977).

Landslides involving soil occur in thick glaciolacustrine deposits and tills, but also thin soils overlying bedrock. Rotational landslides typically have thicknesses of tens of meters and are commonly found along riverbanks and slopes of 13 to 20° (Eisbacher 1977; Parks Canada 1984c). Translational soil slides and flows involve shallow materials. Debris flow initiation is often associated with heavy rainfall and melting ground ice (Parks Canada 1984b; Jackson 1987; Evans and Clague 1988).

Methods

Imagery Collection and Processing

The landslide inventory of this study employs imagery from the Advanced Spaceborne Thermal and Emission Radiometer (ASTER) sensor. The sensor is mounted on the Terra satellite and acquires multi-spectral images of 60 km by 60 km extent with a nominal sampling resolution of 15 m. In addition to nadir viewing, ASTER obtains a corresponding off-nadir (backward-looking) scene at an angle of 27.6°, acquired 60 seconds after a nadir scan, to provide a stereo pair (epipolar pair) of near-infrared images similar to stereo aerial photographs (Abrams et al. 2002; Kääb et al. 2002).

I processed 14 ASTER images to identify and map landslides in the Nahanni region. I rectified and corrected each scene for topographic distortion using PCI Geomatica digital image processing software. National Topographic Data Base (1:50,000 scale) digital maps provided identifiable features such as small lakes or stream confluences that could be used as ground control points (GCPs). I collected approximately 15 uniformly distributed GCPs for each ASTER stereo pair with a root mean square error (RMSE) of 25 m (Table 2.1). At times it was difficult to find enough lakes or river junctions to use as GCPs. I realized after identifying and mapping landslides (described in the sections below) that the limited distribution of control points caused seven images to be offset from water body (lakes and rivers) control points. One image had offsets up to 350 m; the others had offsets less than 100 m. To account for the image distortion, I adjusted affected images and landslide data layers using water body and topography data as a guide to fit the offset layers to their appropriate locations. Following image rectification, I generated epipolar satellite pairs to view the images in 3D. The PCI Geomatica software allows the display of epipolar pairs as red-blue anaglyph images that can be viewed in stereo.

Table 2.1: ASTER imagery acquisition details.

Image Number	Data of Acquisition	Image Centre's Coordinates		RMSE (m)
		Longitude (degrees decimal)	Latitude (degrees decimal)	
AST_L1A_003_09120034200354_09212003164625	9/1/2003	-126.70	61.68	24
AST_L1A_003_09172003200356_10012003122505	9/17/2003	-127.61	62.39	22
AST_L1A_003_08182004200354_08302004110318	8/18/2004	-128.28	61.62	30
AST_L1A_003_09262005193912_09292005095826	9/25/2005	-124.59	61.15	32
AST_L1A_003_07172000200129_06242002102900	7/17/2000	-124.96	60.98	22
AST_L1A_003_10023000201226_02152003153935	10/3/2000	-127.30	62.00	24
AST_L1A_003_08092003195735_0823003181323	8/9/2003	-127.77	62.07	21
AST_L1A_003_10032003200426_10162003135530	10/3/2003	-128.24	61.92	27
AST_L1A_003_05162004195228_05312004112255	5/16/2004	-125.43	61.39	24
AST_L1A_003_9092002194749_09292002113020	9/9/2002	-124.27	60.88	20
AST_L1A_003_03222004194624_04072004125110	3/22/2004	-125.14	61.72	30
AST_L1A_003_0910200020072_01202003135031	9/102000	-123.97	61.74	22
AST_L1A_003_09122003194532_0927200313433	9/12/2003	-123.34	61.37	24
AST_L1A_003_09262005193903_09292005095816	9/26/2005	-124.25	61.66	33
			AVG RMSE	25

Note: RMSE (m) column identifies the root mean square error (RMSE) for each ASTER image.

Landslide Identification and Inventory Production

I identified landslides on ASTER images by distinguishing texture and colour tone differences. Landslides were classified as active if they were bright, vivid toned and had clearly defined hummocky or flowing features compared to the surrounding area. I classified landslides as inactive or dormant, if the texture and tone were similar to the surrounding area. I typed landslides according to the nomenclature of Cruden and Varnes (1996;see Appendix A: Description of Terms provides definitions and illustrations of landslides classes). I also used the Park Warden's knowledge of the area and 1949 aerial photos to estimate ages of some landslides.

I used both polygons and points to symbolize landslides in the study area. Polygons delineate landslides with areas larger than 1 ha and denote single failures or headscarp clusters. Points demarcate landslides smaller than 1 ha or those too narrow (width <30 m) to map at 1:275,000 scale (Appendix B: Landslide Type and Location Map). I entered information for identified landslides into a geographic information system (GIS) to compile information pertinent to each feature based on the Cruden and Varnes (1996) classification scheme (Table 2.2).

Table 2.2: Description of landslide attributes in GIS database.

FIELD NAME	FIELD DESCRIPTION
ID	Unique value given to all entries in the database
Poly/Point	Identifies if the feature is represented as a point or polygon
IMID	The image # used to identify the specific entry
IMTYPE	Type of medium used (e.g. ASTER image)
IMYEAR	Year the image was taken
LSTYPE	Type of landslide e.g. debris flow or rock slide
LSMOVE	Type of movement e.g. flow, slide, slide/flow
MATERIAL	Type of material that failed e.g. rock, debris, earth
LSCODE	Acronym for landslide type e.g. Df for debris flow or Rs-df for rock slide – debris flow
YEAR	Approximate age range of a landslide. Pre or post-dating air photos and ASTER scenes.
QUANTITY	Number of landslides identified by a single point or polygon
COMMENTS	Any additional comments made to describe landslide or for future references.

Map Production

I produced a base map from National Topographic Data Base (NTDB) digital map data (1:50,000 and 1:250,000) using ArcMAP 9.2 and projected it in UTM Zone 10 (NAD 1983). The base map includes a 1:50,000-scale digital elevation model (DEM), major water bodies, and the 2009 Nahanni National Park Reserve boundary. I used a colour-classification scheme to differentiate landslide types and other mapped deposits (see Appendix A: Description of Terms and Appendix B: Landslide Type and Location Map). I also included geologic fault data produced by the Northwest Territories Geoscience office.

Field Observations

I completed limited field work between the Ram Plateau, the northern point of the Tlogotsho Plateau, and Cathedral Creek from a helicopter during July 2006. I visited four large landslides in different materials and with different modes of movement. Field investigations provided the opportunity to evaluate data obtained from ASTER interpretation, as well as collect detailed information on bedrock lithologies, morphological features, and failure mechanisms for several types of landslides that cannot otherwise be identified on aerial imagery. Poor weather conditions and logistical difficulties made it impossible to validate most of the mapping through field work. Consequently, landslide mapping is chiefly the product of satellite interpretation.

Results

Imagery Interpretation

I classified 13 landslide types based on the tone, texture, and morphology in the ASTER imagers. The inventory includes 4477 landslides (369 landslides symbolized using polygons and 4108 landslides denoted as points) (Table 2.3; Appendix B: Landslide Inventory, and Landslide Type and Distribution Map). The smallest feature that I identified was a talus cone approximately 1,000 m^2 in area, which is an acceptable lower limit size class for regional-scale mapping (Soeter and van Westen 1996). The number of landslides in the inventory is thus a minimum of the number in the study area and is limited by the resolution of the ASTER imagery.

The most common landslide type is debris flow. Most debris flows have areas less than 1 ha and are located predominantly in the western portion of the study area. Failures larger than 1 ha includes rock and earth slides, debris and earth flows, and complex landslides comprising rock slide – debris flows, rock fall – debris flows, earth slide - debris flow, and earth slide - earth flows. Most large landslides occur in the eastern portion of the study area, generally in Paleozoic limestone and shale lithologies. While debris flows are the most abundant landslide type, debris flow deposits cover the total spatial area within the watershed. Rock slides cover the greatest spatial area (43.2 km^2, Table 2.3). The largest landslide identified is an 8 km^2 rock slide located southeast of the First Canyon where the failed material traveled 2.4 km (Table 2.3). The second largest landslide is a 7 km^2 rock slide - earth flow and had the longest runout - 4 km (Table 2.3).

I had difficulty differentiating small rock slide - debris flow, rock fall - debris flow and debris flow on ASTER images. For small debris flows (<1 ha), it was not possible to identify the initial mode of failure. To account for this problem, I combined rock slide - debris flow, debris slide – debris flow, and rock fall – debris flow into the debris flow class because in these cases, the duration of the initial slide was short lived prior to its transition to a debris flow, making the latter the main mode of movement.

Table 2.3: Landslide frequency. Total number of landslides identified based on landslide type and size.

Landslide Type	Total Landslides	Landslides <1 ha	Landslides >1 ha			
			Landslides >1 ha	Spatial Frequency (%)	Max. Runout Distance (km)	Largest Landslide (km^2)
Debris flow (df, ds-df, rs-df, rf-df)	4214	4054	160	0.4	3.27	3.2
Debris slide	20	18	2	0.3	0.6	0.2
Earth flow	36	4	32	21.4	3.3	3.5
Earth slide - debris flow	5	5	0	2.1	2.0	1.93
Earth slide - earth flow	29	0	29	18.2	3.8	5.9
Earth slide	70	0	70	12.9	3.0	4.1
Rock slide (rs, rt-rs)	96	26	70	43.2	3.6	10.1
Rock slide - earth flow	7	1	6	1.4	4.0	2

Field Observations

Field observations are an important component of landslide inventories. Even without full ground-truthing, field observations of selected landslides can reveal important details about the mode of failure and material that constitutes the landslide. I observed, for example, permafrost, jointing, and rupture surfaces in the field. These features were not discernable on the imagery.

The regions visited are the Tlogotsho and Ram plateaus, and Cathedral and Wrigley creeks (Figure 2.3). Landslides in these regions occurred along steep canyon and cliff faces, on steep slopes within the mountains, and on lower terrain. Landslides also occur on slopes underlain by permafrost.

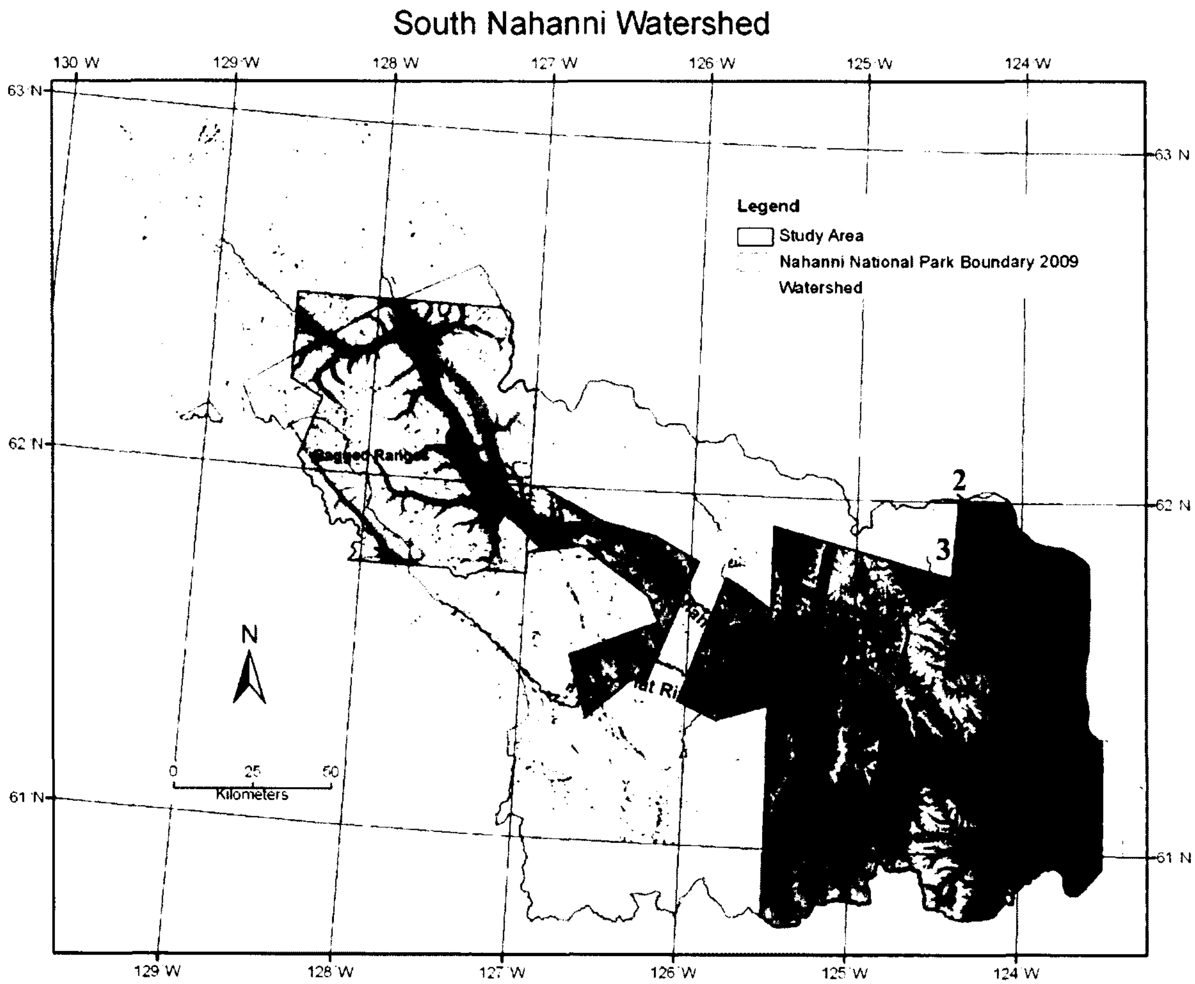

Figure 2.3: Map of landslide field investigation locations: 1) complex rock slide-earth flow, Tlogotsho Plateau; 2) rock slide, Ram Plateau; 3) complex earth slide-earth flow (flowslide), Ram Plateau; 4) debris slide, Wrigley Creek.

Complex Rock Slide – Earth Flow, Tlogotsho Plateau

I interpreted ASTER imagery of the Tlogotsho Plateau and identified long-runout earth flows on low-gradient (typically less than 7°), mainly north-facing slopes. Head-scarp features were not clear because of the presence of shadows on north-facing slopes. Similar limitationsare evident in the 1949 air photos, although subtle geological detail can be observed on the rock faces (Figure 2.4a and b) in the air photos. I traversed one of these landslides in the field and classified it as a complex landslide that traveled approximately 4 km down slope (Figure 2.4c). The upper portion (30 m) of the slide displays both rotational and translational movement in jointed sandstone and siltstone along a shale rupture surface (Figure 2.4d). The middle to lower portions of the landslide involved flowing and minor sliding of cohesive soil on a gradient of 3°. The landslide can thus be classified as a rock slide – earth flow. Based on aerial photos, satellite imagery, and field work observations, this slide was first active prior to 1949 and achieved its current form and extent nine years ago (Figure 2.4a and b). The long runout of this and other similar slides may be caused by undrained loading of cohesive earth materialgenerated by the rock slide. Similar landslides have been described by Geertsema et al. (2006) in northern British Columbia.

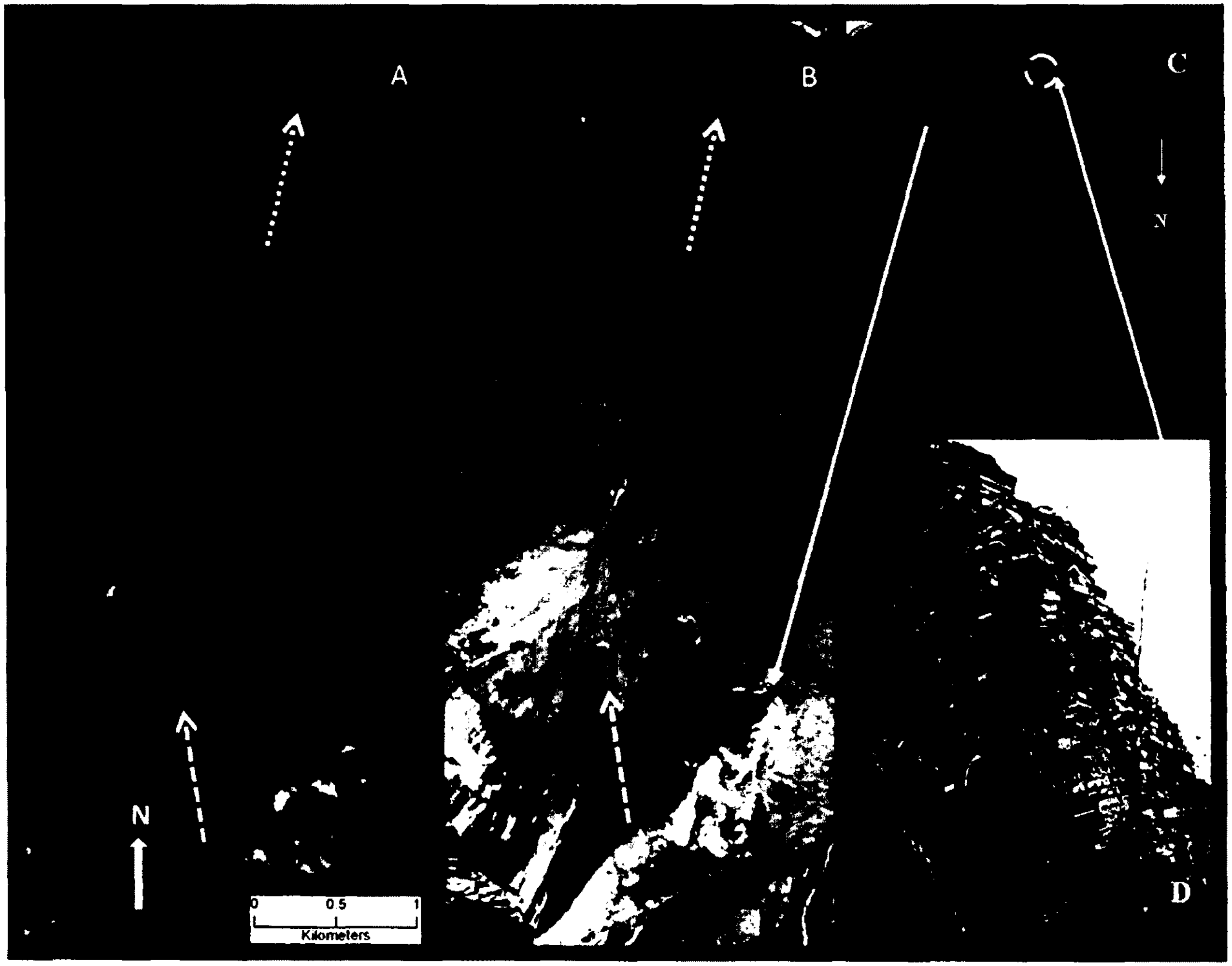

Figure 2.4: Imagery of the rock slide-earth flow in the Tlogotsho Plateau. White dashed lines represent rock slide movement and white dotted lines signify earth flow movement. A) ASTER ortho-image: shadows on north-facing slopes obscure exposed bedrock. B) 1:40,000 scale, cropped 1949 air photo; A12295-182. Shadows appear on north-facing slopes, but image resolution is higher than in ASTER image, with some exposed bedrock evident in shadowed areas. C) Oblique photo illustrating rock slide-earth flow features. D) Jointed siltstone located at the base of a rotational rock slide (location identified by the circle in photo C).

Landslides in the Ram Plateau

Landslides on the Ram Plateau include earth slides and flows, rock falls, debris flows, and complex landslides involving permafrost. Ground traverses were completed on two of these landslides; one was a rock slide (Figure 2.5) and the other a complex flowslide involving permafrost (Figure 2.6). Both of these slides impounded streams.

<u>Rock Slide, Ram Plateau</u>

This rock slide is located on an unnamed river within a canyon on the Ram Plateau. The initiation zone was not evident in the field, but the failure could have been triggered by a rock fall from the steep, limestone cliff face (Figure 2.5a). The failure rock rubble moved down slope, entrained lake sediments and ran 20-25 m up the opposite side of the valley (Figure 2.5b and c). The lake is located on the south side of the landslide deposit and was originally 4 m higher than at present (Figure 2.5c). I determined the previous highest level of the lake from the presence of a spillway marked by accumulation of woody debris and lateral margins formed in the rock debris. The rock slide was not visible on 1949 airphotos indicating that the failure post dates 1949. In addition, the absence of vegetation and disturbance of the landslide deposits and fresh preservation of the spillway (Figure 2.5d) suggest this failure was recent. Due to cloud cover over the failed region, it was not possible to determine if this rock slide pre- or post-dated the ASTER scene.

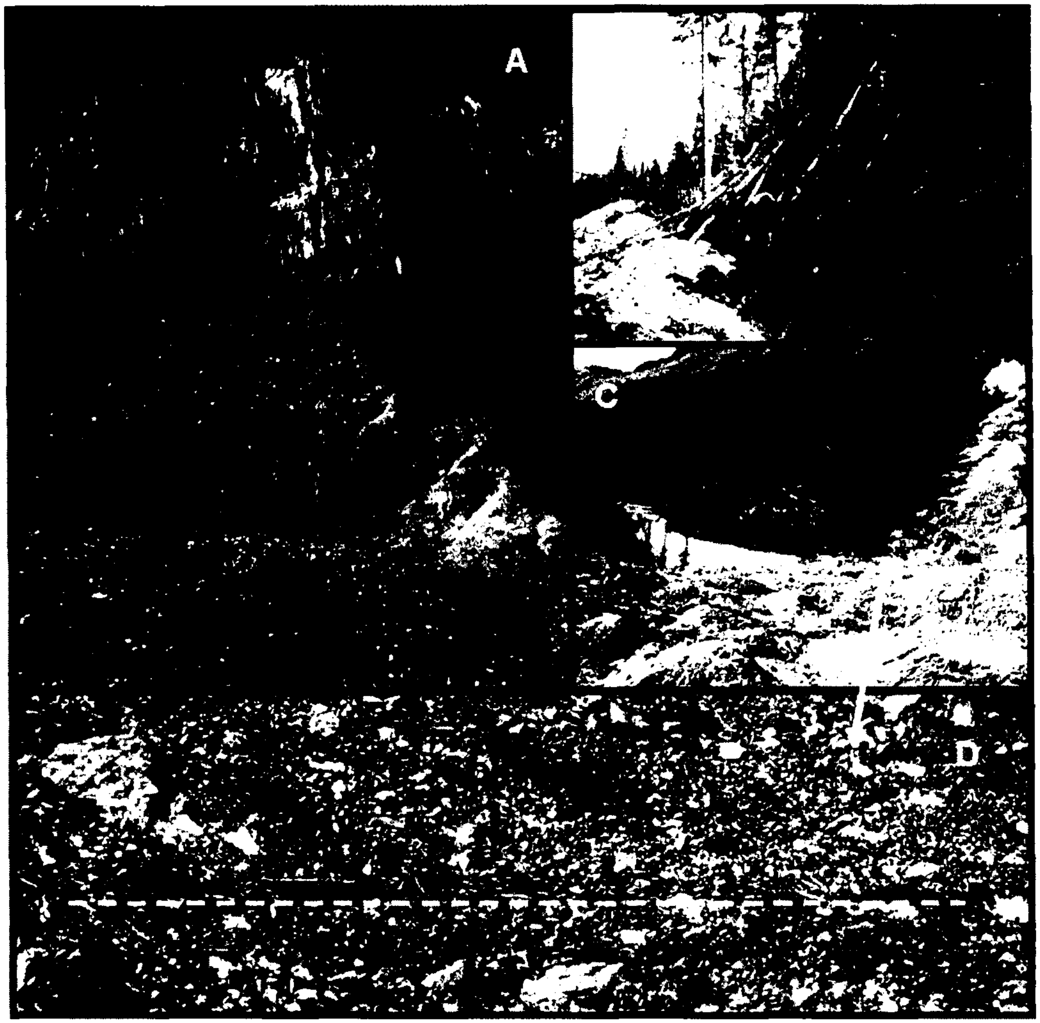

Figure 2.5: Ram Plateau rock slide 1: A) rock slide failure surface; B) uprooted trees caused by run-up of debris during the rock slide event; C) landslide-dammed lake; D) spillway.

Active Complex Earth Slide – Earth Flow (Flowslide), Ram Plateau

I located an active complex landslide south of the rock slide in the canyon on the Ram Plateau (Figure 2.6a-d). Based on field observations, it appears that riverbank erosion exposed fine-grained glacial lake sediments, causing an earth slide - earth flow that dammed the river (Figure 2.6a, b, d). The flowslide exposed permafrost (ground ice) and angular rubble in a talus slope (Figure 2.6c). The exposed permafrost probably then melted resulting in retrogressive thaw flows. The ASTER scene did not provide additional information about the failure because of strong shadows. Field observations suggest the failure post-dates the ASTER scene acquired in 2000 because retrogressive thaw flow activity was ongoing during our visit.

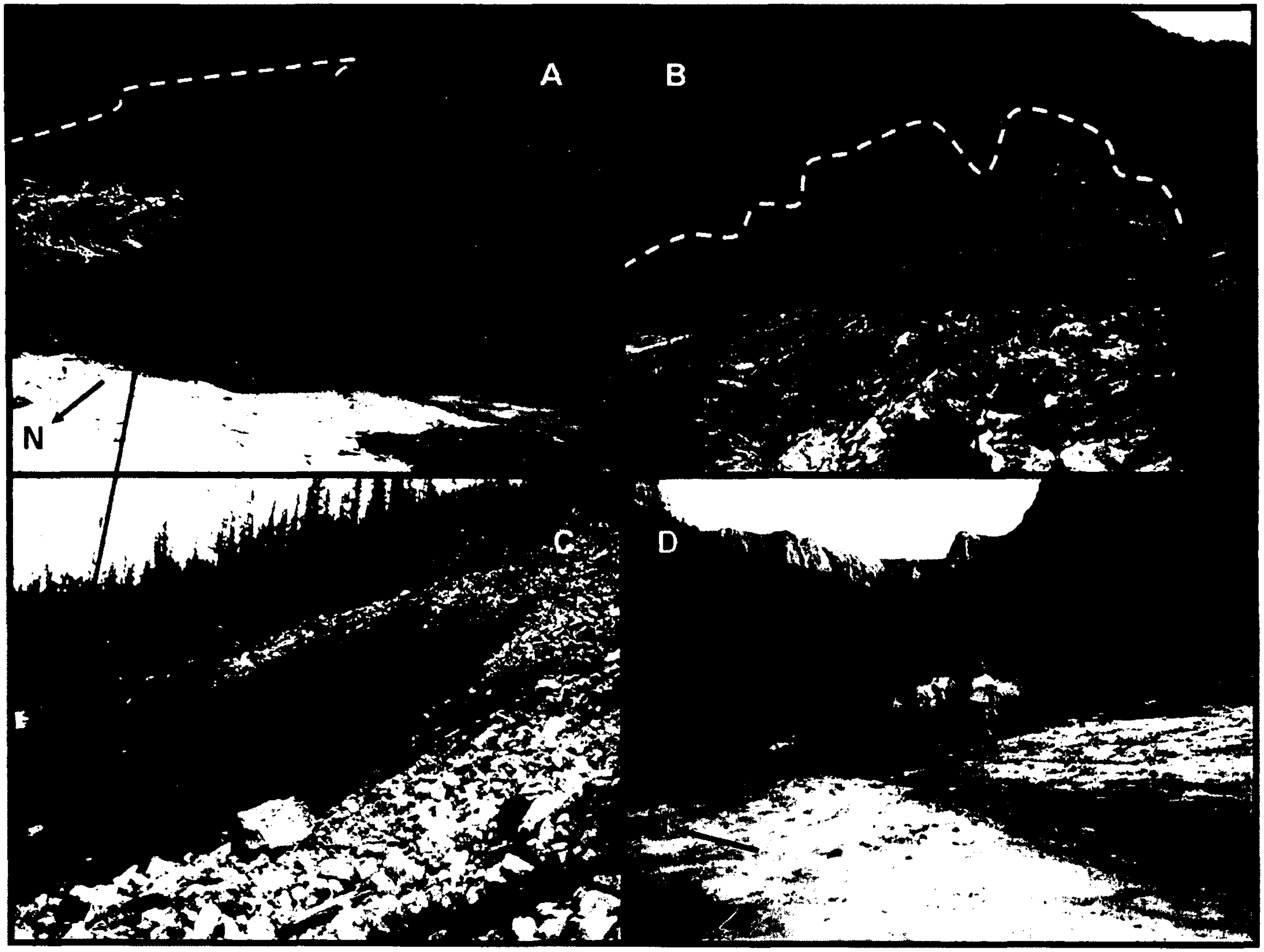

Figure 2.6: Ram Plateau earth slide-earth flow (flowslide). Dashed line delineates headscarp: A) earth flow movement within a complex landslide; B) rotational earth slide movement within a complex slide; C) ground ice exposure; D) landslide-dammed lake. Photos taken by Dr. Marten Geertsema.

Debris Slide, Wrigley Creek

I initially characterized the Wrigley landslide (Figure 2.7a and b) as a rock slide during ASTER imagery interpretation because of its tone and blocky texture (Figure 2.7a). Subsequent field visitation indicated that the slide was a translational debris slide (Figure 2.7a, c, d, and e). The failed material is of matrix-supported diamicton containing sub-rounded to angular clasts (Figure 2.7d). A landslide-dammed lake was located on the north side of the deposit, and based on strandlines on the shore, the lake was 10 m deeper than at the time of our field visit (Figure 2.7e).

I compared a 1949 air photo with an ASTER scene of the Wrigley slide area to evaluate the limitations of using ASTER imagery (Figure 2.7a and b). In both the ASTER scene and air photo, the surrounding slope appears dark grey to black in tone with steep and sharp topography, suggesting bedrock. In contrast, the west side of the valley has gently sloping, smooth-textured, dark grey toned slopes, which I interpret as unconsolidated material (Figure 2.7a and b). In the field we identified large conical piles of debris (molards), up to 12 m in height, across the entire deposition zone (Figure 2.7c). The molards give the landslide its blocky texture in the ASTER scene.

Figure 2.7: Wrigley Creek debris slide: A) ASTER scene (white dashed line identifies the debris slide); B) 1949 air photo A12319-230: 1:40,000 scale. The image pre-dates the landslide. The air photo has a higher resolution than the ASTER scene. Geomorphological detail is comparable in the two aerial images. Because the air photo pre-dates the landslide event, gully formation in the headscarp region is visible. The presence of gullies suggest that the material is glacial in origin (white dashed line identifies the debris slide); C) molards; D) failed diamicton; and E) view of the landslide-dammed lake. Photos taken by Dr. Marten Geertsema.

Discussion

This study is the first to comprehensively identify and inventory landslides in the South Nahanni watershed. Results show that many types of failures occur in the watershed. In the Ram Plateau and the Ragged Ranges, debris flows and rock falls predominately originate along cliffs in karst gorges and on steep mountain slopes. Rock slide-debris flow failures, also common in these regions, initiate along bedding planes on steep valley walls. Huntley and Duk-Rodkin (2006) identified similar failure mechanisms in the neighbouring Mackenzie Valley. The Tlogotsho Plateau contains many complex rock slide-earth flows and earth flows. Complex slides occur where jointed sandstone and siltstone fail along incompetent shale. Earth flows initiate in shale lower on escarpments. Complex earth slides are found at low elevations within the watershed where glacial deposits are most abundant. They occur predominately along active tributaries and river systems. Morphology of some earth slides in the Ram Plateau area resembles features illustrated by Huntley et al. (2006), suggesting that these failures are active layer detachments or retrogressive-thaw flows caused by permafrost degradation. Landslide activity in the Ragged Ranges of the Mackenzie Mountains is characterized by debris flows and rock slides; the latter appear to slide on bedding planesin agreement with the conclusions of Eisbacher (1977, 1979) and Jackson (1987) who also found that bedrock landslides in this area are controlled by rock structure. Moreover, this study also supports Jackson's (1987) observation that small debris avalanches are the most abundant landslide type.

ASTER Imagery

In the course of my research, I identified several limitations in using ASTER imagery for landslide mapping. A disadvantage of ASTER imagery for remote-based studies is the need to use previously georeferenced data to generate stereopair ASTER scenes. For seven scenes, it was difficult to find enough GCPs to orthorectify the images. Rectification of an image depends on the resolution of the image (15 m for ASTER) and the accuracy of the corresponding DEM and reference map. A recommendation to avoid this problem in the future is to obtain more control points if possible or to use a high precision Global Positioning System (GPS) in the field to obtain additional GCPs.

Previous studies have indicated that ASTER satellite imagery is not adequate for detailed landslide investigations because of its limited resolution (Singhroy 2005; Nichol et al. 2006). Singhroy (2005, 2008) suggests that a 1:25,000scale is the smallest for analyzing slope instability because any image with a cell size >3 m makes characterizing and classifying landslides difficult, unless the features are large or contrast marked with the surrounding terrain. Nichol et al. (2006) concluded that ASTER imagery is inadequate for landslide identification in re-vegetated areas. With South Nahanni's rugged alpine and low-density forests, identifying re-vegetated landslides is possible. ASTER's image resolution remains a limitation in this study, as it is affected by cloud cover and shadows on north-facing slopes and in steep canyons. In both cases, these limitations can be minimized by supplementing ASTER imagery with aerial photography or satellite images obtained during favorable weather and times of the day and year.

In agreement with Nichol et al. (2006) and Singhroy (2005), poor spatial resolution is the most limiting factor for landslide identification, particularly for features smaller than 1 ha. Large landslides (>1 ha) identified on the ASTER scenes appear to be consistent with what was seen on the ground. Details such as tension fractures were difficult or impossible to identify. The absence of these features on some of the small landslides became apparent during field investigation. Although the major modes of movement were correctly identified, the initial movement was incorrect. In some cases material type was also inaccurately identified. For example, prior to the field investigation, the Wrigley Creek landslide was classified as a rock slide from its appearance, texture, and tone (Fig. 2.7a and b). In the field, it was discovered that the failed material consisted of diamicton, making it a debris slide. The rock slide - earth flow headscarps in the Tlogotsho Plateau were complex features involving minor spreading, toppling, and rotational movement. These features were not visible on ASTER scenes because of their small size. Shadowed north-facing slopes also reduced recognition of the geological details (Figure 2.3a and b). Limitations associated with ASTER imagery identified above, however, are similar to those encountered in aerial photography investigations.

Although ASTER imagery is not suitable for large-scale landslide investigations, this study identified several benefits that significantly offset its limitations for small- to medium-scale studies. I found ASTER's large spatial coverage and viewing capabilities to be important advantages in mapping large areas. The large spatial coverage reduces the number of images required for the study and, once images are geo-referenced, they can be viewed on the computer screen using anaglyph glasses making images easier to manipulate because they can be viewed at various scales and still maintain topographic detail in 3D (Nichol et al.

2006). Features can also be digitized as they are being outlined, which saves a considerable amount of processing time and reduces common transfer errors. Weirich and Blesius (2006) and Fourniadis et al. (2007) also found ASTER imagery useful when conducting regional landslide studies.

Reduced image processing time is advantageous for landslide studies conducted in remote regions with limited budgets and tight deadlines. Mapping with aerial photographs can be almost 70 times more expensive than with ASTER imagery. Table 2.4, inspired by Nichol et al. (2006), shows the cost-benefits of both types of imagery. Considering the scope of the study, I found the cost and benefits of ASTER imagery to be the most viable option for landslide identification and mapping in the South Nahanni watershed.

Table 2.4: Cost comparison between aerial photos and ASTER imagery for a landslide survey in 24,000km^2 area based on stereo images. This comparison is for imagery acquisition and interpretation only; it does not include field work related costs.

	Aerial photo [g]	**ASTER**
No. of images	2200[a]	14
Material cost of image ($CDN)[c]	$33,000[b]	$1400[b]
Time (h)/cost (geo-referencing/digitizing)[d]	4400hr/$132,000	42hr[f]/$1,260
Time/cost (interpretation and mapping)[e]	5500hr[f]/$165,000	70hr[f]/$2,100
Total job cost[e]	$330,000	$4,860

[a] Rounded values based on 24,000 km^2.

[b] Prices are rounded. Aerial photo costs are based on the National Air Photo Library 2009 prices ($14.99 ($CDN)/image). ASTER imagery costs are based on 2009 cost (~100 $CDN/scene).

[c] Costs could vary. Image acquisition could accrue more costs (i.e. flight time or data processing). Archive data in some cases can be acquired for free.

[d] Assuming 1 hr/photo at $30 ($CDN)/hr wages.

[e] Assuming 2.5hr/image at $30 ($CDN)/hr wages.

[f] Time estimates cited from Nichol et al. (2006).

[g] Aerial photo study assumes manual interpretation and processing not digital.

Conclusions

This study provides a regional assessment of landslide susceptibility in the Nahanni region. The methods I used can be applied to other large remote regions or developing countries where a rapid landslide inventory is required. Data derived using this approach can also be applied in hazard and susceptibility models to delineate areas of unstable terrain that can be used in planning field work logistics and help make preliminary land-use decisions.

The landslide inventory identified the Tlogotsho and Ram plateaus, in the eastern part of the watershed, as especially prone to failure. Based on field studies and the interpretation of remotely sensed imagery, landslide activity in this area is explained by geology (rock type, rock structure, and surficial materials), river undercutting of slopes, and the presence of permafrost.

ASTER imagery proved to be an effective tool to detect landslides in the Nahanni region at regional scale. I required 14 ASTER scenes, as opposed to 2,220 aerial photos, to complete the inventory. Interpretation of many individual aerial photos over extensive areas is costly and time-consuming. Epipolar satellite images allow landslides to be mapped and digitized directly from the image, saving time, money, and minimizing transfer errors that are common in traditional mapping methods.

Despite resolution limitations that censor small landslides, use of ASTER imagery is still considered adequate for regional-scale landslide studies based on criteria proposed by Soeter and van Westen (1996). However, additional ground truthing and the use of higher resolution imagery would have helped validate the map and resolve some uncertainties with ASTER interpretation.

CHAPTER 3: LANDSLIDE SUSCEPTIBILITY MAPPING USING LOGISTIC REGRESSION; SOUTH NAHANNI WATERSHED, NWT

Abstract

The South Nahanni watershed contains over 4000 landslides. To determine areas susceptible to slope failure, I analyzed the relationships between environmental factors and debris flow, earth slide, earth flow, and rock/debris slide occurrence using logistic regression analysis. I used statistical results to generate individual susceptibility maps for debris flows and rock/debris slides in a GIS. Earth slide and earth flow results were inconclusive due to limited input data. I determined the success of the models was 75% for predicting debris flows and 85% and 77% for predicting rock/debris slides, using test and validation models, respectively. I used debris flow and rock/debris slide validation models to produce the final susceptibility maps. The quality of susceptibility maps depends on the type and scale of data input into the regression models. The landslide susceptibility maps produced in this study can provide insight into landslide activity in the South Nahanni watershed and can be used to improve land-use planning strategies to prevent and mitigate landslides.

Keywords: Landslides, landslide susceptibility, logistic regression, Northwest Territories

Introduction

The South Nahanni watershed, located in Northwest Territories, Canada, includes a national park and two mines. The region is prone to landslides (Evans et al. 1987; Wetmiller et al. 1988), which pose a hazard to recreation and mining activities. A better understanding of the factors that control slope stability and development of strategies to identify landslide-prone terrain are required to minimize landslide risk in the South Nahanni basin.

For decades, researchers have examined the association between landslides and terrain attributes with the goal of identifying regions of unstable terrain. These associations have been determined using qualitative (Castellanos Abella and van Westen 2008; Ruff and Czurda 2008), semi-quantitative (Larsen and Torres-Sanchez 1998; Ayalew and Yamagishi 2005; Riopel et al. 2006; Dominguez-Cuesta et al. 2007), and quantitative approaches (Carrara 1983, 1988; Carrara et al. 1991, 2008; Gokceoglu and Aksoy 1996; Turrini and Visintainer 1998; Guzzetti et al. 1999; Gokceoglu et al. 2000; Dai et al. 2001; Lee and Min 2001; Rollerson et al. 2001, 2002a, b; Lee et al. 2002, 2004; Jordan 2003; Lee and Dan 2005; Clerici et al. 2006; Dymond et al. 2006; Gorsevski et al. 2006; Komac 2006; van den Eeckhaut et al. 2006; Chen and Wang 2007; Demoulin and Chung 2007; Wang et al. 2007; Chung and Febbri 2008; Frattini et al. 2008; Nefeslioglu et al. 2008). No single approach is universally applicable for predicting the susceptibility of slope failure (Guzzetti et al. 1999, 2006; Süzen and Doyuran 2004; Komac 2006; Frattini et al. 2008), but heuristic, bivariate, and multivariate methods are most commonly applied in regional-scale landslide hazard maps (Clerici et al. 2006; Guzzetti et al. 2006).

To determine landslide susceptibility in the South Nahanni watershed, I used multivariate logistic regression analysis. This approach is preferred over alternative methods because it does not heavily rely on expert opinion (Nefeslioglu et al. 2008), it can analyze more than two variables at a time, and it can determine relationships between the independent and dependent variables (Clerici et al. 2006; Wang et al. 2007). In addition, logistic regression does not require a linear relation between independent and dependent variables, and it also does not require variables to be normally distributed (Süzen and Doyuran 2004; van den Eeckhaut et al. 2006; Carrara et al. 2008). Logistic regression analysis determines the best-fit function to describe the relationship between the presence and absence of landslides and a set of parameters that might cause slope failure, such as lithology, structure, topography, geomorphology, tectonics, hydrology, and roads (Ayalew and Yamagishi 2005; Ayalew et al. 2005; Kamp et al. 2008). The analysis requires that the input data include binary dependent variables (absence or presence of a landslide) and a set of predetermined explanatory variables in the form of continuous or discrete variables known as indicator variables (Hosmer and Lemeshow 2000; Ayalew and Yamagishi 2005; Nefeslioglu et al. 2008). Results of the logistic regression analysis are used to calculate probability, with values ranging from 0 to 1. Zero represents no likelihood of a landslide and one signifies that a landslide will occur. The probability of a landslide at any pixel location in a raster map determined through the multivariate logistic regression analyses can be expressed as:

$$P_{(Y=1)} = 1 / 1 + e^{-z} \tag{1}$$

where

$$z = \alpha + \beta_1 \cdot X_1 + \beta_2 \cdot X_2 + \ldots + \beta_n \cdot X_n \tag{2}$$

and $P_{(Y=1)}$ is the probability of landslide presence, z is the logit, which is linearly related with the independent variables, β_i (i = 1, 2, 3, …, n) is the coefficient for each independent variable, α is the intercept, and X_i (i = 1, 2, 3, …, n) is the i-th independent variable (Süzen and Doyuran 2004; van den Eeckhaut et al. 2006; Wang et al. 2007).

The objective of this paper is to produce and verify small-scale susceptibility maps for debris flow, earth flow, earth slide, and rock/debris slides for a portion of the South Nahanni watershed. I used publically available input data acquired from several different sources to analyze the associations between landslides and causative factors (i.e. geologic and physiographic factors) using logistic regression models. The methodology developed herein can be used for any remote-based landslide survey and can assist in land-use and development planning in the South Nahanni watershed and in other areas in northern Canada.

Study Area

The study area comprises 24,000 km^2 of the South Nahanni watershed as described in Chapter 2 - Study Area (Figure 2.1). Refer to Chapter 2 for the study area description.

Data and Methods

Landslide-Causing Parameters

Multivariate logistic regression models are useful for landslide susceptibility studies because they can analyze multiple causative factors with different data scales at one time (Hosmer and Lemeshow 2000). Obtaining adequate datasets for landslide prediction is not always possible (Yesilnacar and Topal 2005); data commonly are small-scale and differ in quality. Susceptibility studies are only as reliable as the data used in the model, therefore, it is important to review and understand data prior to and during interpretation of the results. Several criteria must be met when using logistic regression analysis for landslide prediction. Independent variables should: 1) have an association with landslide occurrence, 2) be spatially continuous throughout the study area, 3) be spatially variable, 4) be expressible using any measuring scale (e.g. ordinal, interval, nominal, or ratio scales), and 5) be non-redundant,i.e. two outcomes cannot be possible in the final results (Ayalew and Yamagishi 2005).

I acquired input data for the logistic regression models from government and educational institutions, including Natural Resources Canada, Parks Canada, and the

University of Northern British Columbia. Data used in this study include bedrock, bedrock structure, land cover, and a digital elevation model (DEM). I could not use surficial geology and river networks in the analysis because of the smallscale of the surficial geology (1:5,000,000) and the incompleteness of the river network data. Land cover and the DEM were, respectively, 70 m and 30 m cell resolution raster data, whereas bedrock and surficial geology data were in vector format. I used the DEM to generate derivative data products that included slope, aspect, and plan and profile curvature. I also combined bedrock lithology, slope gradient, and bedrock structure data to generate a vector-based, bedding-slope structure layer. Map scales of the remaining data ranged from 1:50,000 to 1:1,000,000.

The data required additional processing prior to analysis. The first processing requirement involved choosing an appropriate spatial scale to complete the analysis. I selected a ground sampling distance of 30 m to maintain resolution of the topographic parameters, which were variable across small areas relative to other parameters. As a result, I resampled the land cover raster from 70 m to 30 m cell size to accommodate the selected sampling distance. Although 30 m provides a smaller cell resolution than the original,the re-sampling does not increase the spatial information contained in the data (i.e., a pixel with a category value of 1 at 70 m will have a value of 1 at 30 m).

The more variables and classes included in the model, the greater the chance the model will become over-fit. Model over-fitting can occur when there are too many model parameters, and an over-fitted model performs poorly on independent data. To prevent over-fitting, all vector categories were collapsed to the smallest number of classes that could still represent scientifically meaningful results. Over-fitting is particularly a problem when models have too many variables relative to the sample size. Studies that have large samples are less vulnerable to over-fitting and can incorporate a larger number of variables (Harrell et al. 1996; Hosmer and Lemeshow 2000). Revised categories are explained in the corresponding variable descriptions below.

Topography Parameters

A 30-m digital elevation model (DEM) was generated by tiling over 300 DEMs acquired from Geobase (Canadian Council on Geomatics 2009) and then reprojected to UTM NAD 83, Zone 10 in SAGA GIS using spine interpolation (Figure 3.1). I used this DEM to identify elevation values and to calculate first and second derivatives to obtain slope, aspect, and plan and profile curvature using Spatial Analyst in ArcGIS 9.2 (Figure 3.2 to 3.5; Kamp et al. 2008). Slope gradient is one of the most important contributors to slope instability.Instability is common were a slope is steeper than the angle of repose of the material (Kamp et al. 2008), and the steeper the slope the greater the chance of a landslide (Lee et al. 2004). The probability of a landslide also increases when the cohesion of the material is reduced (Kamp et al. 2008). To calculate slope, Spatial Analyst determines the maximum change in elevation over the distance between a cell and its eight neighbouring cells.

Aspect is the direction of the maximum rate of change of a slope, determined from the value of each cell and its surrounding eight neighbours. Slope aspect may be factor in mass movement because of its association with weathering, precipitation, snow meltwater, land cover, and soil conditions (Kamp et al. 2008).

Plan and profile curvature may have a bearing on landslides occurrence because they influence the direction and velocity of movement. Curvature output values are a second derivative product derived from the DEM. Plan curvature is perpendicular to maximum slope and influences water flow convergence or divergence; profile curvature is parallel tothe direction of maximum slope and directly controls downslope water flow velocity and slope erosion (Nefeslioglu et al. 2008). Positive plan curvature values indicate the surface is convex upward and negative values indicate the surface is concave upward. Conversely, profile curvature is concave if the value is positive and convex if the value is negative. A zero value in both plan and profile curvature indicates the area is flat (ESRI 2009).

All topographic parameters show spatial variability across the study area. The watershed has an elevation range of 147to 2700 m asl and is characterized by slope gradients mainly between 3 and 15°, in every cardinal direction, slope plan curvature of -0.15 to 0.11 /100 m and profile curvature of 0.16 to 0.43 /100 m (Figures 3.1 to 3.5).

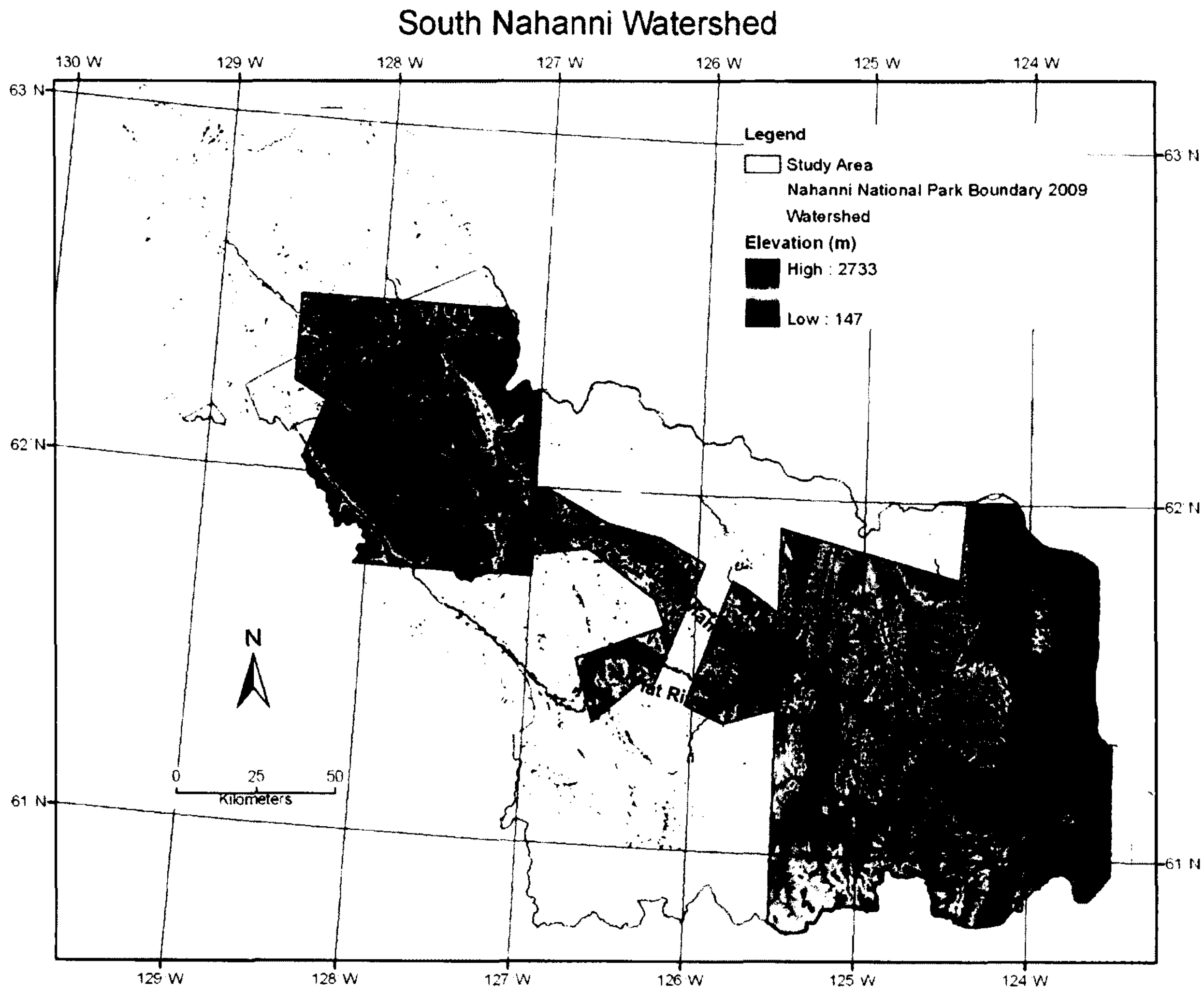

Figure 3.1: Primary and derivative terrain data - elevation.

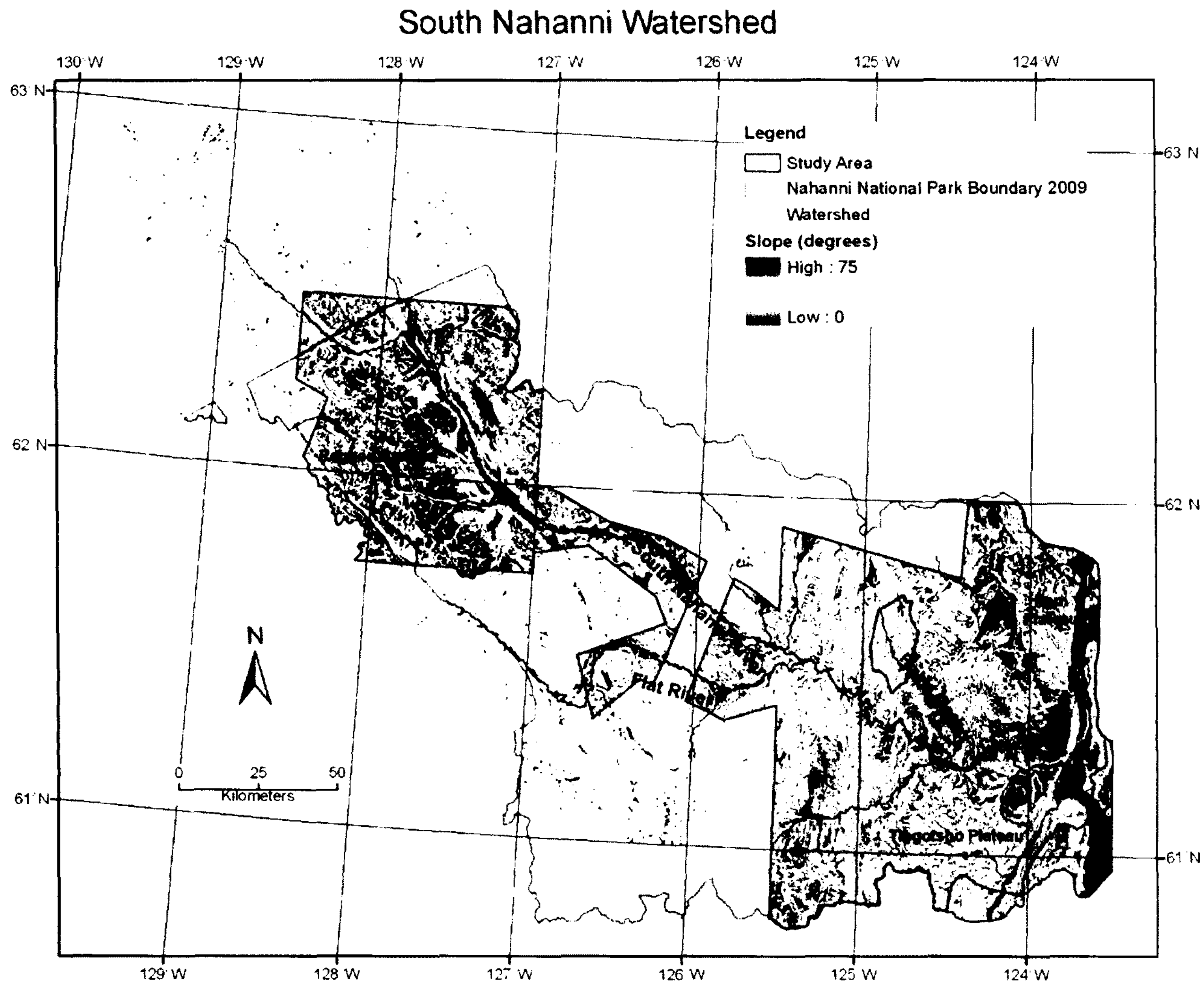

Figure 3.2: Derivative terrain data – slope gradient.

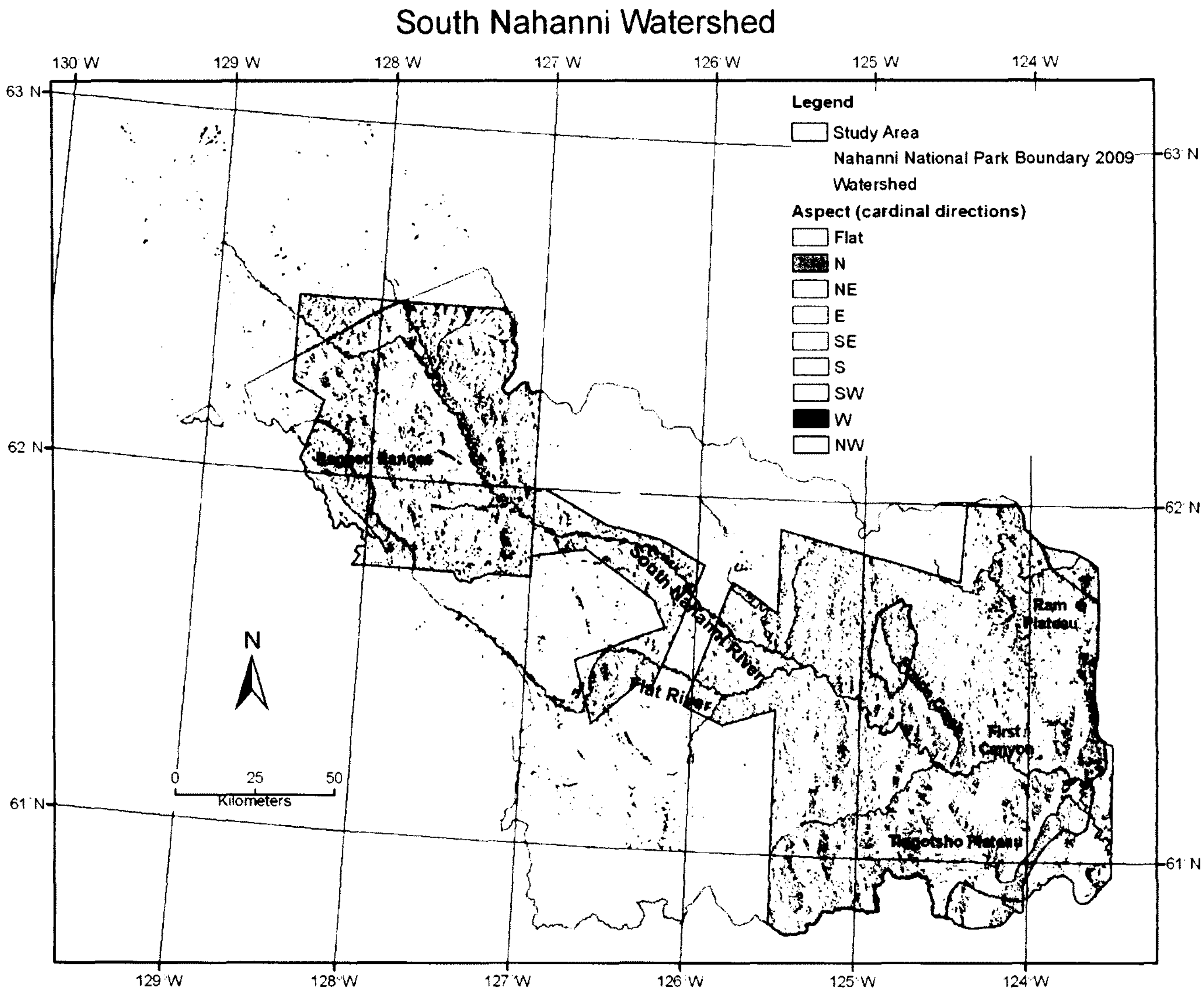

Figure 3.3: Derivative terrain data -aspect.

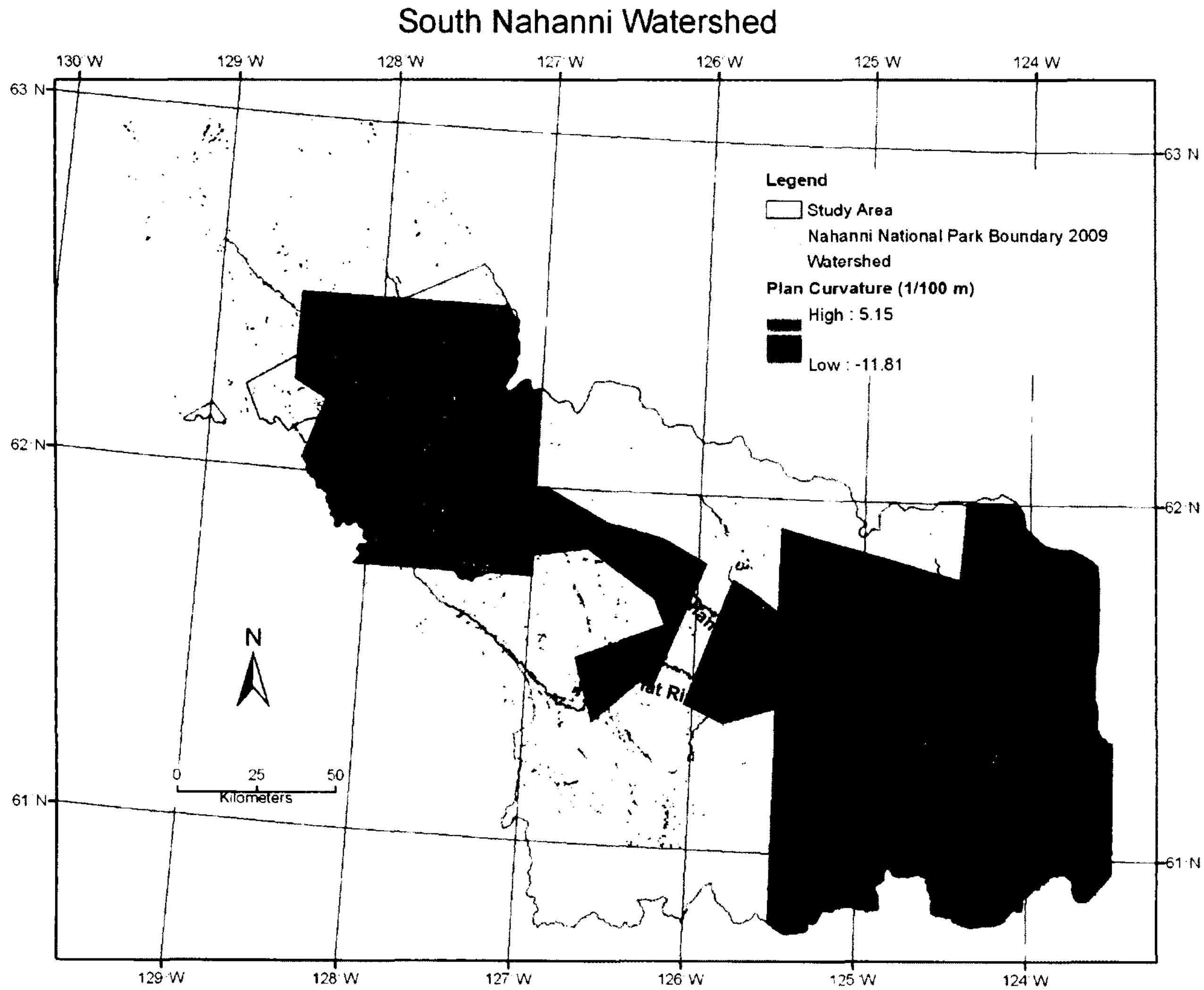

Figure 3.4: Derivative terrain data –plan curvature.

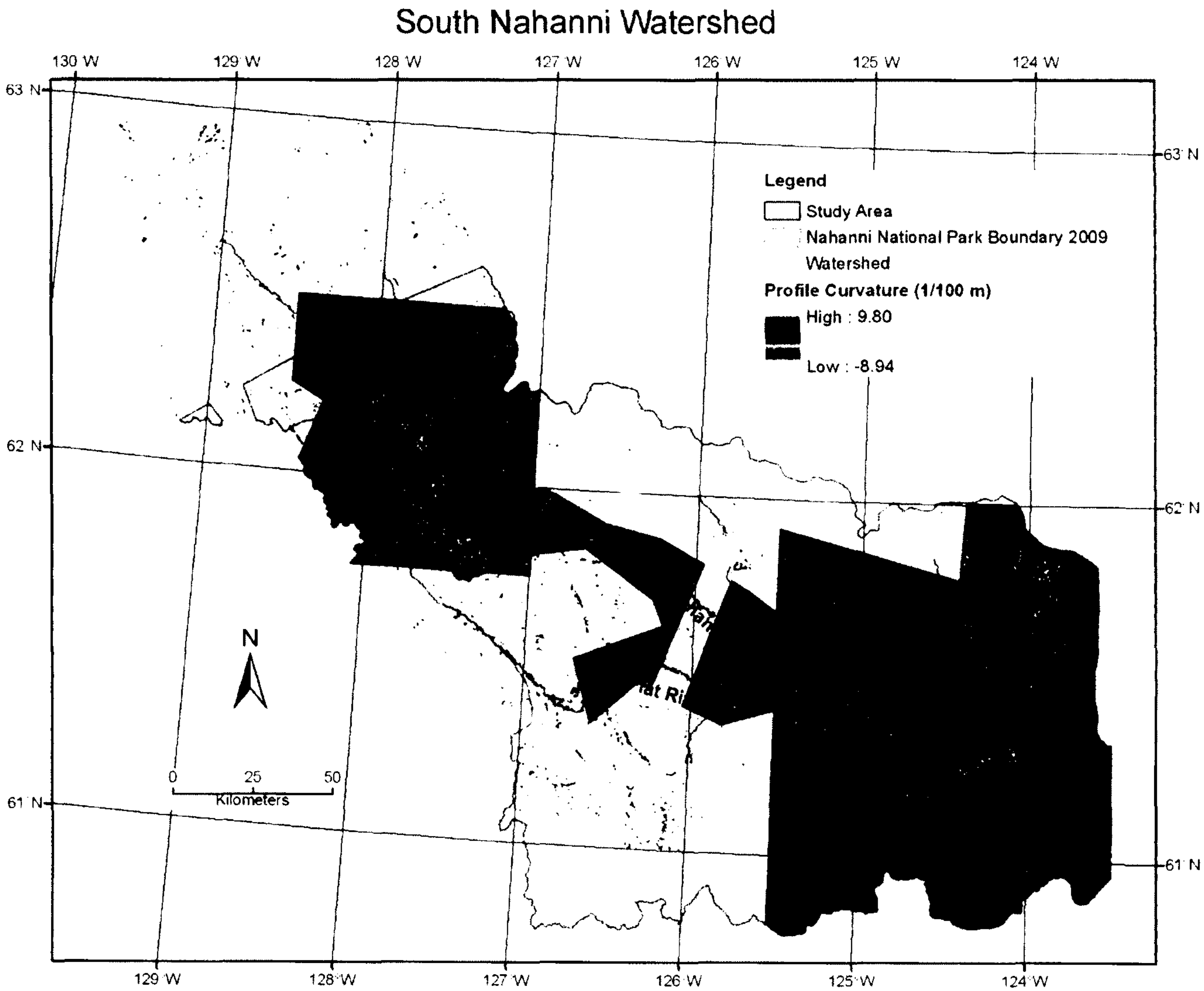

Figure 3.5: Derivative terrain data - profile curvature.

Geological Parameters

Bedrock Lithology

I used the 1:1,000,000-scale digital bedrock lithology map of Wright et al. (2007) (Figure 3.6), which was generalized from 1:250,000 and 1:1,000,000-scale geology maps. Stratigraphic terminology follows Jefferson et al. (2003): Cambrian to Lower Devonian platformal carbonate rocks, Cambrian to Lower Devonian transitional clastic rocks, Cretaceous Plutonic Suite, Cretaceous Tungsten Suite, Late Devonian to Early Mississippian transitional shale, Lower Carboniferous carbonate rocks, Middle Devonian to Carboniferous platformal shale, Middle Devonian transitional to basinal shale, Neoproterozic Windermere Super Group carbonate rocks, Neoproterozic Windermere Super Group transitional shale, and Triassic to Cretaceous clastic rocks (Figure 2.2). I aggregated these map units into four general lithologic classes: carbonate, mixed rocks (mixture of shale, clastic rocks and carbonates), igneous rocks, and shale (Figure 3.6). The study area comprises 45% carbonates, 27% mixed, 4% igneous rocks, and 24% shale by area.

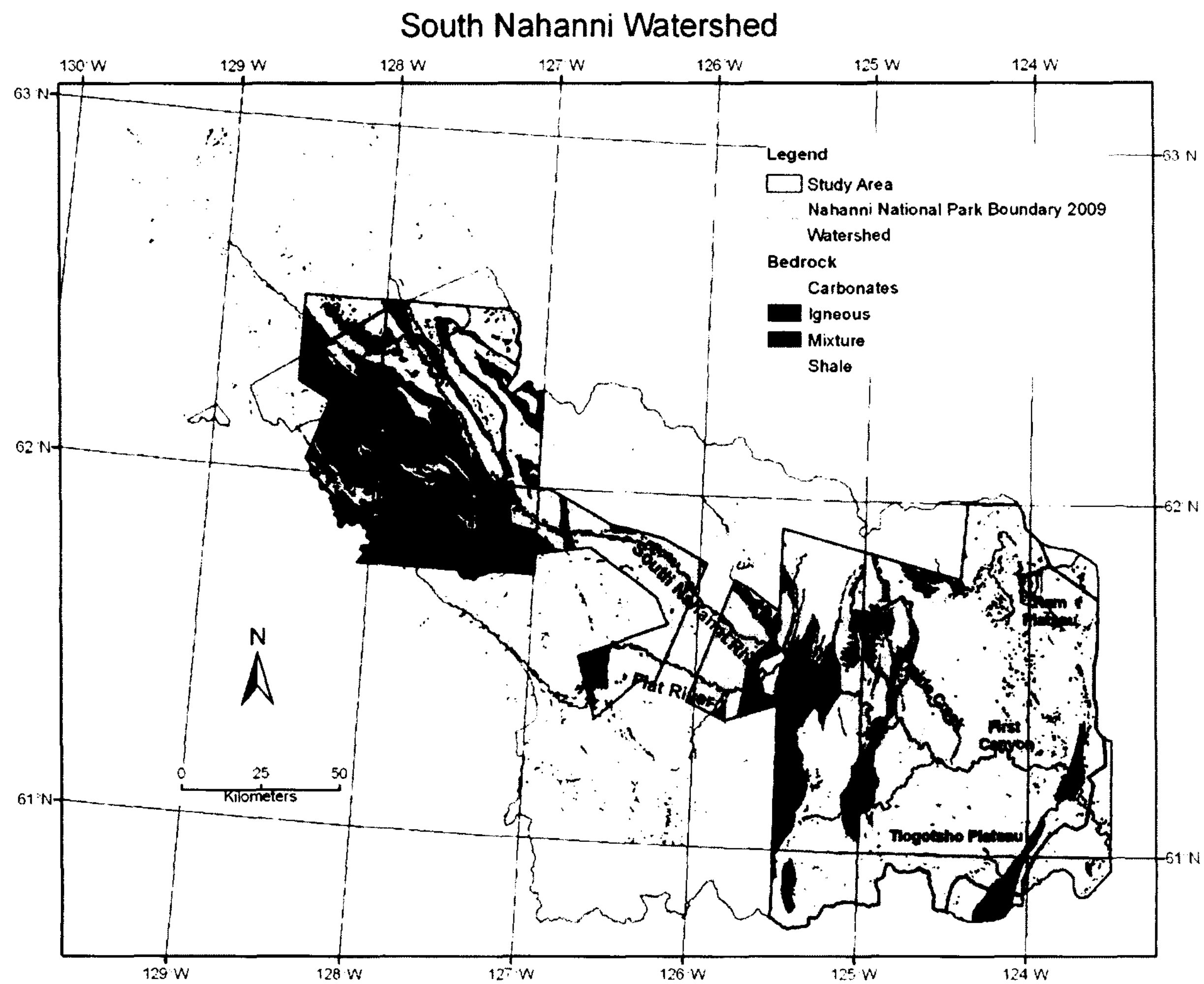

Figure 3.6: Aggregated bedrock classes for the study area.

Bedding-Slope Structure Setting

I obtained information on the dip and dip direction of sedimentary rocks from the 1:250,000-scale geological maps. I digitized bedding attitude as points and then drew large polygons around the points, based on topography and geology and assuming uniform attitudes around the points. Because these data are sparse - one data point per 70 square kilometres on average, they only crudely represent the regional structure. I then combined the bedding attitude and slope data to generate bedding-slope structure classes using the sedimentary rock slope classification of Cruden and Hu (1996) and Cruden (2000, 2003).

Cruden (2000) classifies sedimentary hillslopes (Figure 3.7) on the basis of the relation between dip direction and slope aspect: anaclinal slopes (beds dipping into slopes), cataclinal slopes (beds dipping out of slopes), and orthoclinal slopes (bedding perpendicular to slopes). Anaclinal and cataclinal slopes may be further subdivided based on the relation between slope angle and dip angle. Using the method of Meentemeyer and Moody (2000), I created eight structural classes: cataclinal-underdip slopes, cataclinal overdip slopes, cataclinal dip slopes, anaclinal subdued escarpments, anaclinal normal escarpments, anaclinal steepened escarpments, orthoclinal slopes, and an "other" category including horizontal strata, complex structure, and non-sedimentary bedrock (Figure 3.8; Clerici et al. 2006).

The areal distribution of structure categories in the study area is: 28% orthoclinal slopes, 16% cataclinal overdip slopes, 13% anaclinal steepened slopes, 11% cataclinal underdip slopes, 9% anaclinal subdued escarpments, 9% cataclinal dip slopes, 8% anaclinal normal escarpments, and 6% horizontal, complex or non-sedimentary lithologies.

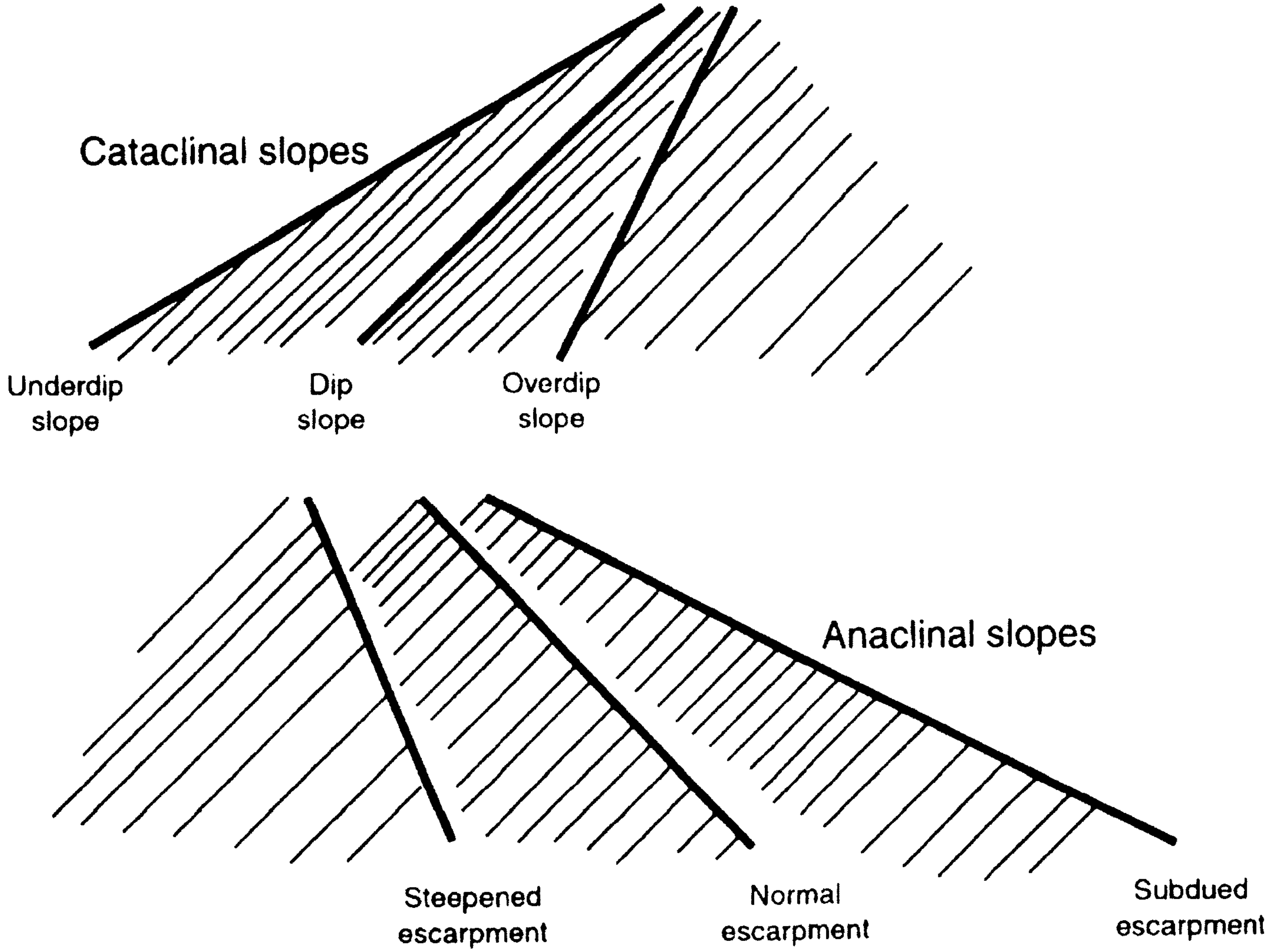

Figure 3.7: Slope classification. Bedding that is dipping out of the slope is classified as cataclinal, whereas bedding dipping into the slope is anaclinal (Cruden, 2000, 2003).

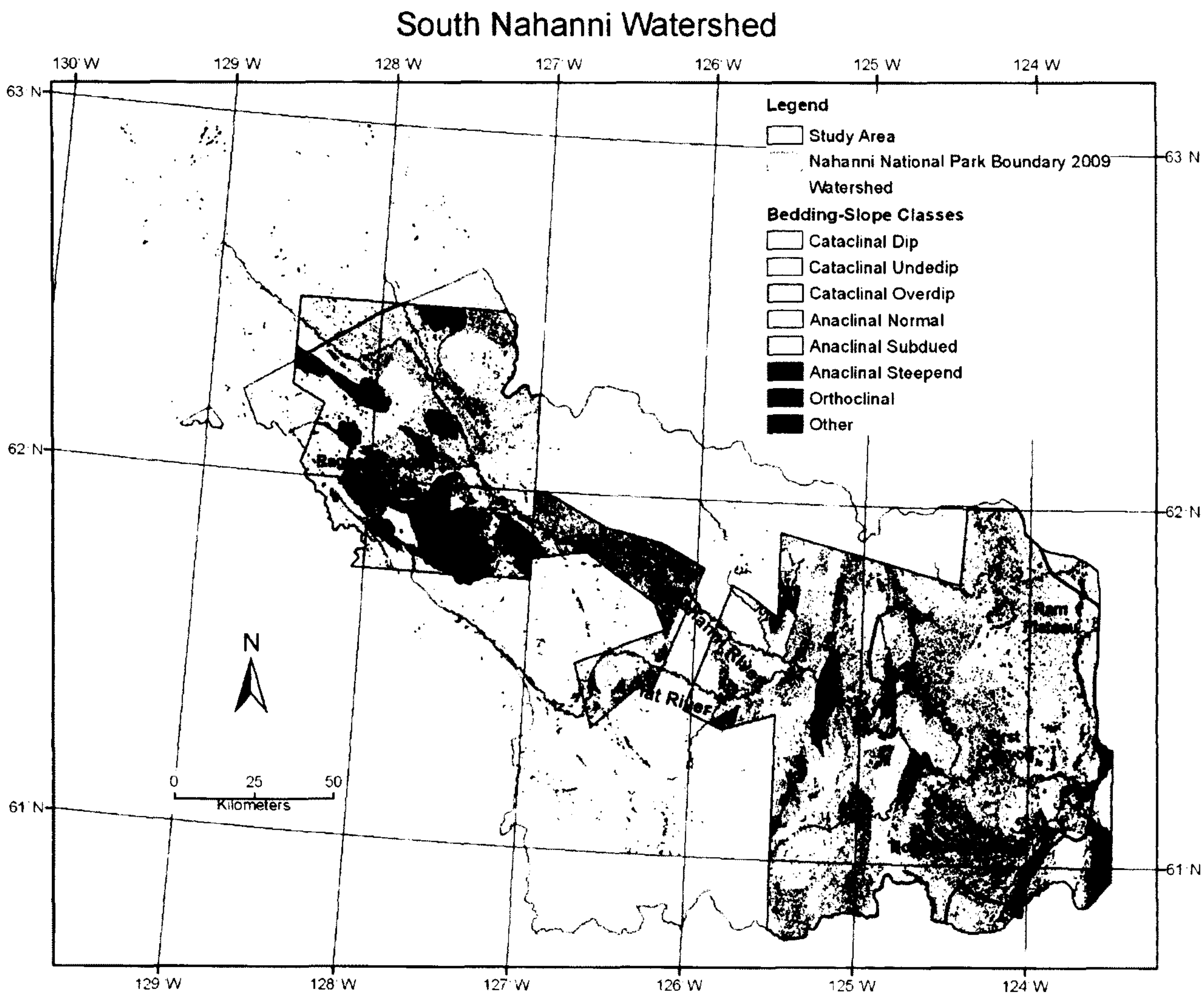

Figure 3.8: Spatial distribution of bedding-slope structure classes.

Land Cover

Stow and Wilson (2006) produced a 150-m-resolution land cover map by amalgamating Canada Centre for Remote Sensing (CCRS) land cover classes with Parks Canada Vegetation and Biophysical Inventory digital mapsproduced in 1979 (Gimbarzevsky et al. 1979). The digital map was than resampled to 70-m pixel resolution. Limitations of the data include no ground-truthing, possible change in land cover since the inventory was completed 30 years ago, presence of cloud cover and shadows, and generalization of land cover classes. The land cover map comprises 14 categories: shadow or closed spruce forest, closed deciduous forest, montane spruce forest – lichen woodland, pine - aspen woodland, montane – subalpine open woodland, montane – subalpine savannah and lichen, subalpine lichen tundra, subalpine low vegetation tundra, rock, recent burns, water, snow and ice, and wetland. Vegetated slopes with strong and big root systems improve slope stability by increasing cohesion (Zhou et al. 2002). To discriminate slopes with strong and weak root systems, I condensed vegetation classes into two categories: forested (combination of woodland and forested categories) and nonforested (tundra, savannahs, burned areas, rock, water, snow, ice and wetlands) (Figure 3.9).

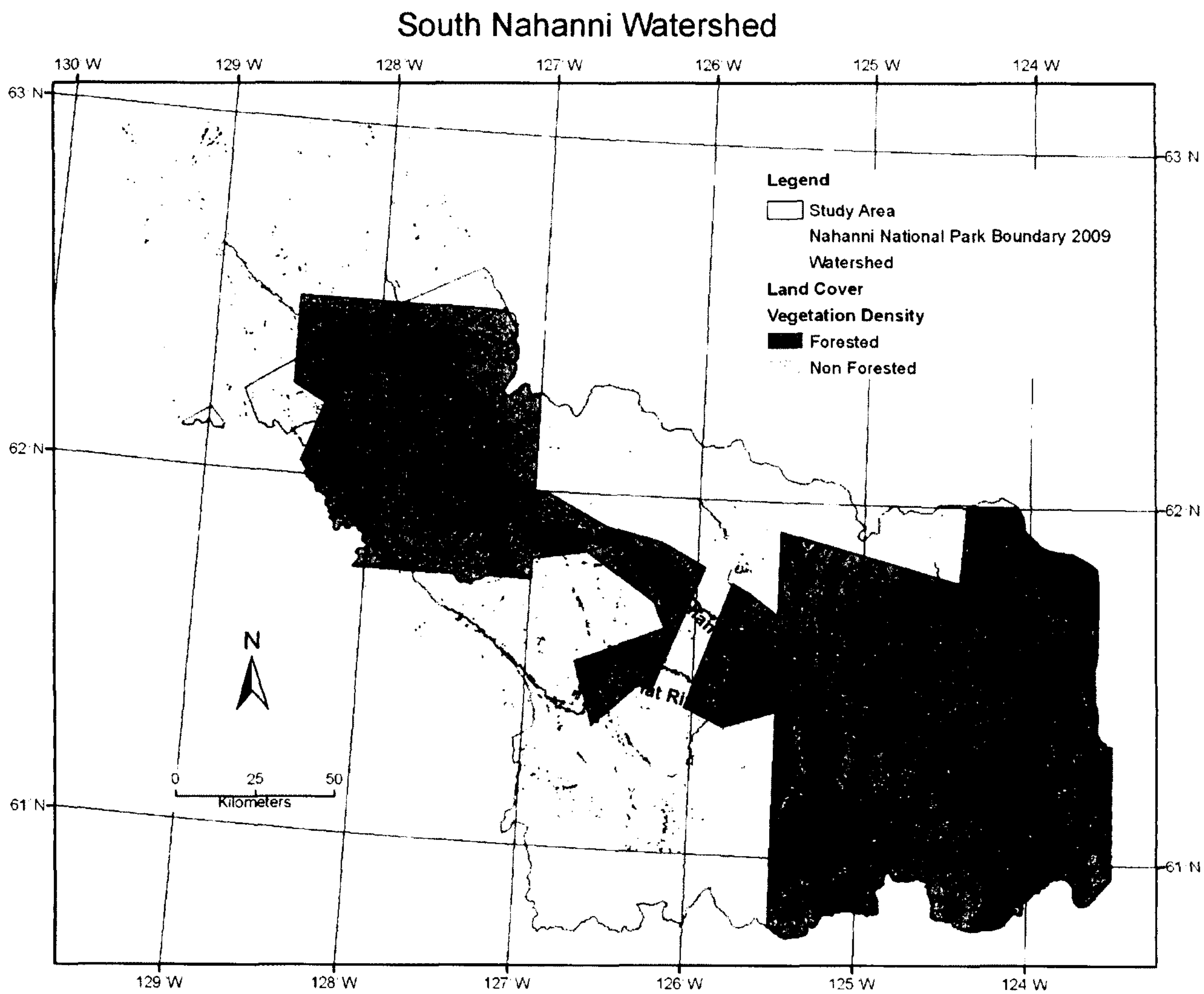

Figure 3.9: Spatial distribution of forested and non-forested areas in the study area.

Response Parameters

Landslides Inventory

Landslides included in this study are described in Chapter 2. The inventory identified slope failures as points and polygons. Points represent areas of small landslide headscarps, whereas polygons identify large landslide areas and include both initiation and accumulation zones. The types of landslides contained in the inventory include flows, topples, falls, slides and complex slides (see Appendix A-B for descriptions of terms and landslide type and location map and inventory). I developed predictive models for each major landslide type to facilitate understanding of the relations between controlling factors and the type of movement (Yesilnacar and Topal 2005; Clerici et al. 2006; Komac 2006).

I had to modify the data to conduct a susceptibility analysis. To properly capture pre-failure conditions around the initiation zones, I used a 50-m buffer area surrounding landslide headscarps (Chung and Fabbri 1999; Chung et al. 2002; Donati and Turrini 2002; Fernandez et al. 2003; Remondo et al. 2003; Süzen and Doyuran 2004; Ayalew and Yamagishi 2005; Yesilnacar and Topal 2005; Clerici et al. 2006; van den Eeckhaut et al. 2006). To isolate headscarp regions, I converted each landslide polygon into a line feature and removed any line segments from the original landslide polygon located below the crown and flanks of the landslide. I then created the 50-m buffer to surround both line and point features. I chose a 50-m buffer because it most consistently captured the desired spatial area when the data were converted from vector to raster. Depending on the position of a headscarp, polygons of the same size do not always comprise the same number of pixels when converted to a raster grid. A 50-m buffer provided the most consistency with headscarps of the same area compared to a 30-m buffer.

The next modification involved aggregating landslide types into four categories: debris flow, earth flow, rock/debris slide, and earth slide. Because I only included areas within the initiation zone and did not account for secondary modes of movements, only the initial failure type of complex slides is considered. For example, I reclassified rock slide-earth flows as rock slides, and earth slides-earth flows as earth slides. Modifications to debris flow and rock slide groupings are described in Chapter 2. In total, the analysis included 4477 landslides of which 4219, 104, 119, and 35 are, respectively, debris flows, earth slides, rock/debris slides, and earth flows.

Non-Landslide Inventory

I created an inventory of non-landslide cases using point data with a spacing of 30 m, consistent with the nominal resolution of the topographic data. Points were generated at the centre of each 30-m grid cell in the DEM. I thus assumed that information derived from vector or raster data and transferred to each point is representative of the surrounding 30 m. I then eliminated any points that fell in landslide areas to ensure that the dataset included only non-landslide points.

Statistical Analyses

Sampling

Small sample bias limits most studies of landslide susceptibility. In an attempt to account for this bias, previous researchers have increased the number of "landslide events" by sampling multiple cells (seed cells) from a landslide headscarp and treating eachcell as an independent sample. Although collecting multiple samples from an area increases the precision of estimated landslide properties, it does not increase the number of independent samples. Treating multiple samples from a single landslide unit as individual cases gives rise to pseudoreplication errors (Hurlbert 1984). Studies containing pseudoreplication are not necessarily flawed, but a re-analysis of the data may be needed or it may become apparent that the sample size is too small for the analysis and an alternative analytical procedure may be required (Lazic 2010). Van den Eeckhaut et al. (2006) comment on population size limitations and the assumption underpinning logistic regression that data are statistically independent. They propose an alternative approach, rare event logistic regression, which retains the appropriate independent landslide events and accounts for the small sample limitation through several correction algorithms. Each landslide is represented by one cell, located in the center of the headscarp. I used a modified "seed cell" approach (see below) that eliminates pseudoreplication errors. I also used standard logistic regression analysis because it is more widely used than rare event logistic regression and has yielded successful results (Guzzetti et al. 1999; Dai et al. 2001; Süzen and Doyuran, 2004; Ayalew and Yamagishi 2005; Ayalew et al. 2005; Yesilnacar and Topal 2005; Clerici et al. 2006; Chen and Wang 2007; Wang et al. 2007; Chung and Fabbri 2008; Melchiorre et al. 2008; Nefeslioglu et al. 2008). The modified seed cell approach is easy to understand, meets statistical assumptions, and maintains familiar logistic regression calculation used in previous studies.

Modified "Seed Cell" Approach

I characterized all pre-failure conditions for each headscarp and non-landslide areas contained in the inventories with a modified "seed cell" approach. Collection of multiple samples within an experimental unit improves precision of the analyzed properties (Hurlbert 1984). Therefore, landslide-related parameters for each landslide type are best characterized by considering the entire headscarp region that is the area within the buffer zone. The simplest and most reliable approach is to express the characteristic of each parameter within a headscarp as a single value, the mean value of the seed cells sampled (Hurlbert, 1984). I generated mean values for slope gradient, elevation, plan and profile curvature for these regions, and I also calculated the mean aspect of each headscarp (see Appendix C-I: Data Used, Independent variables, ASPECT for further details). In the case of nominal data, for which it is not possible to obtain a mean value, I assumed that the category that occupied the largest area within a polygon represented the pre-failure state of the initiation zone. However, because small-scale data were used in this study, the relation between vector contacts and landslides should be addressed in future, more detailed studies.

To characterize non-landslide areas, a 30 x 30 m area "seed cell" was used to identify a non-landslide case. As any area outside of landslide zones is assumed to be stable, a 30 m cell for each non-landslide area provides adequate information to characterizea landslide-free area.

Logistic Regression

I used R 2.9.2 statistical software (R Development Core Team 2008) to conduct logistic regression analyses. R software uses the general linear model (glm) to estimate the models coefficients and their significance level (Appendix C-II: Scripts). Model coefficients are values that maximize the probability of explaining the presence or absence of a landslide. I considered a coefficient to be significant if its significance level was $p \leq 0.05$ (Hosmer and Lemeshow 2000; van den Eeckhaut et al. 2006).

To properly interpret the meaning of the model coefficients, I calculated the odds ratio, which is the ratio of the likelihood that a landslide will occur to the likelihood of it being absent when all other variables included in the model are fixed. To obtain the odds ratio, the coefficient is expressed as a power of the natural log ($e^{\beta i}$). If a coefficient is positive, its transformed log will be greater than one and a landslide is more likely to occur. As a coefficient increases, the probability increases. Conversely, if a coefficient is negative, the log value will be less than 1 and a landslide is less likely to occur. A coefficient of zero will not affect the odds either way (Hosmer and Lemeshow 2000; Ayalew and Yamagishi 2005).

Data Matrix Production

Logistic regression requires data matrices for each landslide class. Each row in the matrix is an individual case, either a landslides or non-landslide area. Columns are each independent and dependent, continuous or nominal variables. Susceptibility models require independent data to validate their effectiveness (van den Eeckhaut et al. 2006). I created test and validation matrices for each landslide type. The matrices for each landslide type include equal numbers landslide and non-landslide cases (see Appendix C; Dai and Lee 2002; Ayalew and Yamagashi 2005; Wang et al. 2007; Nefeslioglu et al. 2008). To build the matrices, I subdivided landslide inventories in two halves by random sampling (Beyer 2008). I then randomly sampled an equal number of non-landslides and incorporated them into the data matrix. For example, a total of 4217 debris flows were subdivided into a test set, with 2109 debris flow cases and 2109 non-debris flow cases; the validation set also comprised 2108 debris flow and 2108 non-debris flow sites.

There should be a minimum of 3-5 events per variable in each dataset to generate a valid susceptibility model; 10 or more events are ideal for logistic regression analysis (Hosmer and Lemeshow 2000). The earth flow datasets had 36 events in total and thus was inadequate for model building using multivariate logistic regression analysis. Therefore, earth flows were excluded from further analysis.

Landslide Frequency Distribution

Prior to conducting logistic regression analysis, I analyzed the frequency distribution of each landslide type to causative parameter (Table 3.1). Multivariate logistic regression identified variable interactions and their statistical significance, but it does not recognize the distribution of landslides within each parameter. I used the distribution table to better understand the importance of each factor and identify if any categories contain zeros to help in the interpretation of the logistic regression results.

Model Building

Prior to conducting multivariate logistic regression analysis, I had to determine explanatory variables. I used Hosmer and Lemeshow's (2000) procedure as a guide in selecting variables for this study. First, I conducted univariate logistic regression on each factor toquantify that factor's effect on landslides without the influenceof other variables. After completing the univariate analyses, I selected variables that had significant levels of $p \leq 0.25$ (Hosmer and Lemeshow 2000), as well as variables with a significance level $p > 0.25$ but have been identified by experts to be geologically important in causing landslides. Hosmer and Lemeshow (2000) argue that a more traditional significance level of $p \leq 0.05$, fails to identify variables known to be important and that a value higher than 0.25 is likely to include variables with little importance. I eliminated from further analysis all remaining factors that did not meet these criteria.

I then conducted multivariate analyses on the variables that I identified through the univariate logistic regression to determine the mix of variables that make up the final models. Variables selected for the final model had to have the following characteristics: they are considered geologically relevant based on previous expert knowledge of the specific landslide type;and they had a p-value ≤ 0.05 in the preliminary logistic regression analysis or a value close to 0.05 in one of the datasets but a value of ≤ 0.05 in the other set in the preliminary logistic regression analysis. I selected and used all variables meeting these criteria for the final probability expression. I then repeated the procedure for each data matrix created.

I constructed final susceptibility models for each data matrix using the best collection of explanatory variables. Susceptibility cannot be directly defined through logistic regression analyses, but it can be inferred using probability values (Ayalew and Yamagishi 2005). For example, if an area contains a probability value of 0.25 then the susceptibility of the area would be considered low, with a 0.25 probability of a landslide to occur. To calculate probability, I converted all data layers into 30m cell size rasters and reclassified cells to express the estimated coefficient values derived from the final multivariate analyses. I then used ArcGIS 9.2, Raster Calculator to compute logit (equation 2) and probability (equation 1) rasters for each landslide type using the variables' reclassified rasters.

Cross Validation

I used a cross-validation technique to determine the quality and success of the logistic regression models (Wang et al. 2007; Chung and Fabbri 2008; Melchiorre et al. 2008). Landslide sites from the validation dataset are superimposed on the corresponding landslide susceptibility map derived from the data in the test set. I then repeated validation procedures using the test data matrices. I selected the most successful model to represent each landslide type.

I classified susceptibility zones into three categories: low (<0.40), medium (0.40-0.60), and high (>0.60), then used Zonal Statistics in ArcGIS 9.2 to evaluate model success.

Values less than or equal to 0.40 represent areas least susceptible to landslides and most likely to comprise non-landslide areas; values greater than 0.40 and less than or equal to 0.60 indicate areas that could contain landslides but may have none; and values greater than 0.60 represent areas most likely to have landslides. These categories are the same as those used by Guzzetti et al. (1999), except that he had a fourth category (very low susceptibility).

A measure of the model's success is the percentage of landslides that have an average probability value of 0.40 or greater (moderate to high susceptibility). I then evaluated the model's ability to correctly classifying non-landslide areas. The success in identifying non-landslide areas was determined by superimposing validation non-landslide points on susceptibility maps derived from test set models. The total percent of non-landslide points that contain a probability value lower than 0.60 (moderate to low landslide susceptibility) provides an indication of the success of the model in properly predicting relatively stable areas.

Results

Landslide-Causing Factors

Landslides in the study area are not randomly distributed (Table 3.1). They occur on convex slopes with plan curvatures, in areas of moderate relief, and at elevations between 500 to 1000 m asl. However, the maximum elevation is >2500 m asl for debris flows (Table 3.1). Slope aspect directions differamong landslide types. Dominant aspect directions include southeast and southwest for debris flows; northeast slopes for earth flows; north slopesfor earth slides, and southwest and east slopes for rock/debris slides (Table 3.1).

All landslide types occur in forested areas. About 63% of all debris flows, 94% of all earth flows, 95% of all earth slides, and 97% of all rock/debris slides are within forested terrain. However 37% of debris flows occur in nonforested terrain. The association of landslides with forested regions may reflect the prevalence of forest at the lower elevations where landslides are predominant (Table 3.1).

Although landslides typically occur on moderately steep slopes (Wang et al. 2007), slope relief (mean slope) differed between landslides in earth material and those in rock or debris. Earth slides and flows are most common on moderate to steep slopes of 15-35°, whereas rock slides and debris flows are most common on slopes $\geq 26°$. Slopesof 0° to 3°have the lowest frequency of landslides, (Table 3.1; Howes and Kenk 1996).

Most landslides in the South Nahanni watershed occur are in carbonate or shale lithologies (Table 3.1). Debris flows and rock slides predominately occur in carbonate, shale, and mixed lithologies, whereas landslides composed of earth most commonly occur in areas comprising of weak shale (Table 3.1). In terms of the number of events per square kilometres, debris flow are most common in igneous lithology, earth flows are most abundant in shale and earth slides and rock/debris slides predominately occur in areas comprising shale and carbonate lithologies (Table 3.1).

Bedrock structure was found to be not statistically significant for predicting landslides. Previous work, however, has indicated the importance that structure plays in mass movement (Cruden and Hu 1996; Cruden 2000). The lack of significance of structure in this study may be the result of sparse bedding attitude data (1 point per 70 km^2) and over-simplification of rock slope classification polygons. Because of the non-significant results, the structure layer was removed from further analyses.

Table 3.1: Frequency distribution of landslide type versus (vs) explanatory variable.

Variable				Debris Flow		Earth Flow		Earth Slide		Rock Slide	
Variable Type	Category	Area (km²)	% area of total study area	Frequency	Df / 1000 km²	Frequency	# Ef / 1000 km²	Frequency	# Es / 1000 km²	Frequency	# Rs / 1000 km²
Elevation	<500	1920	10	162	84	3	2	18	9	10	5
	500-1000	7410	38	1452	196	20	3	73	10	75	10
	1000-1500	6613	33	1262	191	11	2	12	2	28	4
	1500-2000	2889	15	1096	379	0	–	1	0	3	1
	2000-2500	917	5	246	268	0	–	0	–	1	1
	>2500	7	0	1	137	0	–	0	–	0	–
Slope Gradient	0–3	2005	10	33	16	0	–	1	1	–	–
	3–15	7047	36	775	110	19	3	69	10	25	4
	15–26	4646	24	996	214	14	3	29	6	56	12
	26–35	4005	20	1448	362	1	–	4	1	22	5
	>35	2052	10	967	471	0	–	1	0	11	5
Plan Curvature	<-0.75	215	1	28	130	0	–	0	–	0	–
	-0.75 – (-0.50)	412	2	126	306	0	–	0	–	2	5
	-0.50 – (-0.25)	1291	7	401	311	10	8	0	–	4	3
	-0.25 – 0	8487	43	1430	168	24	3	29	3	37	4
	0-0.25	7157	36	1567	219	0	–	75	10	66	9
	0.25-0.50	1446	7	450	311	0	–	0	–	5	3
	0.50-0.75	452	2	119	263	0	–	0	–	3	7
	>0.75	295	1	62	210	0	–	0	–	0	–
Profile Curvature	<-0.75	251	1	56	223	0	–	0	–	6	24
	-0.75 – (-0.50)	371	2	99	267	0	–	0	–	3	8
	-0.50 – (-0.25)	1372	7	388	283	1	1	1	1	7	5
	-0.25 – 0	7917	40	1671	211	26	3	70	9	61	8
	0-0.25	7369	37	1717	233	6	1	33	4	34	5
	0.25-0.50	1784	9	243	136	1	1	0	–	3	2
	0.50-0.75	476	2	32	67	0	–	0	–	2	4
	>0.75	216	1	13	60	0	–	0	–	1	5
Aspect		423	2	0	–	0	–	0	–	0	–
	N	2116	11	324	153	7	3	17	8	8	4
	NE	2695	14	557	207	2	1	4	1	8	3
	E	2898	15	581	200	4	1	12	4	22	8
	SE	2381	12	653	274	6	3	14	6	13	5
	S	2085	11	387	186	3	1	13	6	13	6
	SW	2372	12	686	289	1	0	7	3	21	9
	W	2492	13	536	215	7	3	14	6	17	7
	NW	2295	12	495	216	4	2	23	10	15	7
Landcover	Forested	13760	70	2663	194	32	2	99	7	114	8
	Nonforested	5996	30	1556	259	2	0	5	1	3	1
Bedrock Lithologies	Carbonates	8941	45	1868	209	7	1	12	1	74	8
	Mixture	5330	27	1370	257	2	0	2	0	9	2
	Igneous	826	4	326	395	0	–	1	1	0	–
	Shale	4660	24	655	141	25	5	89	19	34	7

Logistic Regression Models

The logistic regression models reveal the importance of several environmental factors on landslides in the South Nahanni watershed (Table 3.2 and Table 3.3). Results from univariate and multivariate tests for each landslide model can be found in Appendix C-III: Results.

Debris Flow

Debris flow models have the largest and most diverse set of controlling factors. Slope gradient and bedrock are the strongest factors. Odds ratios indicate that the most susceptible areas for debris flows are steep southeast-facing slopes in shale and mixed lithologies. All parameters of the debris flow models are individually significant. However, in the multivariate analysis, land cover was only significant in the debris flow validation model, not in the model derived from the debris flow test data set. I preserved land cover in the final models (Table 3.2) because forest cover plays an important role in the stability of steep slopes that are susceptible to debris flows (Sidle 2005).

The validation models for debris flow classified 55% (57%), 22% (23%), and 22% (20%) of the total area as, respectively, low, moderate, and high susceptibility. Regions of high debris-flow susceptibility are at high elevation located near steep cliff faces (Table 3.3, Figures 3.10 and 3.11).

Cross-validation analysis confirmed the success of both debris flow models. The debris flow test model is 75% accurate in predicting debris flow initiation zones in high to moderate susceptibility regions and an additional 10% of debris flows initiation zones were within 50 m of a high to moderate zone. According to Guzzetti et al. (1999) 73% is considered above the threshold for a successful result. The test model's accuracy is 77% for predicting regions of low to moderate debris flow susceptibility. The debris flow validation model produced similar results to the test model; with 75% success in predicting debris flow susceptible areas and 79% success in predicting non-landslide areas in stable terrain (Table 3.3).

Table 3.2: Multivariate logistic regression results for debris flow test and validation sets.

		Debris Flow Test Set					Debris Flow Validation Set				
Variables		**Estimate**	**Odds Ratio**	**Std. Error**	**Pr(>|z value|)**		**Estimate**	**Odds Ratio**	**Std. Error**	**Pr(>|z value|)**	
(Intercept)		-2.72	0.07	0.18	<2.00E-16	***	-2.34	0.10	0.18	<2.00E-16	***
BEDROCK	Mixed Lithologies	0.44	1.55	0.09	4.46E-07	***	0.47	1.61	0.08	1.83E-08	***
	Igneous	0.24	1.27	0.17	1.42E-01		0.10	1.10	0.17	5.80E-01	
	Shale	0.92	2.51	0.11	2.43E-16	***	0.92	2.51	0.11	<2.00E-16	***
LAND COVER	Nonforested	-0.11	0.90	0.10	2.76E-01		-0.26	0.77	0.10	5.94E-03	**
ASPECT	NE	0.53	1.70	0.15	3.89E-04	***	0.34	1.40	0.15	2.36E-02	*
	E	0.75	2.12	0.15	1.00E-06	***	0.36	1.43	0.15	1.77E-02	*
	SE	0.77	2.16	0.16	8.83E-07	***	0.50	1.64	0.15	1.06E-03	**
	S	0.49	1.63	0.16	2.74E-03	**	0.06	1.06	0.16	7.03E-01	
	SW	0.69	1.99	0.15	5.03E-06	***	0.38	1.47	0.15	1.00E-02	*
	W	0.57	1.77	0.15	2.19E-04	***	0.09	1.09	0.15	5.62E-01	
	NW	0.43	1.54	0.15	5.50E-03	**	0.22	1.25	0.15	1.54E-01	
ELEV		0.00	1.00	0.00	2.33E-07	***	0.00	1.00	0.00	1.78E-06	***
SLOPE		0.10	1.11	0.00	<2.00E-16	***	0.10	1.11	0.00	<2.00E-16	***
CURVPL		-0.55	0.58	0.14	9.68E-05	***	-0.37	0.69	0.13	6.75E-03	**
CURVPF		-1.01	0.36	0.16	3.56E-10	***	-1.01	0.37	0.16	4.52E-10	***

Note:

Significance codes: 0 '***' 0.001 '**' 0.01 '*' 0.05 '.' 0.1 ' ' 1. + identifies variables comprising close to zero events making exceptionally large coefficients and standard error values. *Description of table headings:* ***Variables***: Causative factors selected to identify their association with rock/debris slides (ELEV = elevation, CURVPF = profile curvature, and CURVPL = plan curvature). ***Estimate***: Maximum likelihood estimate. These values identify the "most likely" value for the variable given the data that was observed. ***Odds Ratio***: The ratio of the probability of an event to no event occurring (considers all other variables to be zero). ***Std. Error***: Is the standard deviation of the means of samples taken from a parent population (Porkess 2005). ***Pr(>|z value|)***: Represents the significance level. The value identifies how significant a variable is in contributing or not contributing to rock/debris slides. *Referenced categories for nominal variables:* **Bedrock** categories are in relation to carbonate bedrock, **Landcover** categories are in relation to forested areas, and **Aspect** categories are in relation to North aspect.

Table 3.3: Cross-validation results illustrating model accuracy (in percent) for each landslide type and a list of factors used to generate the models.

LANDSLIDE TYPE	SUSCEPTIBILITY ZONE CATEGORIES (based on probability values)	PERCENT OF WATERSHED COVERED BY ZONE (%)	LANDSLIDES IN HIGH/MEDIUM ZONES SUCCESS (%)	LANDSLIDES WITHIN 50 m of HIGH/MEDIUM ZONES (%)	NON-LANDSLIDES CORRECTLY ID in LOW/MEDIUM ZONES (%)	MODEL VARIABLES
Debris Flow Test	Low: 0-0.40	55	-	-	54	bedrock, land cover, aspect, elevation, slope, plan curvature, profile curvature
	Medium: 0.40-0.60	22	32	21	23	
	High: ≥0.60	22	43	64	-	
	Total	**100**	**75**	**85**	**77**	
Debris Flow Validation	Low: 0-0.40	57	-	-	57	bedrock, land cover, aspect, elevation, slope, plan curvature, profile curvature
	Medium: 0.40-0.60	23	32	22	22	
	High: ≥0.60	20	43	63	-	
	Total	**100**	**75**	**85**	**79**	
Rock/Debris Slide Test	Low: 0-0.40	56	-	-	61	bedrock, land cover, slope
	Medium: 0.40-0.60	21	31	31	0	
	High: ≥0.60	23	54	54	-	
	Total	**100**	**85**	**85**	**61**	
Rock/Debris Slide Validation	Low: 0-0.40	49	-	-	57	bedrock, land cover, slope
	Medium: 0.40-0.60	25	15	7	25	
	High: ≥0.60	26	62	85	-	
	Total	**100**	**77**	**92**	**82**	

Earth Slide

Limited data availability, such as a large-scale surficial geology data, hindered statistical modeling of the earth slides. As a result, I removed earth slides from further analysis.

Rock/Debris Slide

Rock/debris slide models identified bedrock and land cover to be the most significant explanatory variables for these types of failures in the South Nahanni watershed. Hillslope gradient was only significant in the test set model. I incorporated slope in both models because slope is known to play an important role in rock/debris slope failures (Ayalew and Yamagishi 2005; Ayalew et al. 2005; Clerici et al. 2006; van den Eeckhaut et al. 2006; Chen and Wang 2007; Wang et al. 2007).The odds ratios for the logistic regression models reveal that steep forested slopes in shale and carbonate lithologies are most closely associated with rock/debris slide events (Table 3.4).

Landslide susceptibility maps reveal that 56% of the terrain in the study area has low rock/debris slide susceptibility; 44% of the terrain is in moderate and high zones (Table 3.3). The eastern portion of the study area is most susceptible to these types of failures (Figure 3.12 and 3.13). A likely reason for this association is the abundance of carbonate and shale bedrock in this part of the study area.

Both models were successful in predicting rock/debris slide areas, but the test set model only moderately successfully in predicting non-landslide areas. The test model had an accuracy of 85% predicting rock slides in high to moderate zone, but only 63% predicting areas of stable terrain, perhaps implying that the randomly sampled non-landslide points could be located where landslides have not yet occurred. This hypothesis could be tested by increasingthe sample size of rock/debris slides and stable terrain locations.

The validation model was 77% successful predicting landslide locations in high to moderate susceptibility zones and 82% successful predicting no landslides in low to moderate zones (Table 3.3).

Table 3.4: Final multivariate logistic regression results for rock/debris slide test and validation sets.

		Rock Slide Test Set					Rock Slide Validation Set				
Variables		Estimate	Odds Ratio	Std. Error	Pr(>|z|)		Estimate	Odds Ratio	Std. Error	Pr(>|z|)	
(Intercept)		-0.19	-	0.52	7.11E-01		-0.41	-	0.60	4.92E-01	
BEDROCK	Mixed Lithologies	-2.58	0.08	0.67	1.28E-04	***	-1.97	0.14	0.62	1.57E-03	**
	Igneous	-18.77	0.00	1626.62^{+}	9.91E-01		-13.82	0.00	1028.82	9.89E-01	
	Shale	-0.48	0.62	0.55	3.86E-01		0.37	1.45	0.54	4.92E-01	
LAND COVER	Nonforested	-3.18	0.04	0.77	3.82E-05	***	-3.04	0.05	0.88	5.35E-04	***
SLOPE		0.06	1.06	0.02	4.69E-03	**	0.06	1.06	0.02	2.39E-02	*

Notes: Significance codes: 0 '***' 0.001 '**' 0.01 '*' 0.05 '.' 0.1 ' ' 1. + Identifies variables containing close to zero events making exceptionally large negative maximum likelihood estimates and positive odds ratios. *Description of table headings:* ***Variables***: Causative factors selected to identify their association with rock/debris slides (ELEV = elevation, CURVPF = profile curvature, and CURVPL = plan curvature). ***Estimate***: Maximum likelihood estimate. These values identify the "most likely" value for the variable given the data that was observed. ***Odds Ratio***: The ratio of the probability of an event to no event occurring (considers all other variables to be zero). ***Std. Error***: Is the standard deviation of the means of samples taken from a parent population (Porkess 2005). ***Pr(>|z value|)***: Represents the significance level. The value identifies how significant a variable is in contributing or not contributing to rock/debris slides. *Referenced categories for nominal variables:* **Bedrock** categories are in relation to carbonate bedrock and **Landcover** categories are in relation to forested areas.

Susceptibility Map Accuracy

I used the final debris flow and rock/debris slide validation models to develop landslide susceptibility maps (Figures 3.11 and Figure 3.13). I selected these two models because they were most successful in predicting unstable and stable terrain. Although the models produce maps with a resolution of 30 m, the map scale accuracy depends on the smallest scale data incorporated in the models. Bedrock lithology at 1:1,000,000-scale were the smallest scale data incorporated into debris flow and rock/debris slide models. Therefore, debris flow and rock/debris slide susceptibility maps were resampled to 500 m pixel resolution to appropriately represent their map scale accuracy (Tobler 1988; Appendix C).

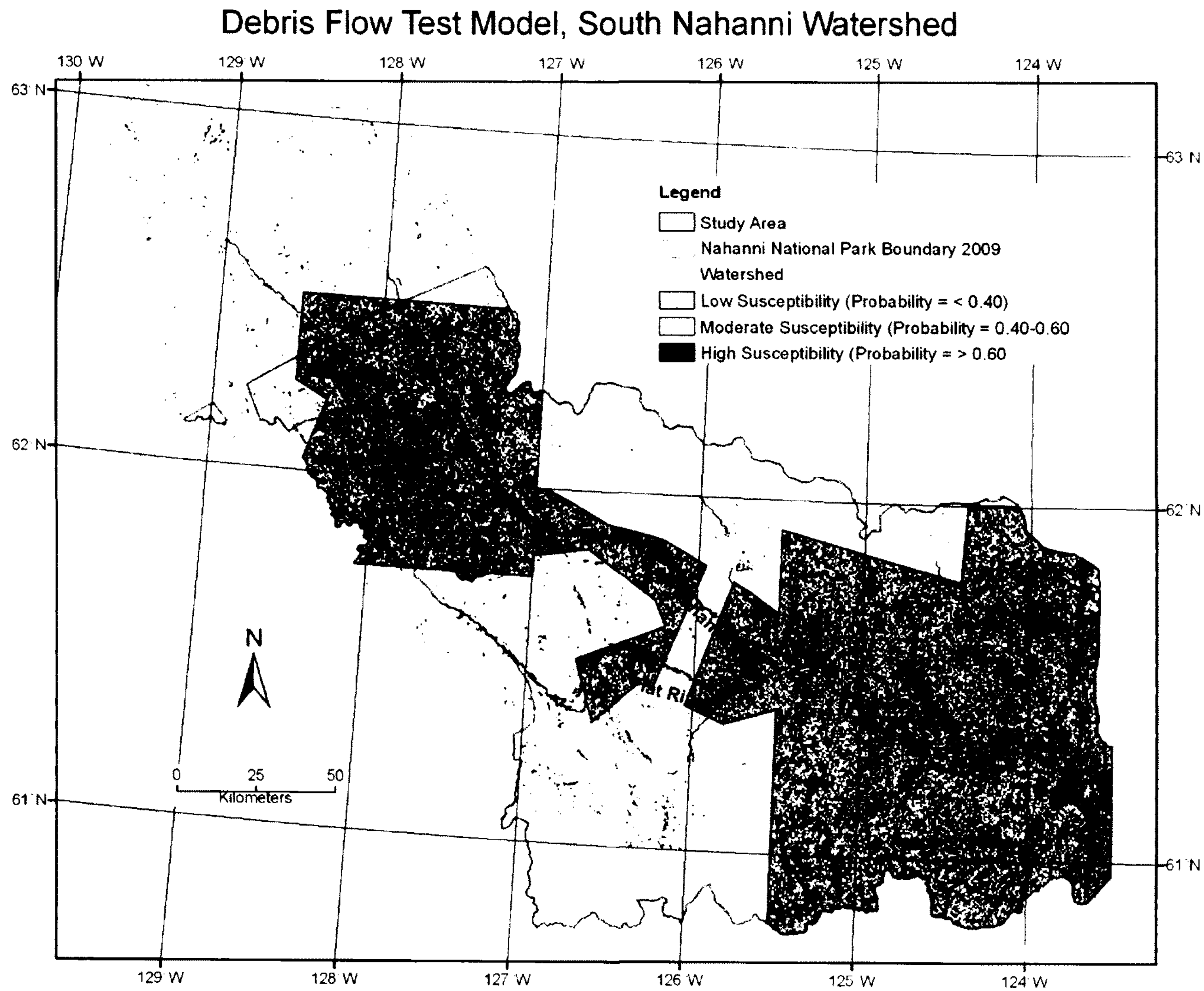

Figure 3.10: Debris flow test susceptibility map derived from bedrock, land cover, aspect, elevation, slope, and plan and profile curvature.

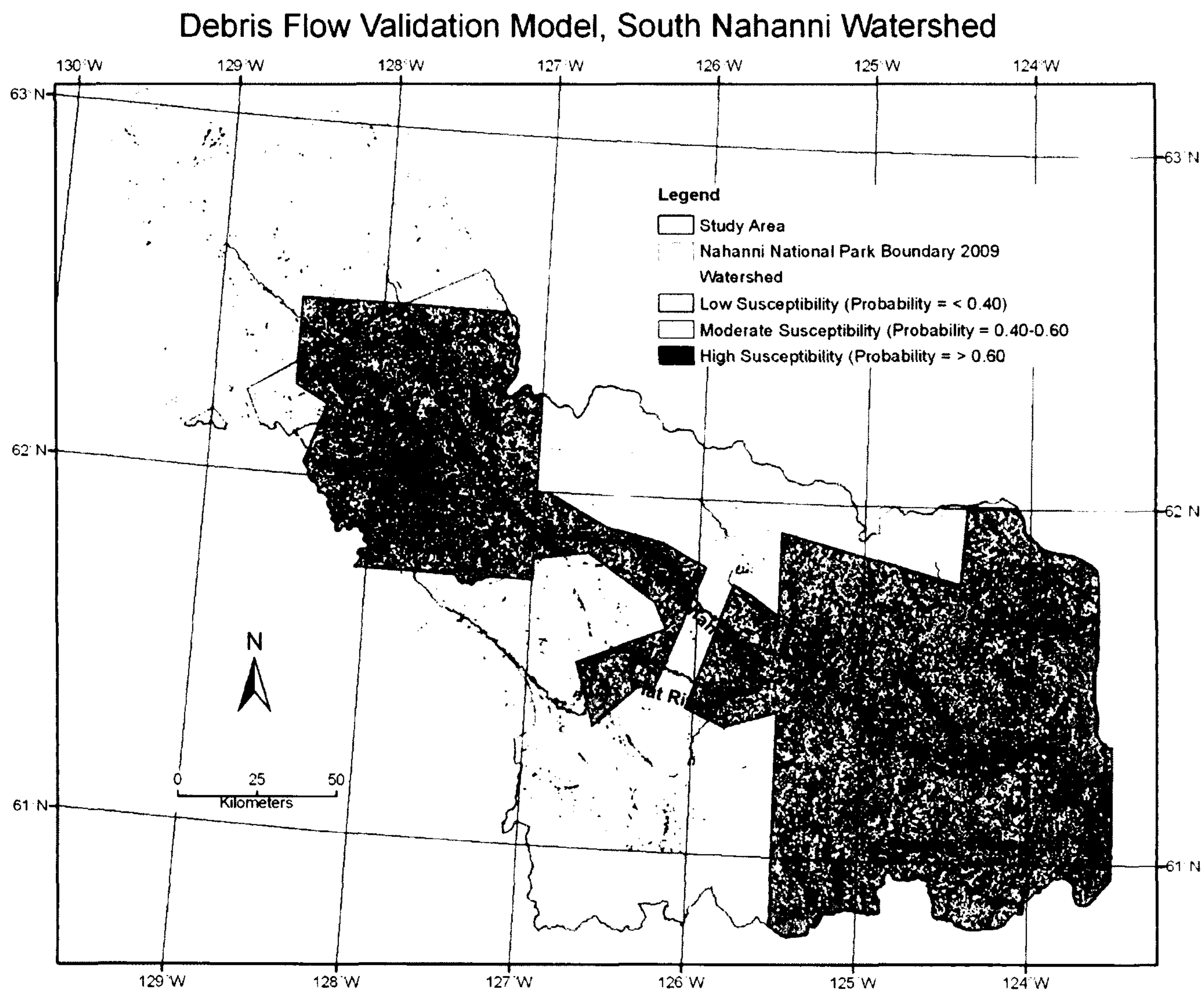

Figure 3.11: Debris flow validation susceptibility map derived from bedrock, land cover, aspect, slope, profile curvature.

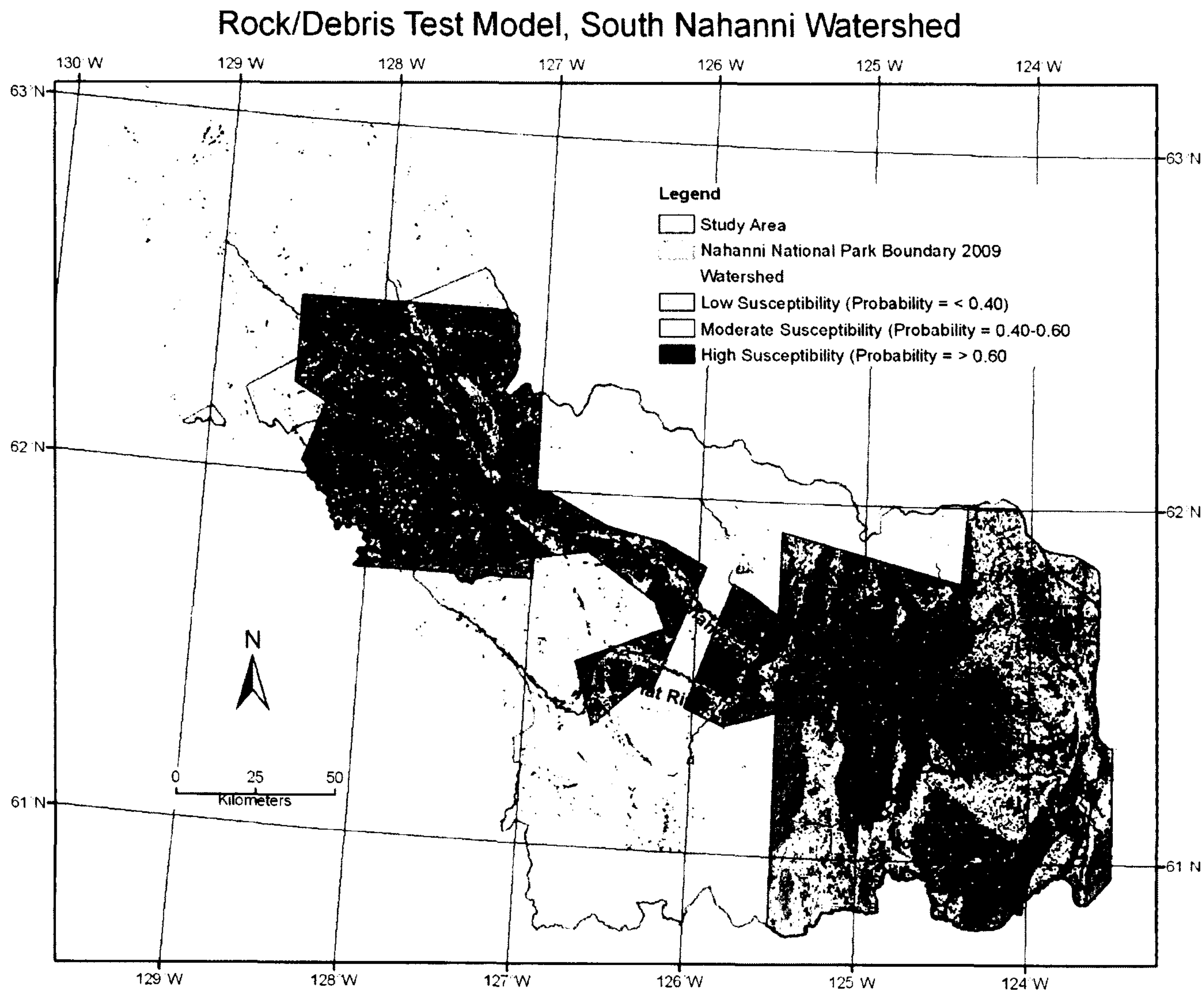

Figure 3.12: Rock/debris slide test susceptibility model bedrock, land cover, and slope.

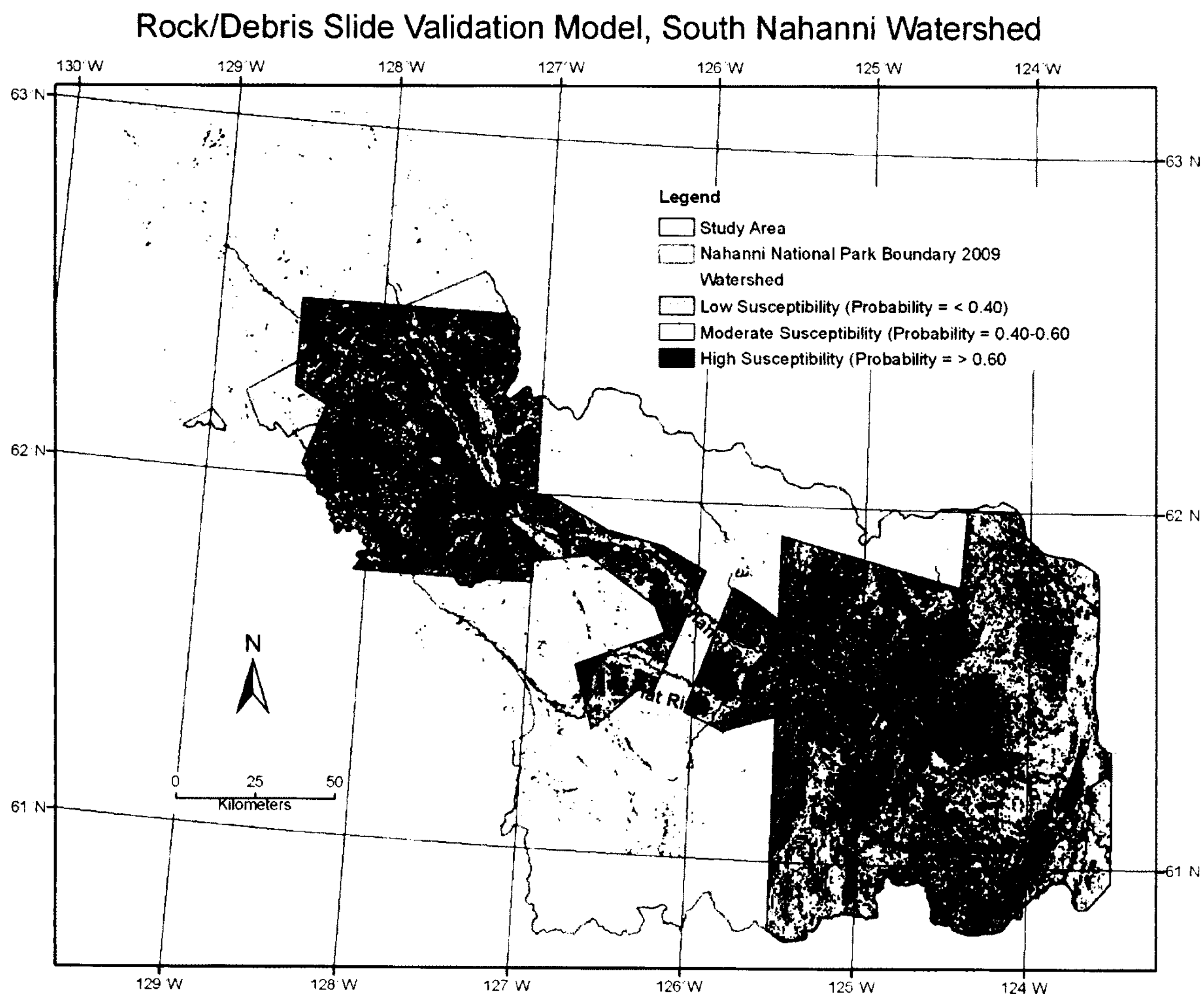

Figure 3.13: Rock/debris slide validation susceptibility model bedrock, land cover, and slope.

Discussion

The objective of this study was to produce and validate preliminary landslide susceptibility maps for the main types of slope failures in the South Nahanni watershed. I used the landslide inventory completed in Chapter 2, publicly available geospatial data obtained from government agencies, a GIS, and free statistical software to analyze factors affecting slope instability and to produce susceptibility maps.

Landslide-causing factors selected by the logistic regression analysis produced successful susceptibility models for the two dominant failure modes, debris flow and rock/debris slide. In both models, slope gradient is identified as the most significant factor affecting instability in the study area. Associations between landslides and causative factors identified from the analysis agree with results from other landslide studies in Northwest Territories (Eisbacher 1977; Jackson 1987; Aylsworth et al. 2000; Huntley et al. 2006).

Debris flows are the most abundant and distributed of the landslide types in the study area (Takahashi 1981). They favour steep, concave slopes in igneous, shale, or mixed lithologies. The results of this study are in accord with previous work on the controls of debris flow activity (Aylsworth et al. 2000; Lyle et al. 2004; Bertolo and Wieczorek 2005; Sidle 2005; Huntley et al. 2006; Marchi and Cavalli 2007; Wang et al. 2007). Studies conducted in the Mackenzie Valley, for example, concluded that debris flows favour soils underlain by shale bedrock (Aylsworth et al. 2000; Huntley et al. 2006).

Earth slides are less common than debris flows in the study area, but are larger failures. Earth slide predictive models could not be developed with sufficient predictive capacity, given the lack of large-scale terrain data required for the analysis. Many previous studies describe the importance of surficial geology, permafrost, bank erosion, and forest fires on controlling the distribution of earth slides (Code 1973; McRoberts and Morgenstern 1973; Ford 1976; Eisbacher 1977; Evans et al. 1987; Evans and Clague 1989; Dyke 1990; Clague 1992; Evans and Clague 1994; Aylsworth et al. 2000; Lyle et al. 2004; Couture and Riopel 2006; Huntley and Duk-Rodkin 2006; Huntley et al. 2006; Lipovsky and Huscroft 2007). Qualitative results ofthis study revealed that earth slides occur at low elevations in gentle to steeply sloping terrain underlain by shale and unconsolidated sediments.

Rock/debris slide test and validation models contain three controlling factors: bedrock, slope, and land cover. Bedding-slope structure is a significant contributor to rock mass instability in most sedimentary rock environments (Cruden and Hu 1996; Cruden 2000, 2003; Aylsworth et al. 2000; Huntley et al. 2006), but the data available in my study area were insufficient for this analysis. The large number of rock/debris slides in forested terrain was unexpected, as slope stability typically increases with the presence of vegetation due to the increased cohesion added by tree roots (Turner 1996). Several factors could explain the abundance of rock/debris slide on forested slopes: (1) both forested slopes and rock/debris slides are located at similar elevations; (2) vegetation support may have been removed by forest fires prior to failure; or (3) the resolution of the land cover data is too coarse to capture local vegetation effects.

Identification of debris slides was difficult (discussed in Chapter 2), and, as a result, specific controlling factors affecting debris slides are not known. In the Mackenzie Valley, debris slides are common in till and are controlled by till-bedrock interfaces (Aylsworth et al. 2000). Based on field and airphoto observations of the Wrigley Creek debris slide, slope morphology suggests the slope failed at a diamicton-rock interface, similar to failures described by Aylsworth et al. (2000).

The accuracy of the susceptibility maps in this study suggest that the modified "seed cell" approach for characterizing pre-landslide conditions using logistic regression techniques is adequate for small- to medium-scale landslide susceptibility maps. Debris flow and rock/debris slide models were successful, in part because of their large sample sizes. Earth slides and flow modelshad small sample sizes – too few to statistically identify causative associations. To further improve the analysis, detailed site investigations for data collection and more advanced statistical analyses, such as rare event logistic regression, could be beneficial.

Conclusion

This study revealed several important environmental factors that control debris flow and rock/debris slide failures in the South Nahanni watershed. Identified controls are consistent with results of previous landslide studies in western Canada. Cross-validation of debris flow and rock/debris slide models demonstrated that the modified sampling technique I applied to the logistic regression analysis is suitable for creating successful landslide susceptibility models, assuming adequate data are used. Advanced statistical methods might further improve results given the small sample size of several landslide types.

Success of any susceptibility model is dependent on the quality and type of data analyzed. Incomplete and sparse datasets are a reality when conducting susceptibility analysis, especially for large remote regions. As a result, data should be carefully reviewed, and the results of the analysis should be considered relative to the quality of the data used.

Despite differences in mapping scales, removal of three parameters (rivers, bedrock structure, and surficial geology), and the relatively small sample size, debris flows and rock/debris slide models produced accurate small-scale susceptibility maps. Final susceptibility map accuracy depends on the smallest map scale or resolution included in the model. Debris flow and rock/debris slide models yield susceptibility maps of 1:1,000,000 scale because they include bedrock geology data available at that scale. I recommend using geologic data at 1:1,000,000scale and topographic data at 1:50,000 scale as the smallest scale limit for national or regional scale studies. Further investigation is required to determine reasonable scales for bedding-slope structure.

Susceptibility models and maps can be used for planning protection and mitigation in vulnerable areas in the South Nahanni watershed. They also identify areas that require more intensive, field-based studies (e.g. regions with high landslide frequency that were notpredicted by the regression models).

CHAPTER 4: CONCLUSIONS

ASTER satellite imagery proved to be a reliable tool with which to conduct a regional-scale landslide inventory. Fewer images were required for analysiscompared to aerial photos, and landslides could be directly digitized during mapping. This direct digitization reduces transfer errors. The main limiting factor involved in using ASTER satellite imagery is its coarse resolution, whichprecludes mapping landslides less than 1 ha in size. Lack of high-resolution base maps and geocoded imagery increased positional errors of the rectified ASTER images. Cloud cover and shadows also compromised image quality. Despite these limitations, I found that ASTER interpretation is adequate for preliminary landside inventory projects.

Using ASTER imagery, I identified over 4000 landslides, which I grouped into different types of flow, slide, and complex movements. The eastern portion of the watershed contains a diversity of landslide types and contains the majority of large landslides. The east area comprises uplifted and folded sedimentary rock formations, incised plateaus, and thick glacial lake sediments, which create favourable conditions for several types of mass movements. The terrain in the west comprises steep, rugged mountain ranges, which is dominated by debris flows and rock slides.

Landslide susceptibility models incorporating logistic regressions were successful for two types of landslides - debris flows and rock/debris slides. Verification and cross-validation exercises indicate that both models achieve accuracies between 75-85%. Despite the limitation in the structure data, rock/debris slide models produced successful predictions of landslides in areas of high-to-moderate landslide susceptibility. Debris flow susceptibility models performed best overall. In addition to the successful predictive power of the models, the identified relationships between environmental factors and landslides were consistent with prior research on those environmental factor that influence landslides in the region.

This study employed publicly available data and open-source statistical software to minimize expenses in data acquisition and in data analysis. A constraint when using publicly available data for a detailed landslide study is the limited availability of applicable data at reasonable scales. The smallest scale of the causative factors used in the model defines final accuracy of the map data. The debris flow models include the most diverse set of causative factors and produce a map with an accuracy of 1:1,000,000 scale. The rock/debris flow map also has a spatial accuracy of 1:1,000,000 scale, but the models contain less explanatory variables including bedrock lithologies, land cover and slope. Few mapped earth slides and lack of important geospatial data at a suitable map scale precluded development of reliable earth slide susceptibility models.

Data availability and resolution were the most limiting factors for landslide mapping in the South Nahanni watershed.In my opinion, regional landslide inventories are only achievable when 1:50,000 scale topographic data exist and where bedrock geology and land cover is available at scales of 1:250,000 to 1:1,000,000 or larger. The appropriate scale for bedding-slope structure data is uncertain. These findings should serve as general guidelines for regional landslide mapping.

Land-use planners, engineers, and geoscientists can use the landslide mapping methods applied in this study as a preliminary assessment tool during landslide prevention and mitigation projects. The low cost associated with the methodology provides reasonable alternatives to traditional approaches for landslide inventories.

Future landslide studies in the South Nahanni watershed should includefieldwork to validate the landslide maps produced in this study. This fieldwork should also consider estimating the age of landslides where possible. Further investigations should build on information gathered in Chapter 2 to finalize the landslide inventory to be used for future hazard and risk analysis in the region. Regions of particular interest include secondary headscarp areas associated with complex slides, lithological contacts located within landslide initiation zones, and areas where landslides are found in low-susceptibility zones. An attempt should also be made to improve the inventory of large-scale causative factor data in the area. Generating susceptibility models using the newly derived data and advanced statistical procedures would also be beneficial. It is likely that additional landslides will be identified during detailed investigation, especially when higher resolution imagery is used. Further investigation of landslide activity in the watershed will improve the understanding of the initial causes of slope movement and the impacts they have on the watershed and can be applied to land-use planning or engineering prevention or mitigation practices prior to any future development.

REFERENCES

Abrams M, Hook S, and Ramachandran B (2002) ASTER User Handbook. NASA Jet Propulsion Laboratory, Pasadena, California, 135 p.

Ayalew L and Yamagishi H (2005) The application of GIS-based logistic regression for landslide susceptibility mapping in the Kakuda-Yahiko Mountains, Central Japan. Geomorphology, 65: 15-31.

Ayalew L, Yamagishi H, Marui H, and Kanno T (2005) Landslides in Sado Island of Japan: Part II. GIS-based susceptibility mapping with comparisons of results from two methods and verifications. Engineering Geology, 81(4): 432-445.

Aylsworth JM, Duk-Rodkin A, Robertson T, and Traynor JA (2000) Landslides of the Mackenzie valley and adjacent mountainous and coastal regions. In: Dyke LD and Brooks GR (eds.), The Physical Environment of the Mackenzie Valley, Northwest Territories: A Base Line for the Assessment of Environmental Change. Geological Survey of Canada, Bulletin 547, p. 167-176.

Bertolo P and Wieczorek GF (2005) Calibration of numerical models for small debris flows in Yosemite Valley, California, USA. Natural Hazards and Earth System Sciences, 5: 993-1001.

Beyer HL (2010) Hawth's analysis tools for ArcGIS, version 3.27 [online]. Available from: http://www.spatialecology.com/htools. Last accessed: June 2010.

Brown RJE. (1978) Permafrost map of Canada. In: Hydrological Atlas of Canada. Ottawa: Department of Fisheries and Environment, Ottawa, Plate 32, scale 1:10000000.

Canadian Council on Geomatics (2009) Geobase. Retrieved August, 2009, from www.geobase.ca.

Carrara A (1983) Multivariate models for landslide hazard evaluation. Mathematical Geology, 15(3): 304-427.

Carrara A (1988) Landslide hazard mapping by statistical methods: A "Black Box" approach. In: Workshop on Natural Disaster in Europe Mediterranean Countries. Perugia, Italy. Consiglio nazionale delle Ricerche, Perugia, p. 205-224.

Carrara A, Cardinali M, Detti R, Guzzetti F, Pasqui V, and Reichenbach P (1991) GIS techniques and statistical models in evaluating landslide hazard. Earth Surface Processes and Landforms, 16: 427-445.

Carrara A, Crosta GB, and Frattini P (2008) Comparing models of debris-flow susceptibility in the alpine environment. Geomorphology, 94: 353-378.

Castellanos Abella, EA and van Westen CJ (2008) Qualitative landslide susceptibility assessment by multicriteria analysis: A case study from San Antonio del Sur, Cuantanamo, Cuba. Geomorphology, 94(3-4): 453-466.

Chen Z and Wang J (2007) Landslide hazard mapping using logistic regression model in Mackenzie Valley, Canada. Natural Hazards, 42: 75-89.

Chung CF and Fabbri AG (1999) Probabilistic prediction model for landslide hazard mapping. Photogrammetric Engineering and Remote Sensing, 65(12): 1389-1399.

Chung CF and Fabbri AG (2008) Predicting future landslides for risk analysis – spatial models and cross-validation of their results. Geomorphology, 94: 438-452.

Chung CF, Kojima H, and Fabbri AG (2002) Stability analysis of prediction models for landslide hazard mapping. In: Allison RJ (ed.), Applied Geomorphology: Theory and Practice. New York, John Wiley and Sons Ltd., p. 3-19.

Clague JJ (1992) Chapter 21. In: Gabrielse H and Yorath CJ (eds.), Geology of Cordilleran Orogen in Canada. Geological Survey of Canada. Geology of Canada No. 4, p. 808-815.

Clerici A, Perego S, Tellini C, and Vescovi P (2006) A GIS-based automated procedure for landslide susceptibility mapping by the conditional analysis method: The Baganza valley case study (Italian Northern Apennines). Environmental Geology, 50: 941-961.

Code JA (1973) The stability of natural slopes in the Mackenzie Valley. Environmental-Social Committee, Northern Pipelines, Task Force on Northern Oil Development. Geological Survey of Canada, Report No. 73-9, 18 p.

Couture R and Riopel S (2006) Regional landslide mapping: Landslide spatial database and case studies in the Mackenzie Valley, Northwest Territories, Canada. Abstract for 36th International Arctic Workshop, Boulder, 16-18 March 2006, INSTAAR, University of Colorado. http://instaar.colorado.edu/AW/abstract_detail.php?abstract_id=48.

Cruden DM (2000) Some forms of mountain peaks in the Canadian Rockies controlled by their rock structure. Quaternary International, 68(71): 59-65.

Cruden DM (2003) The shapes of cold, high mountains in sedimentary rocks. Geomorphology, 55: 249-261.

Cruden DM and Hu, XQ (1996) Hazardous modes of rock slope movement in the Canadian Rockies. Environment and Engineering Geoscience, 2: 507-516.

Cruden DM and Varnes DJ (1996) Landslide types and processes. In: Turner AK, Schuster RL (eds.), Landslides, Investigation and Mitigation, Transportation Research Board, National Research Council, Special Report 247, pp. 36-75.

Dai FC, Lee CF, Li J, and Xu ZW (2001) Assessment of landslide susceptibility on the natural terrain of Lantau Island, Hong Kong. Environmental Geology, 40(3): 381-391.

Davis JC (2002) Statistics and Data Analysis in Geology. 3rd ed. Wiley & Sons, Inc. New York, 638 p.

Demoulin A and Chung, CJF (2007) Mapping landslide susceptibility from small datasets: A case study in the Pays de Herve (E Belgium). Geomorphology, 89(3-4): 391-404.

Dominguez-Cuesta MJ, Jimenex-Sanchez M, and Berrezueta E (2007) Landslides in the Central Coalfield (Cantabrian Mountains, NW Spain) geomorphological features, conditioning factors and methodological implications in susceptibility assessment. Geomorphology, 89(3-4): 358-369.

Donati L and Turrini MC (2002) An objective method to rank the importance of the factors predisposing to landslides with the GIS methodology: Application to an area of the Apennines (Valnerina: Perugia, Italy). Engineering Geology, 63: 277-289.

Duk-Rodkin A and Lemmen DS (2000) Glacial history of the Mackenzie region. In: Dyke LD and Brooks GR (eds.), The Physical Environment of the Mackenzie Valley, Northwest Territories: a Base Line for the Assessment of Environmental Change. Geological Survey of Canada, Bulletin 547, p. 11-20.

Duk-Rodkin A, Huntley D, and Smith R (2007) Quaternary Geology and glacial limits of the Nahanni national Park Reserve and adjacent areas, Northwest Territories, Canada. In: Wright DF, Lemkow D, and Harris JR (eds.), Mineral and Energy Resource Assessment of the Greater Nahanni Ecosystem under consideration for the Expansion of the Nahanni National Park Reserve, Northwest Territories. Geological Survey of Canada, Open File 5344, p. 125-129.

Dyke AS (1990) Quaternary Geology of the Frances Lake Map Area, Yukon and Northwest Territories. Geological Survey of Canada, Memoir 426, 39 p.

Dymond JR, Ausseil AG, Shepherd JD, and Buettner L (2006) Validation of a region-wide model of landslide susceptibility in the Manawatu-Wanganui region of New Zealand. Geomorphology, 74: 70-79.

Eisbacher GH (1977) Rockslides in the Mackenzie Mountains, District of Mackenzie. Geological Survey of Canada, Paper 77-1A, p. 235-241.

Eisbacher GH (1979) Cliff collapse and rock avalanches (sturzstroms) in the Mackenzie Mountains, northwestern Canada. Canadian Geotechnical Journal, 16: 309-334.

ESRI, Environmental Systems Resource Institute (2009) ArcMap 9.2. ESRI, Redlands, California.

ESRI Support Center (2009) ESRI Discussion Conferences. Retrieved February 2009. http://forums.esri.com/

Evans SG and Clague JJ (1989) Rain-induced landslides in the Canadian Cordillera, July 1988. Geosciences Canada, 16(3): 193-200.

Evans SG and Clague JJ (1994) Recent climate change and catastrophic geomorphic processes in mountain environments. Geomorphology 10: 107-128.

Evans SG, Aitken JD, Wetmiller RJ, and Horner RB (1987) A rock avalanche triggered by the October 1985 North Nahanni earthquake, District Mackenzie, NWT. Canadian Journal of Earth Sciences, 24: 176-184.

Fernandez T, Irigaray C, El Hamdouni R, and Chacon J (2003) Methodology for landslide susceptibility mapping by means of a GIS. Application to the Contraviesa area (Granada, Spain). Natural Hazards, 30: 297-308.

Ford DC (1976) Evidences of multiple glaciation in South Nahanni National Park, Mackenzie Mountains, Northwest Territories. Canadian Journal of Earth Sciences, 13: 1433-1445.

Ford DC (1980) Threshold and limit effects in karst geomorphology. In: Coates DR and Vitek JD (eds.), Thresholds in Geomorphology. George Allen and Unwin, London, p. 345-362.

Fourniadis IG, Liu JG, and Mason PJ. (2007) Landslide hazard assessment in the Three Gorges area, China, using ASTER imagery: Wushan-Badong. Geomorphology, 84: 126-144.

Frattini P, Crosta G, Carrara A, and Agliardi F (2008) Assessment of rock fall susceptibility by integrating statistical and physically-based approaches. Geomorphology, 94:419-437.

Gabrielse H and Yorath CJ (1992) Geology of the Cordilleran Orogen in Canada. Geological Survey of Canada, Geology of Canada, No. 4, 844 p.

Geertsema, M (2006) Hydrogeomorphic hazards in northern British Columbia. Netherlands Geographical Studies 341, Utrecht, The Netherlands, 185 p.

Geertsema, M, Schwab JW, Jordan P, Millard TH, and Rollerson TP (2010). Chapter 8: Hill slope processes. In Pike RG, Redding TE, Moore RD, Winkler RD, and Bladon KD (eds.), Compendium of Forest Hydrology and Geomorphology in British Columbia. B.C. Ministry of. Forest and Range, Forest Science Program, Victoria, B.C. and FORREX Forum for Research and Extension in Natural Resources, Kamloops, B.C. Land Management. Handbook 66. www.for.gov.bc.ca/hfd/pubs/Docs/Lmh/Lmh66.htm.

Gimbarzevsky P, Peaker JP, Addison P, and Talbot S (1979) Nahanni National Park integrated survey of biophysical resources, Nahanni National Park, Northwest Territories. Unpublished Forest Management Institute, report 169, 460 p.

Gokceoglu C and Aksoy H (1996) Landslide susceptibility mapping of the slopes in the residual soils of the Mengen region (Turkey) by deterministic stability analysis and image processing techniques. Engineering Geology, 44: 147-161.

Gokceoglu C, Sonmez H, and Ercanoglu M (2000) Discontinuity controlled probabilistic slope failure risk maps of the Altindag (settlement) region in Turkey. Engineering Geology, 55: 277-296.

Gorsevski PV, Gessler PE, Boll J, Elliot WJ, and Foltz RB (2006) Spatially and temporally distributed modeling of landslide susceptibility. Geomorphology, 80:178-198.

Guzzetti F, Carrara A, Cardinali M, and Reichenbach P (1999) Landslide hazard evaluation: a review of current techniques and their application in a multi-scale study, Central Italy. Geomorphology, 31:181-216.

Guzzetti F, Reichenbach P, Ardizzone F, Cardinali M, and Galli M (2006) Estimating the quality of landslide susceptibility models. Geomorphology, 81: 166-184.

Harrel FE, Lee K, and Mark DB (1996) Tutorial in biostatistics, multivariable prognostic models: Issues in developing models, evaluating assumptions and adequacy, and measuring and reducing errors. Statistics in Medicine, 15: 361-387.

Hervás J and Bobrowsky P (2009) Mapping: inventories, susceptibility, hazard and risk. In: Sassa K and Canuti P (eds.), Landslides - Disaster Risk Reduction. Springer, Berlin, p. 321-349.

Hosmer DW and Lemeshow S (2000) Applied Logistic Regression 2nd ed. John Wiley & Sons Inc., New York, 375 p.

Howes DE and Kenk E (1997) Terrain Classification System for British Columbia: A System for the Classification of Surfical Materials, Landforms and Geological Processes of British Columbia. Resources Inventory Branch, Ministry of Environment, Lands and Parks, Victoria, B.C., 110 p.

Huntley D and Duk-Rodkin A (2006) Landslide processes in the south-central Mackenzie River valley region, Northwest Territories, Geological Survey of Canada, Current Research, 2006-A9, 7 p.

Huntley D, Duk-Rodkin A, and Sidwell C (2006) Landslide inventory of the south-central Mackenzie River valley region, Northwest Territories. Geological Survey of Canada, Current Research 2006-A10, 11 p.

Hurlbert (1984) Pseudoreplication and the design of ecological field experiments. Ecological Monographs, 54(2): 187-211.

Jackson LE Jr. (1987) Terrain inventory and Quaternary history of Nahanni map area, Yukon and Northwest Territories. Geological Survey of Canada, Paper 86-18, 23 p.

Jackson LE Jr (2002) Landslides and landscape evolution in the Rocky Mountains and adjacent Foothills area, southwestern Alberta, Canada. Geological Society of America Reviews in Engineering Geology, 15: 325-344.

Jefferson CW, Spirito WA, and Hamilton SM (2003) Chapter 3: Geological setting. In: Jefferson CW and Spirito WA (eds.), Mineral and Energy Resource assessment of the Tlogotsho Range, Nahanni Karst, Ragged Ranges and Adjacent Areas under Consideration for Expansion of Nahanni National Park Reserve, Northwest Territories. Geological Survey of Canada, Open File 1686, 21 p.

Jordan P (2003) Landslide and terrain attribute study in Nelson Forest Region. Final report to Ministry of Forests Research Branch, FRBC Project Number: KB97202-ORE1, 61 p.

Kääb A, Huggel C, Paul F, Wessels R, Raup B, Kieffer H, and Kargel J (2002) Proceedings of EARSEL-LISSIG, Workshop Observing our Cryosphere from Space, Bern, March 11-13. EARSELeproceedings No. 2 – Observing Our Cryosphere from Space, p. 43-53.

Kamp U, Growley BJ, Khattak GA, and Owen LA (2008) GIS-based landslide susceptibility mapping for the 2005 Kashmir earthquake region. Geomorphology, 101(4): 631-642.

Kennedy H (2000) Dictionary of GIS terminology. Environmental Systems Research Institute, Inc., ESRI press, Redlands, California, USA, 116 p.

Komac M (2006) A landslide susceptibility model using the Analytical Hierarchy Process method and multivariate statistics in perialpine Slovenia. Geomorphology, 74: 17-28.

Larsen MC and Torres-Sanhez AJ (1998) The frequency and distribution of recent landslides in three montane tropical regions of Puerto Rico. Geomorphology, 24:309-331.

Lazic SE (2010) The problem of pseudoreplication in neuroscientific studies: is it affecting your analysis? BMC Neuroscience, 11(5): 1-17.

Lee S and Dan NT (2005) Probabilistic landslide susceptibility mapping in the Lai Chau province of Vietnam: Focus on the relationship between tectonic fractures and landslides. Environmental Geology, 48: 778-787.

Lee S and Min K (2001) Statistical analysis of landslide susceptibility at Yongin, Korea. Environmental Geology, 40: 1095-1113.

Lee S, Chwae U, and Min K (2002) Landslide susceptibility mapping by correlation between topography and geological structure: The Janghung area, Korea. Geomorphology, 46: 149-162.

Lee S, Ryu JH, Won JS, and Park HJ (2004) Determination and application of the weights for landslide susceptibility mapping using an artificial neural network. Engineering Geology, 71: 289-302.

Lipovsky P and Huscroft C (2007) A reconnaissance inventory of permafrost-related landslides in the Pelly River watershed, central Yukon. In: Emond DS, Lewis LL, and Weston LH (eds.), Yukon Exploration and Geology 2006. Yukon Geological Survey, p. 181-195.

Lyle RR, Hutchinson DJ, and Preston Y (2004) Landslide processes in discontinuous permafrost, Little Salmon Lake (NTS 105L/1 and 2), south-central Yukon. Yukon Exploration and Geology, p. 193-204.

Marchi L and Cavalli M (2007) Procedures for the documentation of historical debris flows: Applications to the Chieppena Torrent (Italian Alps). Environmental Management, 40: 493-503.

McRoberts EC and Morgenstern NR (1973) A study of landslides in the vicinity of the Mackenzie River mile 205 to 660. Environmental-Social Committee, Northern Pipelines, Task Force on Northern Oil Development. Geological Survey of Canada, Report No. 73-35.

Meentemeyer RK and Moody A (2000) Automated mapping of conformity between topographic and geological surfaces. Computers and Geosciences, 26: 815-829.

Melchiorre C, Matteucci M, Azzoni A, and Zanchi A (2008) Artificial neural networks and cluster analysis in landslide susceptibility zonation. Geomorphology, 94: 379-400.

Nefeslioglu HA, Duman TY, and Durmaz S (2008) Landslide susceptibility mapping for a part of tectonic Kelkit Valley (Eastern Black Sea region of Turkey). Geomorphology, 94(3-4): 401-418.

Nichol JE and Wong M-S (2005) Satellite remote sensing for detailed landslide inventories using change detection and image fusion. International Journal of Remote Sensing, 26(9): 1913-1926.

Nichol JE, Shaker A, and Wong M-S (2006) Application of high-resolution stereo satellite images to detailed landslide hazard assessment. Geomorphology 76: 68-75.

Parks Canada (1984a) Section 2: Climatology. Nahanni National Park Reserve Resource Description and Analysis. Natural Resource Conservation Section, Parks Canada, Prairie Region, Winnipeg, Manitoba, 29 p.

Parks Canada (1984b) Section 3: Geology. Nahanni National Park Reserve Resource Description and Analysis. Natural Resource Conservation Section, Parks Canada, Prairie Region, Winnipeg, Manitoba, 27 p.

Parks Canada (1984c) Section 4: Geomorphology. Nahanni National Park Reserve Resource Description and Analysis. Natural Resource Conservation Section, Parks Canada, Prairie Region, Winnipeg, Manitoba, 118 p.

Parks Canada (2003) Nahanni National Park Reserve of Canada: Natural wonders and culture treasures, natural heritage – Geology and Geomorphology. Website: http://www.pc.gc.ca/pn-np/nt/nahanni/natcul/natcul1c_e.asp. Last accessed 2006.

Porkes R (2005) Collins internet-linked dictionary of statistics, second edition. HarperCollins Publishers, Glasgow, Scotland, 316 p.

R Development Core Team (2008). R: A language and environment for statistical computing. R Foundation for Statistical Computing, Vienna, Austria. URL http://www.R-project.org. Last accessed 2010.

Remondo J, Gonzalez A, Diaz de Teran JR, Cendrero A, Fabbri AG, and Chung CF (2003) Validation of landslide susceptibility maps; examples and applications from a case study in Northern Spain. Natural Hazards, 30:437-449.

Riopel S, Couture R, and Tewari K (2006) Mapping susceptibility to landslides in a permafrost environment: Case Study in the Mackenzie Valley, Northwest Territories, Canada. GeoTec Conference, 18-21 June, 2006, Ottawa, Ontario, 13 p. ESS Contribution=2005648.

Rollerson TP, Millard T, Jones C, Trainor K, and Thompson B (2001) Predicting post-logging landslide activity using terrain attributes: Coast Mountains, British Columbia. Forest Research Technical Report, Vancouver Forest Region, Nanaimo, BC.

Rollerson T, Millard T, and Thompson B (2002a) Using terrain attributes to predict post-logging landslide likelihood on southwestern Vancouver Island, Forest Research Technical Report, Vancouver Forest Region, Nanaimo, BC.

Rollerson T, Millard T, and Thompson B (2002b) Post-logging landslide rates in the Cascade Mountains, southwestern British Columbia, Forest Research Technical Report, Vancouver Forest Region, Nanaimo, BC.

Ruff M and Czurda K (2008) Landslide susceptibility analysis with a heuristic approach in Eastern Alps (Vorarlberg, Austria). Geomorphology, 94 (3-4): 314-324.

Sanborn, P and Smith S (2007) Soil landscapes of the Nahanni karst – interim report to Parks Canada, 98 p.

Selby MJ (1993) Hill slope materials and processes 2nd edition Oxford, Oxford University Press, 451 p.

Sidle R (2005) Influence of forest harvesting activities on debris avalanches and flows. Debris-flow Hazards and Related Phenomena, Springer, p. 387-409.

Singhroy V (2005) Remote sensing of landslides. In: Glade T, Anderson M, and Crozier MJ (eds.). Landslide Hazard and Risk. John Wiley and Sons, West Sussex, England, 803 p.

Singhroy V (2008) Satellite remote sensing applications for landslide detection and monitoring. In: Sassa K and Canuti P (eds.), Landslide Disaster risk reduction. Springer-Verlag, Berlin Heidelberg, Germany, 389 p.

Soeter R and van Westen CJ (1996) Slope instability recognition, analysis, and zonation. In: Turner AK and Schuster RL (eds.). Landslides: Investigation and Mitigation. Washington, DC: National Academy Press, p. 129-177.

Stow N and Wilson PW (2006) Aggregated CCRS land cover mapping for the Greater Nahanni Ecosystem. Prepared for the Park Establishment Branch, Parks Canada Agency, 49 p.

Süzen ML and Doyuran V (2004) Data driven bivariate landslide susceptibility assessment using geographic information systems: a method and application to Asarsuyu catchments, Turkey. Engineering Geology, 71: 303-321.

Takahashi T (1981) Debris flow. Annual Review of Fluid Mechanics, 13: 57-77.

Tobler W (1988) Resolution, resampling, and all that. In: Mounsey H and Tomlinson R (eds.), Building Data Bases for Global Science. Taylor and Francis, London, pp. 129-137.

Turner AK (1996) Chapter 20: Colluvium and talus. In: Turner AK, Schuster RL (eds.), Landslides, Investigation and Mitigation. Transportation Research Board, National Research Council, Special Report 247, pp. 525-554.

Turrini MC and Visintainer P (1998) Proposal of a method to define areas of landslide hazard and application to an area of the Dolomites, Italy. Engineering Geology, 50: 255-265.

van den Eeckhaut M, Vanwalleghem T, Poesen J, Govers G, Verstraeten G, and Vandekerckhove L (2006) Prediction of landslide susceptibility using rare events logistic regression: A case-study in the Flemish Ardennes (Belgium). Geomorphology, 76: 392-410.

van Westen CJ, Castellanos E, Kuriakos SL (2008) Spatial data for landslide susceptibility, hazard, and vulnerability assessment: An overview. Engineering Geology, 102: 112-131.

Wang FW, Matsumoto T, and Sassa K (2004) Deforming mechanism and influential factors of giant Jinnosuke-dani landslide, Japan. Annuals of Disaster Prevention Research Institute, Kyoto University, No. 47B, 883-891.

Wang HB, Sassa K, Xu WY (2007) Assessment of landslide susceptibility using multivariate logistic regression: a case study in southern Japan. Environmental and Engineering Geoscience, 13(2): 183-192.

Wang WN, Chigira M, and Furuya T (2003) Geological and geomorphological precursors of the Chiu-fen-erh-shan landslide triggered by the Chi-chi earthquake in central Taiwan. Engineering Geology, 69: 1-13.

Weirich F and Blesius L (2006) Comparison of satellite and aerial photo based landslide susceptibility maps. Geomorphology, 87(4): 352-364.

Wetmiller RJ, Horner RB, Hasegawa HS, North RG, Lamontagne M, Weichert DH, and Evans SG (1988) An analysis of the 1985 Nahanni Earthquakes. Bulletin of the Seismological Society of America, 78(2): 590-616.

Wright DF, Lemkow D, and Harris JR, eds. (2007) Mineral and Energy Resource Assessment of the Greater Nahanni Ecosystem Under consideration for the Expansion of the Nahanni National Park Reserve, Northwest Territories. Geological Survey of Canada, Open File 5344, 557 p.

Wyrwoll KH (1986) Characteristics of a planar rock slide: Hamersley Range, Western Australia. Engineering Geology, 22: 335-348.

Yesilnacar E and Topal T (2005) Landslide susceptibility mapping: a comparison of logistic regression and neural networks methods in a medium scale study Hendek region (Turkey). Engineering Geology, 79: 251-266.

Zhou CH, Lee CF, Li J, and Xu ZW (2002) On the spatial relationship between landslides and causative factors on Lantau island, Hong Kong. Geomorphology 43: 197-207.

APPENDIX A: Description of Terms

Material terms

Figure A.1: Sandstone on the top of the Tlogotsho Plateau

Rock: A hard or firm consolidated material (possibly containing joints or fractures) that is intact in its original location before failure occurred (Figure A.1). The meaning of rock in "rock slides" does not include previously transported rubble or rock debris (Geertsema et al. 2010). Rock has a coarse, blocky, massive appearance on the satellite imagery.

Earth: Small grained material, with grain size <2mm (Cruden and Varnes, 1996), generally unsorted, plastic material (Figure A.2). Earth materials are normally observed in valleys or low elevated areas (Geertsema et al. 2010). Earth has a smooth textured appearance on the satellite imagery.

Figure A.2: Earth material located in the Ram Plateau.

Debris: A mixture of material containing a significant amount of coarse material (can include trees; Cruden and Varnes, 1996). Debris appears to have a combined coarse and smooth texture appearance on the satellite image. Debris is normally identified where rock masses are broken into boulders and cobbles and do not appear to be a massive unit (Figure A.3). The material is also classified as debris when rock combines with earth materials (material with a smooth textured appearance) during movement along the transport zone.

Figure A.3: Diamicton from the Wrigley slide deposits

Landslide type description

Rock slide (Rs): Rock slides fail as blocky or massive movements along the rupture surface (Figure A.4a and b). Rock slides can fail as planar slides along bed dip direction, joints or fracture surfaces. Diagnostic features used to classify rock slides are massive debris, hummocky texture, and that the slide failed along a rupture surface in a non-channelized movement.

Figure A.4a: ASTER image of the Cathedral Creek Rock slide

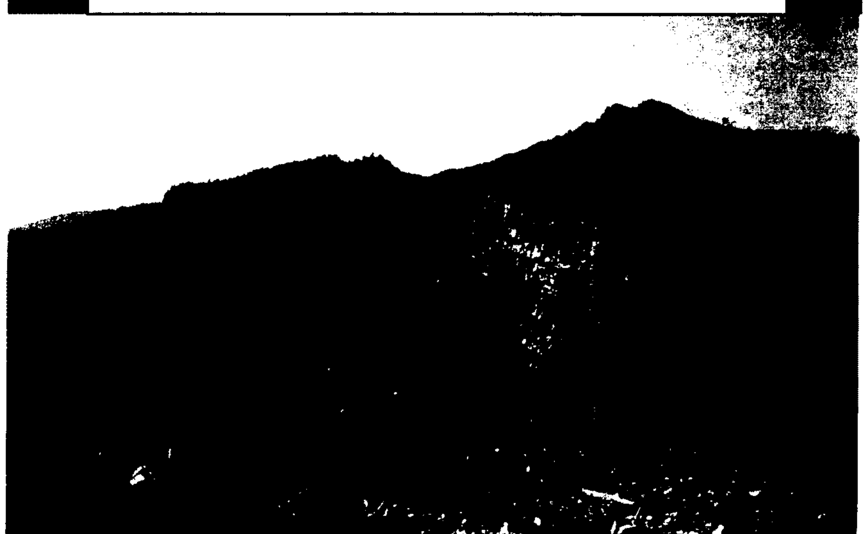

Figure A.4b: Oblique photo of the Cathedral Creek rock slide

Rock fall (RF): Rock falls occur on steep slopes and can form talus cones at the base of the slope. Evidence of rock falls are most often observed in canyons and on steep mountain slopes. Diagnostic features of rock falls on satellite imagery are steep slopes with talus cones at the base and little to no evidence of a channelized transport zone (Figure A.5).

Figure A.5: ASTER image of the Ram Plateau.

Rock fall – debris flow (Rf-df): Rock fall – debris flows occur where steep slopes are present at the top of the slope and grade into a gentler slope. The failure initiates on vertical slopes as rocks fall and then transform into a debris flow when the talus material below becomes activated. These processes can be rapid. Diagnostic features to identify rock fall – debris flows are where the initiation zones are located on vertical slopes and then transformed into a channelized flow causing the landslide's dimensions to have a larger length-to-width ratio (Figure A.6).

Figure A.6: Ram Plateau

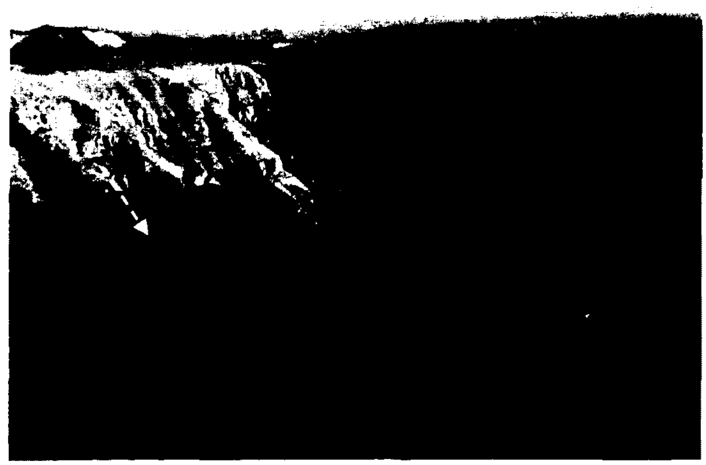

Rock slide – debris flow (Rs-df): Rock slide – debris flows initiate as rock slides that fail along the surface of rupture and then start to break up during transport causing the material to transform into a debris flow further down slope (Figure A.7a). As the material moves down slope it can also incorporate underlying material (i.e. lake sediments, trees, rubble) changing the material composition from massive rock to predominantly debris. Diagnostic features used to classify rock slide – debris flows were steep initiation zones that failed along a surface of rupture in massive rock that transitioned into a channelized transport zone (Figure A.7b). Rock slide – debris flows often have a fan at the base of the slope.

Figure A.7a: Rockslide – debris flows north of the South Nahanni River

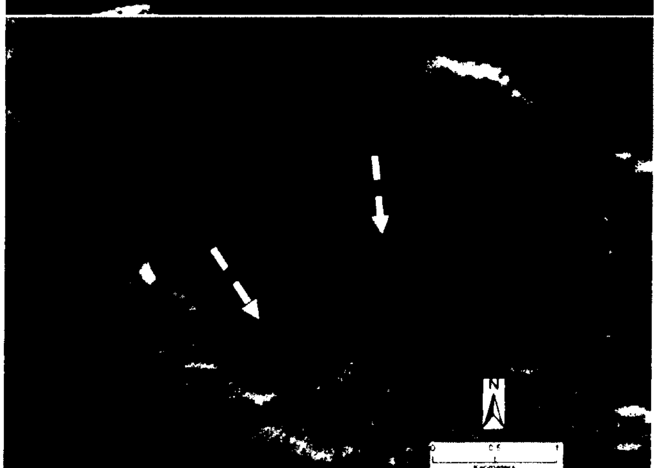

Figure A.7b: Rockslide – debris flows north of the South Nahanni River

Rock slide – earth flow (Rs-ef): Rock slide – earth flows differ from rock slide – debris flows because they occur as two individual modes unlike rock slide – debris flows where the initial failure becomes incorporated into the secondary failure. The landslide initiates as a rock slide along the failure surface and triggers fine grained sediments (eg. lake sediments) to fail further down slope. An example of a rock slide – earth flow was observed on the Tlogotsho Plateau (Grizzly slide; Figure A.8). The slide was initiated as a rotational rock slide transforming into a translational rock slide along a weak, fine grained shale rupture surface that later transformed into a rotational earth slide followed by a earth flow. Diagnostic characteristics of a rock slide – earth flow are steep escarpments in massive rock at the initiation zone followed by a secondary failure scarp in smooth textured materials further down slope.

Figure A.8: Rock slide – earth flow; Tlogotsho Plateau: ASTER scene of slide (left), oblique photos of slide (top, right), close up oblique photo of rock slide (bottom, right).

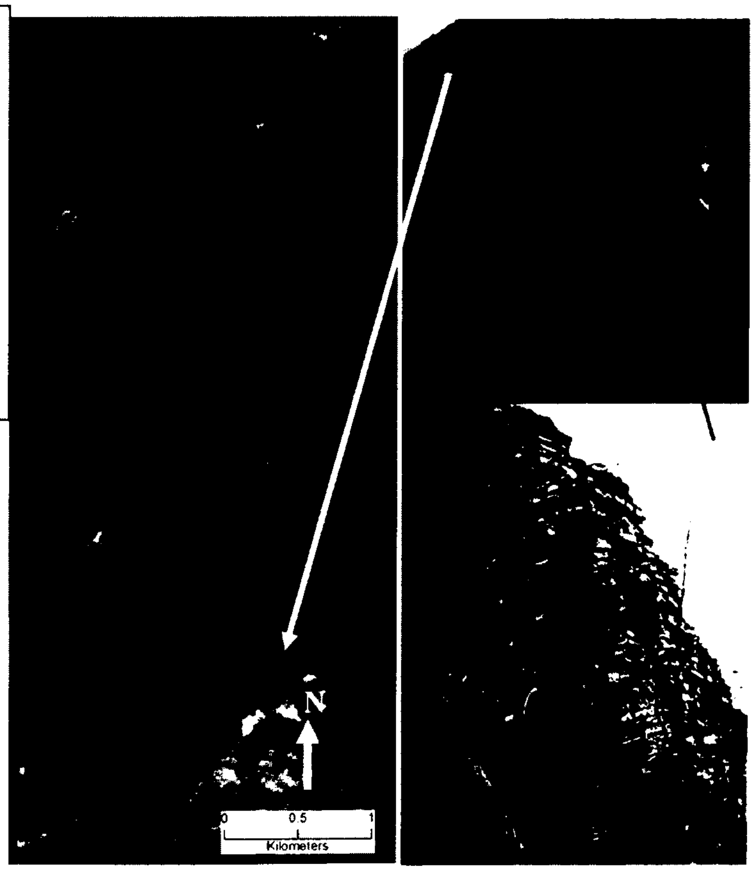

Rock topple – debris flow (Rt-df): Rock topple – debris flows occur when rock that has a forward rotation along a point or axis below the center of gravity fail and then are transported down slope by channelized movement. Rock topple – debris flows are observed along escarpments in the Tlogotsho Plateau (Figure A.9; e.g. toppling initiation). Toppling occurred in sandstone on the Tlogotsho Plateau, possibly because it contained major joints parallel and perpendicular to the edge of the escarpment.

Figure A.9: Rock topple;Tlogotsho Plateau

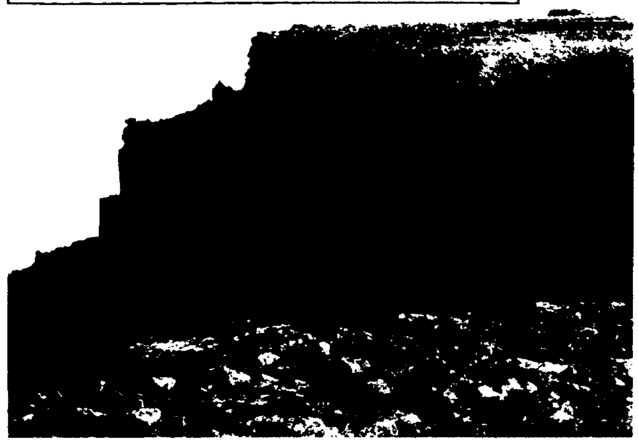

Earth slide (Es): Earth slides fail as smooth massive movements along the rupture surface. They were observed most often in lake sediments, terraces, and along river banks in Nahanni. Diagnostic features used to classify earth slides are massive, smooth textures that fails along a surface of rupture.

Figure A.10: Earth slide, South Nahanni River

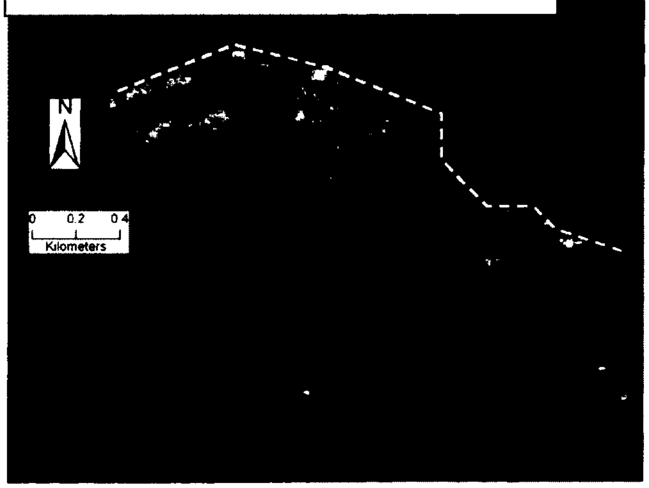

Earth flow (Ef): Earth flows occur in fine-grained material saturated with water (Figure A.11). When permafrost is involved earth flows are known as active layer detachments or thaw flows. The permafrost extent is not known in Nahanni. However, many slides observed resemble permafrost landslides. Diagnostic features such as smooth homogenous textures, and low slope gradients are common.

Figure A.11: Earth slide, Tlogotsho Plateau

Earth slide – debris flow (Es-df): Earth slide – debris flows occur when landslides originate as homogeneous earth material that fails along a surface of rupture. Earth slides then trigger rock and other materials down slope to fail resulting in different materials being incorporated into the deposits (Figure A.12). Diagnostic features used to classify this landslide type are smooth textures, evidence of a failure plane at the initiation zone that transform into hummocky mixed textures with flow-like characteristics further down slope.

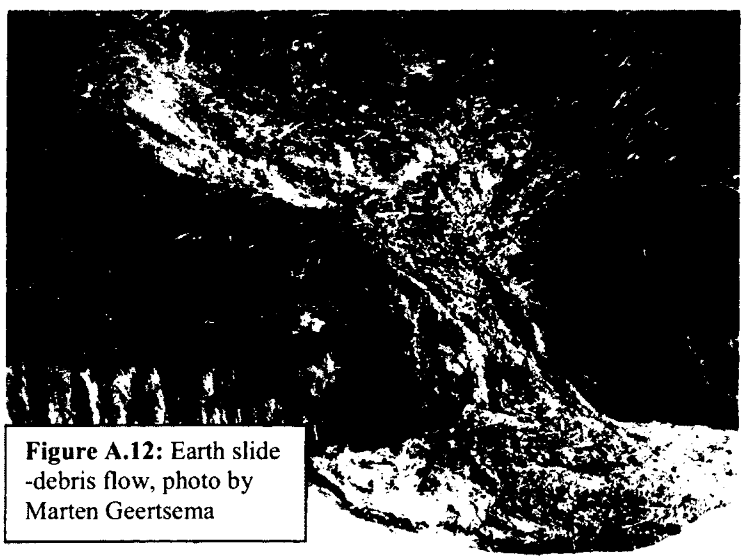

Figure A.12: Earth slide -debris flow, photo by Marten Geertsema

Earth slide – earth flow (Es-ef): Earth slide – earth flows occur when landslides originate as homogeneous earth material that fail along a failure surface maintaining a uniform width that transform into a flow containing similar material further down slope (Figure A.13). Diagnostic features used to classify earth slide – earth flows are smooth textures, uniform width and evidence of a failure plane at the initiation zone, transforming into smooth flow-like characteristics further down slope.

Figure A.13: Earth slide – earth flow

Debris flow (Df): Debris flows occur in material with different grain sizes consisting of loose boulders, cobbles and fine-grained sediments. They initiate where the slope gradients exceed the angle of repose or when material is entrained in water and transported down slope. Debris flows are transported down slope in a channelized manner (Figure A.14). They can travel as slow or rapid movements and can run out for long distances. A debris flow in Nahanni was observed in real-time. The debris flow was slow moving and occurred in highly saturated material and did not fail as a uniform movement within the channel but failed periodically in different locations along the transport zone. The water source on this slide came from melting ground ice. It is possible that the velocity of the slide would increase if there was a rapid introduction of water to the area (e.g. heavy rain fall or rain on snow event). In addition, debris flows commonly fail as fast moving torrents during heavy rainfall. Channelized morphology is the most diagnostic feature of a flow. Material is classified as debris when there is a combined coarse and fine textured appearance and when the deposits initiate in rock, flow in a channelized form and appear to have finer deposits at the base of the slope. Talus cones are often present at the base of debris flows.

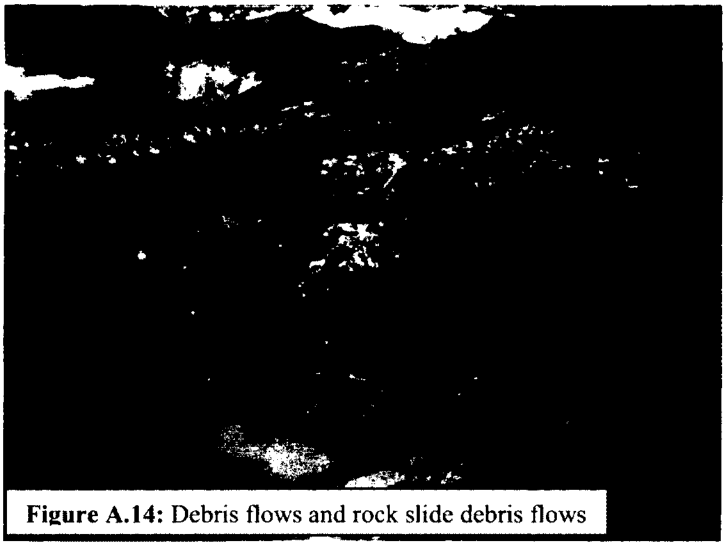

Figure A.14: Debris flows and rock slide debris flows

***Debris slide (Ds)*:** Debris slides fail along the surface of rupture. They occur in material with different grain sizes and tend to fail as one massive movement (Figure A.15C). Debris slides are different from debris flows because they are not channelized during transport and their run out is normally not as extensive. Diagnostic features used to classify debris slides are landslides that appeared coarse texture like rock slides but on less steep slopes within material that contain geomorphological features that suggest fine to coarse materials (i.e. gully formation; Figure A.15A and B). Material is made up of a combination of broken up rock material and finer sediments, and possibly vegetation debris during movement down slope (Figure A.15D and E).

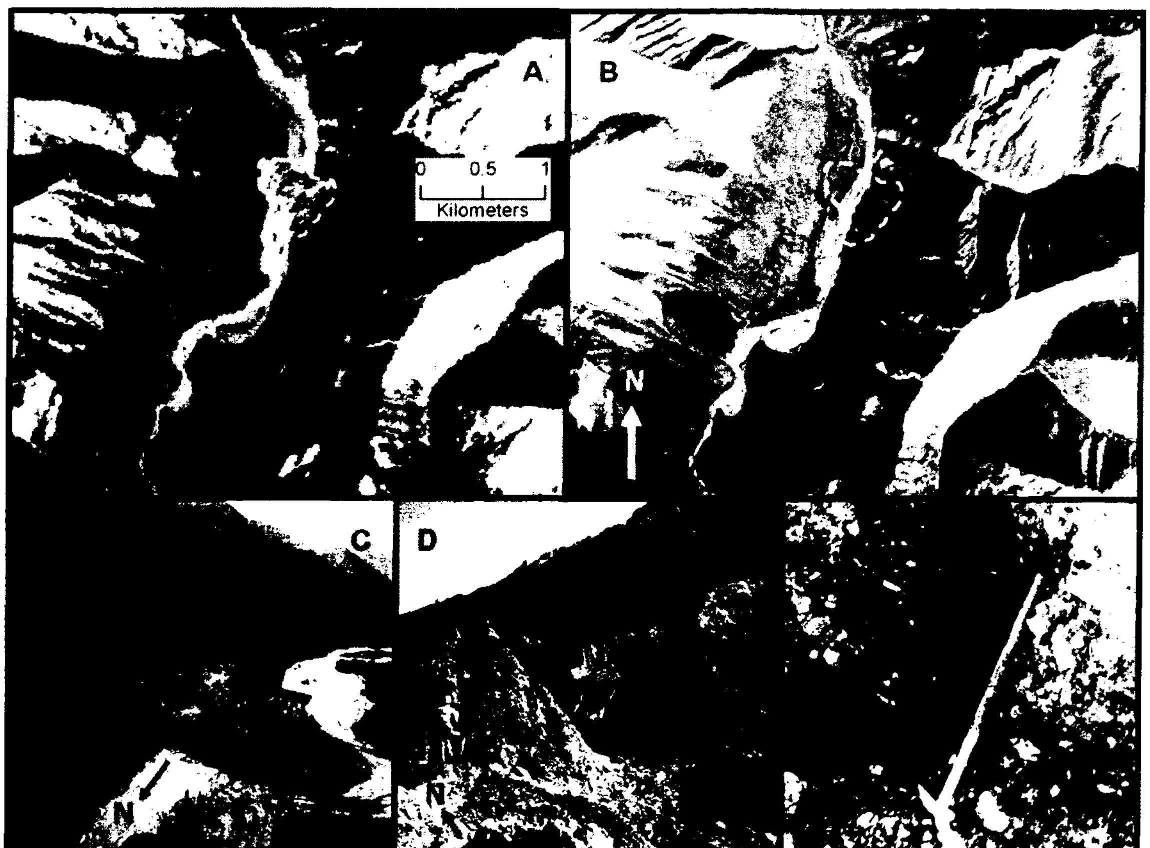

Figure A.15: Wrigley Creek Debris slide. A) Satellite image of debris slide, B) 1949 Air photo of debris slide location, C) Oblique photo of slide, D) Molard on top of slide debris, E) Close up of slide debris.

Debris slide – debris flow (Ds-df)**:** Debris slide – debris flows are complex slides. They initiate as debris slides and transform into flows with descent. Diagnostic features that are used to identify debris slide – debris flows are the smooth and coarse texture appearance throughout the slide. The initiation zone failed as a uniform movement along the surface of rupture and transformed into a channelized movement further down slope.

APPENDIX B: Landslide Type and Location Map and Inventory

Note: Please contact Dr. Brian Menounos at menounos@unbc.ca or Courtney Jermyn at courtney.jermyn@gmail.com to request aPDF copy of the landslide type and distribution map and landslide inventory.

APPENDIX C: Model Building Procedures, Scripts, and Results

Note: Please contact Dr. Brian Menounos at menounos@unbc.ca or Courtney Jermyn at courtney.jermyn@gmail.com to request aPDF copy of the debris flow and rock/debris slide susceptibility maps and data.

Model building, procedures, scripts, and results can be found below.

APPENDIX C-I: Model Building Procedures

Assumption made:

- Factors that caused landslides in the passed will be the same in the future
- Variables characteristics are uniform across a landslide head scarp (see notes below on how this was assumption was accounted for).
- Debris flow initiation occurs within 50 m of the head scarp in complex landslides that involve rock slide - debris flows (see note under Debris flows)

Data Used

Dependent variable:

- Landslides (1s): Each landslide type is a separate dataset and will be modeled independently from one another.
  - Debris flows (DF):
    - Total: 4219
    - Mapped from ASTER satellite imagery
    - Points and polygons, include head scarps only with 100m buffer
  - **Note**: During field work, large scale debris flows were found to be part of a complex landslide that was not previously detected on ASTER scenes. The initial failures were short lived and debris flows were the main movement type. In this study debris flow type class includes: debris flows, rock topple-debris flows, rock slide-debris flows, debris slides-debris flows, and rock fall-debris flows.
  - Earth Flows (EF):
    - Total: 35
      - Mapped from ASTER satellite imagery
      - Points and polygons include head scarps with 50 m buffer around head scarp.
      - Sample size is too small to conduct analysis.
  - Earth Slides (ES):
    - Total: 104
    - Mapped from ASTER satellite imagery
    - Points and polygons include head scarps only with 50 m buffer around head scarp.
  - **Note**: As head scarps of the initiation zone are the only areas considered in the analysis the first landslide type class in a complex landslide is the only type considered (for the exception of DF where initial failures are very short lived). Earth slide type class includes: earth slides, earth slide-debris flow, and earth slide-earth flow.

- Rock Slides (RS):
  - Total: 119
  - Mapped from ASTER satellite imagery
  - Points and polygons include head scarps only with 50 m buffer around head scarp.
  - **Note:** As rock and diamicton were difficult to distinguish on ASTER scenes, rock slide dataset comprises, rock slide type class includes: rock slides, debris slides, and rock slide-earth flows.

***Independent variables*:**

- Bedrock (BROCK):
  - Provided by Natural Resources-MERA project (Wright et al. 2007).
  - Vector:1:1,000,000 scale
  - 30 m cell size was used to be consistent with DEM (does not improve data quality)
  - Lithologies were reclassified into 4 categories: 1. Carbonates, 2. Mixture (carbonate/shale/clastic), 3. Igneous, 4. Shale
  - Susceptibility Map: Layer was rasterized using final coefficients from the logistic regression analysis as the cell values.
  - **Note:** BROCK values given to each landslide event in the Logistic regression database are based on the lithology category that has the largest area within a given landslide heads carp (see script in section XX below). For example if a landslide head scarp (Headscarp1) overlies two different lithology categories (4-shale 95% and 1-Carbonates 5%) then Headscarp1 would have a BROCK value of 4 = Shale.
- Bedding-slope Structure (STRUCT):
  - Vector: 1:250,000 scale
  - 30 m cell size to be consistent with DEM (does not improve data quality)
  - I used structure data (dip and strike) from 1:250,000 printed geological maps, 1:250,000 (70m cell size) DEM to identify slope gradient and topography to classify slopes using Cruden and Hu (1996), Cruden (2000), and Meentemeyer and Moody (2000) sedimentary slope classification.
  - Classified into 7 categories: Anaclinal steepened, Anaclinal Subdued, Cataclinal dip-slope, Cataclinal over-dip, Cataclinal under-dip, Orthoclinal, Other
  - Susceptibility Map: Layer was rasterized using final coefficients from the logistic regression analysis as the cell values.
  - **Note**: STRUCT values given to each landslide event in the logistic regression database are based on the unit category that has the largest area within a given landslide heads carp (see script in Section below). For example if a landslide head scarp (Headscarp1) overlies two different unit categories (1- Anaclinal dip slope 20% and 3-Cataclinal subdued 80%) then Headscarp1 would have a STRUCT value of 3 = Cataclinal subdued. **This layer was removed from analysis.**
- Land cover (VEG):
  - Provided by Parks Canada

- Original data generated from Landsat raster with 150 m cell size
- Reclassified into 2 categories: Forested, Non-forested
- Susceptibility Map: raster was reclassified using final coefficients from the logistic regression analysis as the cell values.

- **Note:** VEG values given to each landslide event in the logistic regression database is based on the unit category that has the largest area within a given landslide heads carp (see script in section below). For example if a landslide head scarp (Headscarp1) overlies two different unit categories (1. Forested 90% and 2. Non-forested 10%) then Headscarp1 would have a VEG value of 1 = Forested.

- Slope (SLOPE):
  - DEM generated from 1:50,000 NTS map sheets
  - Raster, 30m cell size
  - Slope values in degrees
- **Note:** SLOPE values given to each landslide event in the logistic regression database is the mean slope gradient found in the head scarp polygon.
- Elevation (ELEV):
  - DEM generated from 1:50,000 NTS map sheets
  - Raster, 30m cell size
  - Elevation values in meters
- **Note**: ELEV values given to each landslide event in the logistic regression database was the mean elevation found in the head scarp polygon.
- Aspect (ASPECT):
  - DEM generated from 1:50,000 NTS map sheets
  - Raster, 30m cell size
  - Aspect values in degrees
- **Note**: ASPECT values given to each landslide event in the logistic regression database is the mean aspect of all the values contained in a landslide head scarp polygon. Cardinal directions were later determined through R code during logistic regression analysis to avoid problems associated with 0 and 360° being equal aspects.
- Mean aspect was based on the equation from Davis (2002):
  - **Tan^{-1}= (sum of cosθ/sum of sinθ)**
  - Using Aspect raster cosθ (in radians) was calculated using Raster calculator
    - **cos([AspectGrid] * (0.01745329))**
  - Using Aspect raster sinθ was calculated using Raster Calculator
    - **sin([AspectGrid] * (0.01745329))**
  - Using zonal statistics using unique ID for each landslide polygon sums of cos and sums of sins were calculated for each landslide polygon.
  - Statistical results were imported to excel to convert aspect from radians to degrees using equation:
    - **=MOD(360+ATAN2(cossums, sinsums)*(180/PI()),360)**
  - Mean Aspect values transferred back into ArcGIS and values were assigned to the appropriate landslide by using Join tool.

- Slope Profile Curvature (CURVPF):
    - DEM generated from 1:50,000 NTS map sheets
    - Raster, 30m cell size
  - Note: CURVPF values are based on the mean curvature calculated, using Zonal Statistics as Table in Spatial Analyst, for each landslide head scarp polygon.
- Slope Plan Curvature (CURVPL):
    - DEM generated from 1:50,000 NTS map sheets
    - Raster, 30m cell size
  - Note: CURVPL values are based on the mean curvature calculated, using Zonal Statistics as Table in Spatial Analyst, for each landslide head scarp polygon.

Sampling Method:

At ratio of 1:1 landslide to non-landslide areas were selected using Hawth's random selection tool.

Models were generated for each landslide type individually. Each landslide type's polygons were divided in half using random sampling (Hawth's tools). Half the dataset were used as a test set and the other for validation. (ID= 1 in the logistic regression database).

To obtain non-landslide points (ID=0 in the logistic regression database), including validation and test sets, a Raster of the study area was converted into points every 30 m (not including areas that have been identified as landslide head scarp areas). Depending on the number of landslides in a given population determined the number of non-landslides sampled.

APPENDIX C-II: Scripts

Script used to select the category with the largest area found in each head scarp polygon:

Step 1: spatially join (one to many) landslide polygon with vector data (eg. vegetation)
Step 2: dissolve new shape file by unique Id and keep VEG code
Step 3: create area field
Step 4: Use code written below (ESRI Support Centre 2009). Change the file names for the following fields to match the current project: AREA_FIELD, NEW_SHAPEFILE_FOLDER, and NEW_SHAPEFILE_NAME.
Step 5: Join results to desired landslide shape file using unique ID (joinID)

Code:

```
Sub mergefeatures()
Const AREA_FIELD = "area"
Const ID_FIELD = "FID_LSPOLY"
Const NEW_SHAPEFILE_FOLDER = "C:\Documents and
Settings\Administrator\Desktop\final_layers"
Const NEW_SHAPEFILE_NAME = "surf2_ls_merge"
'*********************************************
Dim pMxDoc As IMxDocument
Dim pFtrLyr As IFeatureLayer
Dim pFtrCls As IFeatureClass
Dim pCalc As ICalculator
Dim lIDFldIdx As Long
Dim pTblSort As ITableSort
Dim pFtrCsr As IFeatureCursor
Dim pFtr As IFeature
Dim pFlds As IFields
Dim pObjCpy As IObjectCopy
Dim pWrkspcFact As IWorkspaceFactory
Dim pFtrWrkspc As IFeatureWorkspace
Dim pOutFtrCls As IFeatureClass
Dim pOutFtrCsr As IFeatureCursor
Dim pFtrBfr As IFeatureBuffer
Dim pGeomColl As IGeometryCollection
Dim vLastID As Variant
Dim vNextID As Variant

  ' Get a ref to the polygon featureclass
  Set pMxDoc = ThisDocument
  Set pFtrLyr = pMxDoc.FocusMap.Layer(0)
  Set pFtrCls = pFtrLyr.FeatureClass

  ' Populate the area field
```

```
    Set pCalc = New Calculator
    With pCalc
      .Field = AREA_FIELD
      .PreExpression = "dim pArea as IArea" + vbCrLf + "set pArea = [Shape]"
      .Expression = "pArea.Area"
      Set .Cursor = pFtrCls.Update(Nothing, False)
      .ShowErrorPrompt = True
      .Calculate
    End With

    ' Get the index of the ID field
lIDFldIdx = pFtrCls.FindField(ID_FIELD)

    ' Sort the values by ID Ascending, Area Descending
    Set pTblSort = New TableSort
    With pTblSort
      Set .Table = pFtrCls
      .Fields = ID_FIELD + "," + AREA_FIELD
      .Ascending(ID_FIELD) = True
      .Ascending(AREA_FIELD) = False
      .Sort Nothing
      Set pFtrCsr = .Rows
    End With

    ' Create a new empty featureclass based on the existing one
    Set pObjCpy = New ObjectCopy
    Set pFlds = pObjCpy.Copy(pFtrCls.Fields)
    Set pWrkspcFact = New ShapefileWorkspaceFactory
    Set pFtrWrkspc = pWrkspcFact.OpenFromFile(NEW_SHAPEFILE_FOLDER, 0)
    Set pOutFtrCls = pFtrWrkspc.CreateFeatureClass(NEW_SHAPEFILE_NAME, pFlds,
Nothing, Nothing, esriFTSimple, "Shape", "")
    Set pFtrBfr = pOutFtrCls.CreateFeatureBuffer
    Set pOutFtrCsr = pOutFtrCls.Insert(True)

    ' Loop through the features and merge them based on the ID, keeping the attributes
    ' of the feature with the largest polygon area
    Set pFtr = pFtrCsr.NextFeature
    While Not pFtr Is Nothing
      For f = 0 To pFtrCls.Fields.FieldCount - 1
        If pFtrCls.Fields.Field(f).Name <>pFtrCls.OIDFieldName And _
pFtrCls.Fields.Field(f).Name <>pFtrCls.ShapeFieldName Then
pFtrBfr.Value(f) = pFtr.Value(f)
        End If
      Next f
      Set pGeomColl = pFtr.Shape
```

```
vLastID = pFtr.Value(lIDFldIdx)
      Do
         Set pFtr = pFtrCsr.NextFeature
         If Not pFtr Is Nothing Then
vNextID = pFtr.Value(lIDFldIdx)
            If vNextID = vLastID Then pGeomColl.AddGeometryCollectionpFtr.Shape
         End If
      Loop Until vNextID<>vLastID Or pFtr Is Nothing

      Set pFtrBfr.Shape = pGeomColl
pOutFtrCsr.InsertFeaturepFtrBfr
   Wend
End Sub
```

R coding for categorizing aspect into cardinal directions (conducted as one step during the logistic regression analysis):

```
DFTESTSEPT=read.table("C://Documents and Settings//Administrator//My
Documents//Thesis//StatsData //JULY2010//DFTEST.txt", header=T, sep="\t")

binASPECT=

for(i in 1:length(DFTESTSEPT$ASPECT))
{
print(DFTESTSEPT$ASPECT[i])

if(DFTESTSEPT$ASPECT[i]<=22.5){DFTESTSEPT$BinASPECT[i]=1}
else if(DFTESTSEPT$ASPECT[i]>22.5 & DFTESTSEPT$ASPECT[i]<=67.5)
{DFTESTSEPT$BinASPECT[i]=2}
else if(DFTESTSEPT$ASPECT[i]>67.5 & DFTESTSEPT$ASPECT[i]<=112.5)
{DFTESTSEPT$BinASPECT[i]=3}
else if(DFTESTSEPT$ASPECT[i]>112.5 & DFTESTSEPT$ASPECT[i]<=157.5)
{DFTESTSEPT$BinASPECT[i]=4}
else if(DFTESTSEPT$ASPECT[i]>157.5 & DFTESTSEPT$ASPECT[i]<=202.5)
{DFTESTSEPT$BinASPECT[i]=5}
else if(DFTESTSEPT$ASPECT[i]>202.5 & DFTESTSEPT$ASPECT[i]<=247.5)
{DFTESTSEPT$BinASPECT[i]=6}
else if(DFTESTSEPT$ASPECT[i]>247.5 & DFTESTSEPT$ASPECT[i]<=292.5)
{DFTESTSEPT$BinASPECT[i]=7}
else if(DFTESTSEPT$ASPECT[i]>292.5 & DFTESTSEPT$ASPECT[i]<=337.5)
{DFTESTSEPT$BinASPECT[i]=8}
else if(DFTESTSEPT$ASPECT[i]>337.5 & DFTESTSEPT$ASPECT[i]<=370)
{DFTESTSEPT$BinASPECT[i]=1}
else {DFTESTSEPT$BinASPECT[i]=NA}
}
```

Univariate Logistic Regression Models:

R coding used to calculate univariate logistic regression is the same for each landslide type. An example of the code is provided below.

```
DFTbrockmodel=glm(ID~as.factor(BROCK),family=binomial(logit),data=DFTESTSEPT)
DFTstructmodel=glm(ID~as.factor(STRUCT),family=binomial(logit),data=DFTESTSEPT)
DFTvegmodel=glm(ID~as.factor(VEG),family=binomial(logit),data=DFTESTSEPT)
DFTaspectmodel=glm(ID~as.factor(BinASPECT),family=binomial(logit),data=DFTESTSE
PT)
DFTelevmodel=glm(ID~ELEV,family=binomial(logit),data=DFTESTSEPT)
DFTslopemodel=glm(ID~SLOPE,family=binomial(logit),data=DFTESTSEPT)
DFTcurvplmodel=glm(ID~CURVPL,family=binomial(logit),data=DFTESTSEPT)
DFTcurvflmodel=glm(ID~CURVPF,family=binomial(logit),data=DFTESTSEPT)

summary(DFTbrockmodel)
summary(DFTstructmodel)
summary(DFTaspectmodel)
summary(DFTvegmodel)
summary(DFTslopemodel)
summary(DFTelevmodel)
summary(DFTcurvflmodel)
summary(DFTcurvplmodel)
```

Final models:

Multivariate logistic regression models:

Example, debris flow test model:

```
DFTmodel=glm(ID~as.factor(BROCK+as.factor(STRUCT)+as.factor(VEG)+as.factor(BinA
SPECT)+ELEV+SLOPE+CURVPL+CURVPF,family=binomial(logit),data=DFTESTSEPT)

summary(DFTmodel)
```

APPENDIX C-III: Results

Table C.1: Debris Flow Test set (DFT and Debris Flow Validation Set DFV) univariate logistic regression results.

		Debris Flow Test Set					Debris Flow Validation Set				
Variables		Estimate	Std.Error	z value	Pr(>|z value|)		Estimate	Std. Error	z value	Pr(>|z value|)	
(Intercept)		-0.06	0.05	-1.25	2.11E-01		-0.08	0.05	-1.69	9.20E-02	.
BEDROCK	Mixed Lithologies	0.22	0.07	3.08	2.05E-03	**	0.27	0.07	3.76	1.69E-04	***
	Igneous	0.70	0.13	5.24	1.61E-07	***	0.55	0.14	3.87	1.10E-04	***
	Shale	-0.30	0.09	-3.50	4.60E-04	***	-0.19	0.09	-2.20	2.81E-02	*
ASPECT	NE	0.51	0.13	3.85	1.20E-04	***	0.13	0.13	0.99	3.20E-01	
	E	0.66	0.13	4.99	5.99E-07	***	0.18	0.13	1.34	1.81E-01	
	SE	0.90	0.13	6.75	1.46E-11	***	0.42	0.13	3.17	1.53E-03	**
	S	0.51	0.14	3.61	3.11E-04	***	-0.05	0.14	-0.33	7.42E-01	
	SW	0.82	0.13	6.29	3.16E-10	***	0.34	0.13	2.61	8.97E-03	**
	W	0.60	0.13	4.52	6.27E-06	***	0.08	0.13	0.58	5.64E-01	
	NW	0.54	0.13	3.99	6.55E-05	***	0.18	0.14	1.32	1.88E-01	
(Intercept)		-0.12	0.04	-3.07	2.13E-03	**	-0.06	0.04	-1.57	1.16E-01	
LAND COVER	Nonforested	0.34	0.07	5.25	1.50E-07	***	0.18	0.07	2.72	6.44E-03	**
(Intercept)		-1.96	0.08	-23.98	<2.00E-16	***	-1.78	0.08	-22.49	<2.00E-16	***
SLOPE		0.08	0.00	26.71	<2.00E-16	***	0.07	0.00	25.08	<2.00E-16	***
(Intercept)		-0.64	0.08	-7.78	7.53E-15	***	-0.54	0.08	-6.53	6.52E-11	***
ELEV		0.00	0.00	8.38	<2.00E-16	***	0.00	0.00	7.05	1.81E-12	***
(Intercept)		-0.01	0.03	-0.20	8.43E-01		0.00	0.03	-0.11	9.13E-01	
CURVPF		-0.77	0.12	-6.14	8.40E-10	***	-0.73	0.12	-5.83	5.44E-09	***
(Intercept)		0.00	0.03	-0.11	9.10E-01		0.00	0.03	-0.03	9.77E-01	
CURVPL		0.17	0.11	1.56	1.18E-01		0.17	0.11	1.59	1.13E-01	

Notes: Results given for both debris flow data sets (test and validation). **Signif. codes**: 0 '***' 0.001 '**' 0.01 '*' 0.05 '.' 0.1 ' ' 1
+ identifies variables containing close to zero events making exceptionally large coefficients and standard error values. *Description of table headings: **Variables***: Causative factors selected to identify their association with rock/debris slides (ELEV = elevation, CURVPF = profile curvature, and CURVPL = plan curvature). ***Estimate***: Maximum likelihood estimate. These values identify the "most likely" value for the variable given the data that was observed. ***Odds Ratio***: The ratio of the probability of an event to no event occurring (considers all other variables to be zero). ***Z value***: Also known as Wald z statistic is a value that identifies the significance of each coefficient (estimate). Value can be inflated when sample sizes are small (Hosmer and Lemeshow 2000). ***Std. Error***: Is the standard deviation of the means of samples taken from a parent population (Porkess 2005). ***Pr(>|z value|)***: Represents the significance level. The value identifies how

significant a variable is in contributing or not contributing to rock/debris slides. *Referenced categories for nominal variables:* **Bedrock** categories are in relation to carbonate bedrock, **Landcover** categories are in relation to forested areas, and **Aspect** categories are in relation to North aspect.

Table C.2: Earth Slide Test (EST) and Earth Slide Validation (ESV) univariate logistic regression results

		Earth Slide Test Set					Earth Slide Validation Set				
Variables		Estimate	Std. Error	z value	Pr(>|z value|)		Estimate	Std. Error	z value	Pr(>|z value|)	
(Intercept)		-1.61	0.55	-2.94	3.30E-03	**	-1.01	0.41	-2.45	1.43E-02	*
BEDROCK	Mixed Lithologies	-16.96	1537.40^{+}	-0.01	9.91E-01		-0.78	0.87	-0.90	3.69E-01	
	Igneous	1.61	1.5166	1.06	2.89E-01		-16.55	1769.26^{+}	-0.01	9.93E-01	
	Shale	2.89	0.63	4.59	4.49E-06	***	2.18	0.52	4.20	2.73E-05	***
(Intercept)		-0.15	0.56	-0.28	7.82E-01		-1.55	0.95	-1.63	1.02E-01	
ASPECT	NE	-1.23	0.97	-1.28	2.02E-01		-0.61	0.74	-0.82	4.11E-01	
	E	-0.25	0.77	-0.33	7.43E-01		-1.01	0.79	-1.28	2.01E-01	
	SE	0.67	0.76	0.88	3.81E-01		-0.32	0.71	-0.45	6.53E-01	
	S	0.67	0.92	0.72	4.69E-01		-1.26	0.77	-1.64	1.02E-01	
	SW	-0.54	0.90	-0.60	5.49E-01		-0.63	0.77	-0.82	4.13E-01	
	W	0.15	0.73	0.21	8.33E-01		0.93	0.81	1.16	2.47E-01	
	NW	1.17	0.81	1.45	1.48E-01		0.56	0.23	2.43	1.52E-02	*
(Intercept)		0.29	0.22	1.31	1.92E-01		-3.70	1.05	-3.53	4.12E-04	***
LAND COVER	Nonforested	-1.67	0.60	-2.79	5.34E-03	**	-0.25	0.46	-0.55	5.82E-01	
(Intercept)		-1.25	0.44	-2.82	4.78E-03	**	0.01	0.02	0.61	5.42E-01	
SLOPE		0.06	0.02	3.18	1.50E-03	**	2.92	0.63	4.63	3.62E-06	***
(Intercept)		2.08	0.59	3.49	4.78E-04	***	0.00	0.00	-4.62	3.84E-06	***
ELEV		0.00	0.00	-3.62	2.92E-04	***	-0.01	0.20	-0.05	9.62E-01	
(Intercept)		-0.01	0.20	-0.05	9.58E-01		-0.30	0.77	-0.39	6.96E-01	
CURVPF		-1.17	1.18	-0.99	3.21E-01		0.00	0.20	0.00	9.99E-01	
(Intercept)		0.02	0.20	0.10	9.23E-01		1.09	1.03	1.06	2.89E-01	
CURVPL		-0.55	1.10	-0.50	6.16E-01		-	-	-	-	

Notes: Results given for both earth slide data sets (test and validation). Signif. codes: 0 '***' 0.001 '**' 0.01 '*' 0.05 '.' 0.1 ' ' 1
+ identifies variables comprising close to zero events making exceptionally large coefficients and standard error values. *Description of table headings:* ***Variables***: Causative factors selected to identify their association with rock/debris slides (ELEV = elevation, CURVPF = profile curvature, and CURVPL = plan curvature). ***Estimate***: Maximum likelihood estimate. These values identify the "most likely" value for the variable given the data that was observed. ***Odds Ratio***: The ratio of the probability of an event to no event occurring (considers all other variables to be zero). ***Z value***: Also known as Wald z statistic is a value that identifies the significance of each coefficient (estimate). Value can be inflated when sample sizes are small (Hosmer and Lemeshow 2000). ***Std. Error***: Is the standard deviation of the means of samples taken from a parent population (Porkess 2005). ***Pr(>|z value|)***: Represents the significance level. The value

identifies how significant a variable is in contributing or not contributing to rock/debris slides. *Referenced categories for nominal variables:* **Bedrock** categories are in relation to carbonate bedrock, **Landcover** categories are in relation to forested areas, and **Aspect** categories are in relation to North aspect.

Table C.3: Rock/Debris Slide Test (RST) and Rock Slide/Debris Validation (RSV) univariate logistic regression results.

		Rock/Debris Slide Test Set					Rock/Debris Slide Validation Set				
Variables		Estimate	Std. Error	z value	Pr(>|z value|)		Estimate	Std. Error	z value	Pr(>|z value|)	
(Intercept)		0.48	0.25	1.92	5.46E-02	.	0.27	0.26	1.03	3.03E-01	
BEDROCK	Mixed Lithologies	-1.98	0.61	-3.27	1.07E-03	**	-1.70	0.56	-3.03	2.42E-03	**
	Igneous	-17.05	1199.77^{+}	-0.01	9.89E-01		-15.83	1029.12^{+}	-0.02	9.88E-01	
	Shale	-0.33	0.47	-0.70	4.85E-01		0.42	0.47	0.91	3.63E-01	
(Intercept)		-0.92	0.59	-1.55	1.21E-01		-0.69	0.61	-1.13	2.58E-01	
ASPECT	NE	0.31	0.78	0.40	6.91E-01		-0.22	1.04	-0.22	8.30E-01	
	E	1.01	0.74	1.38	1.69E-01		1.15	0.78	1.47	1.42E-01	
	SE	1.07	0.81	1.32	1.88E-01		0.41	0.82	0.50	6.20E-01	
	S	1.25	0.83	1.51	1.32E-01		0.09	0.80	0.11	9.13E-01	
	SW	0.92	0.76	1.21	2.26E-01		1.72	0.80	2.14	3.21E-02	*
	W	1.39	0.82	1.69	9.15E-02	.	0.94	0.79	1.19	2.34E-01	
	NW	1.61	0.85	1.89	5.87E-02	.	0.56	0.80	0.70	4.85E-01	
(Intercept)		0.28	0.20	1.40	1.63E-01		0.41	0.21	1.94	5.29E-02	.
LAND COVER	Nonforested	-2.02	0.66	-3.07	2.18E-03	**	-2.76	0.77	-3.59	3.36E-04	***
(Intercept)		-0.48	0.39	-1.23	2.17E-01		-0.33	0.39	-0.85	3.96E-01	
SLOPE		0.02	0.02	1.40	1.61E-01		0.02	0.02	0.97	3.34E-01	
(Intercept)		1.21	0.55	2.19	2.84E-02	*	1.32	0.47	2.81	4.90E-03	**
ELEV		0.00	0.00	-2.31	2.08E-02	*	0.00	0.00	-3.03	2.46E-03	**
(Intercept)		-0.03	0.19	-0.17	8.64E-01		-0.08	0.19	-0.40	6.86E-01	
CURVPF		-1.07	0.66	-1.60	1.09E-01		-0.90	0.68	-1.32	1.88E-01	
(Intercept)		0.03	0.19	0.17	8.69E-01		-0.01	0.19	-0.04	9.70E-01	
CURVPL		-0.73	0.84	-0.87	3.82E-01		0.14	0.76	0.19	8.50E-01	

Notes: Results given for both rock/debris slide data sets (test and validation). Signif. codes: 0 '***' 0.001 '**' 0.01 '*' 0.05 '.' 0.1 ' ' 1
+ identifies variables containing close to zero events making exceptionally large coefficients and standard error values. *Description of table headings: **Variables***: Causative factors selected to identify their association with rock/debris slides (ELEV = elevation, CURVPF = profile curvature, and CURVPL = plan curvature). ***Estimate***: Maximum likelihood estimate. These values identify the "most likely" value for the variable given the data that was observed. ***Odds Ratio***: The ratio of the probability of an event to no event occurring (considers all other variables to be zero). ***Z value***: Also known as Wald z statistic is a value that identifies the significance of each coefficient (estimate). Value can be inflated when sample sizes are small (Hosmer and Lemeshow 2000). ***Std. Error***: Is the standard deviation of the means of samples taken from a parent population (Porkess 2005). ***Pr(>|z value|)***: Represents the significance level. The value identifies how

significant a variable is in contributing or not contributing to rock/debris slides.*Referenced categories for nominal variables:* **Bedrock** categories are in relation to carbonate bedrock, **Landcover** categories are in relation to forested areas, and **Aspect** categories are in relation to North aspect.

Multivariate logistic regression results:

Table C.4: Debris Flow test model

Variables		Estimate	Odds Ratio	Std. Error	z value	Pr(>|z value|)	
		Debris Flow Test Set					
(Intercept)		-2.72	0.07	0.18		<2.00E-16	***
BEDROCK	Mixed Lithologies	0.44	1.55	0.09		4.46E-07	***
	Igneous	0.24	1.27	0.17		1.42E-01	
	Shale	0.92	2.51	0.11		2.43E-16	***
LAND COVER	Nonforested	-0.11	0.90	0.10		2.76E-01	
ASPECT	NE	0.53	1.70	0.15		3.89E-04	***
	E	0.75	2.12	0.15		1.00E-06	***
	SE	0.77	2.16	0.16		8.83E-07	***
	S	0.49	1.63	0.16		2.74E-03	**
	SW	0.69	1.99	0.15		5.03E-06	***
	W	0.57	1.77	0.15		2.19E-04	***
	NW	0.43	1.54	0.15		5.50E-03	**
ELEV		0.00	1.00	0.00		2.33E-07	***
SLOPE		0.10	1.11	0.00		<2.00E-16	***
CURVPL		-0.55	0.58	0.14		9.68E-05	***
CURVPF		-1.01	0.36	0.16		3.56E-10	***

Notes:
Signif. codes: 0 '***' 0.001 '**' 0.01 '*' 0.05 '.' 0.1 ' ' 1. + identifies variables containing close to zero events making exceptionally large coefficients and standard error values. *Description of table headings:* ***Variables***: Causative factors selected to identify their association with rock/debris slides (ELEV = elevation, CURVPF = profile curvature, and CURVPL = plan curvature). ***Estimate***: Maximum likelihood estimate. These values identify the "most likely" value for the variable given the data that was observed. ***Odds Ratio***: The ratio of the probability of an event to no event occurring (considers all other variables to be zero). ***Z value***: Also known as Wald z statistic is a value that identifies the significance of each coefficient (estimate). Value can be inflated when sample sizes are small (Hosmer and Lemeshow 2000). ***Std. Error***: Is the standard deviation of the means of samples taken from a parent population (Porkess 2005). ***Pr(>|z value|)***: Represents the significance level. The value identifies how significant a variable is in contributing or not contributing to rock/debris slides. *Referenced categories for nominal variables:* **Bedrock** categories are in relation to carbonate bedrock, **Landcover** categories are in relation to forested areas, and **Aspect** categories are in relation to North aspect.

Table C.5: Debris flow validation model

Variables		Estimate	Odds Ratio	Std. Error	z value	Pr(>|z value|)	
		Debris Flow Validation Set					
(Intercept)		-2.34	0.10	0.18	-13.04	<2.00E-16	***
BEDROCK	Mixed Lithologies	0.47	1.61	0.08	5.63	1.83E-08	***
	Igneous	0.10	1.10	0.17	0.55	5.80E-01	
	Shale	0.92	2.51	0.11	8.38	<2.00E-16	***
LAND COVER	Nonforested	-0.26	0.77	0.10	-2.75	5.94E-03	**
ASPECT	NE	0.34	1.40	0.15	2.26	2.36E-02	*
	E	0.36	1.43	0.15	2.37	1.77E-02	*
	SE	0.50	1.64	0.15	3.27	1.06E-03	**
	S	0.06	1.06	0.16	0.38	7.03E-01	
	SW	0.38	1.47	0.15	2.58	1.00E-02	*
	W	0.09	1.09	0.15	0.58	5.62E-01	
	NW	0.22	1.25	0.15	1.43	1.54E-01	
ELEV		0.00	1.00	0.00	-4.78	1.78E-06	***
SLOPE		0.10	1.11	0.00	25.51	<2.00E-16	***
CURVPL		-0.37	0.69	0.13	-2.71	6.75E-03	**
CURVPF		-1.01	0.37	0.16	-6.24	4.52E-10	***

Notes:
Signif. codes: 0 '***' 0.001 '**' 0.01 '*' 0.05 '.' 0.1 ' ' 1. + identifies variables containing close to zero events making exceptionally large coefficients and standard error values. *Description of table headings: **Variables***: Causative factors selected to identify their association with rock/debris slides (ELEV = elevation, CURVPF = profile curvature, and CURVPL = plan curvature). ***Estimate***: Maximum likelihood estimate. These values identify the "most likely" value for the variable given the data that was observed. ***Odds Ratio***: The ratio of the probability of an event to no event occurring (considers all other variables to be zero). ***Z value***: Also known as Wald z statistic is a value that identifies the significance of each coefficient (estimate). Value can be inflated when sample sizes are small (Hosmer and Lemeshow 2000). ***Std. Error***: Is the standard deviation of the means of samples taken from a parent population (Porkess 2005). ***Pr(>|z value|)***: Represents the significance level. The value identifies how significant a variable is in contributing or not contributing to rock/debris slides. . *Referenced categories for nominal variables:* **Bedrock** categories are in relation to carbonate bedrock, **Landcover** categories are in relation to forested areas, and **Aspect** categories are in relation to North aspect.

Table C.6: Earth slide test model

Variables		Estimate	Odds Ratio	Std. Error	z value	Pr(>|z|)	
		Earth Slide Test Set					
(Intercept)		-17.82	-	5.26	-3.39	7.09E-04	***
BEDROCK	Mixed Lithologies+	-25.54	0.00	2779.85+	-0.01	9.93E-01	
	Igneous	-5.94	0.00	2.50	-2.38	1.76E-02	*
	Shale+	11.64	114039.48+	3.41	3.41	6.44E-04	***
ELEV		-	-	-	-	-	
SLOPE		0.57	1.76	0.17	3.35	8.14E-04	***

Notes:
Signif. codes: 0 '***' 0.001 '**' 0.01 '*' 0.05 '.' 0.1 ' ' 1. + identifies variables containing close to zero events making exceptionally large coefficients and standard error values. *Description of table headings:* ***Variables***: Causative factors selected to identify their association with rock/debris slides (ELEV = elevation, CURVPF = profile curvature, and CURVPL = plan curvature). ***Estimate***: Maximum likelihood estimate. These values identify the "most likely" value for the variable given the data that was observed. ***Odds Ratio***: The ratio of the probability of an event to no event occurring (considers all other variables to be zero). ***Z value***: Also known as Wald z statistic is a value that identifies the significance of each coefficient (estimate). Value can be inflated when sample sizes are small (Hosmer and Lemeshow 2000). ***Std. Error***: Is the standard deviation of the means of samples taken from a parent population (Porkess 2005). ***Pr(>|z value|)***: Represents the significance level. The value identifies how significant a variable is in contributing or not contributing to rock/debris slides. *Referenced categories for nominal variables:* **Bedrock** categories are in relation to carbonate bedrock.

Table C.7: Earth slide validation model

Variables		Estimate	Odds Ratio	Std. Error	z value	Pr(>|z|)	
		Earth Slide Validation Set					
(Intercept)		-1.64	-	1.36	-1.20	2.31E-01	
BEDROCK	Mixed Lithologies	-0.03	0.97	1.10	-0.27	7.91E-01	
	Igneous	-1.49	0.23	1410.00+	-0.01	9.92E-01	
	Shale	2.84	17.06	0.84	3.37	7.42E-04	***
ELEV		0.00	1.00	0.00	-3.36	7.72E-04	***
SLOPE		0.01	1.01	0.04	3.71	2.10E-04	***

Notes:
Signif. codes: 0 '***' 0.001 '**' 0.01 '*' 0.05 '.' 0.1 ' ' 1. + identifies variables containing close to zero events making exceptionally large coefficients and standard error values. *Description of table headings:* ***Variables***: Causative factors selected to identify their association with rock/debris slides (ELEV = elevation, CURVPF = profile curvature, and CURVPL = plan curvature). ***Estimate***: Maximum likelihood estimate. These values identify the "most likely" value for the variable given the data that was observed. ***Odds Ratio***: The ratio of the probability of an event to no event occurring (considers all other variables to be zero). ***Z value***: Also known as Wald z statistic is a value that identifies the significance of each coefficient (estimate). Value can be inflated when sample sizes are small (Hosmer and Lemeshow 2000). ***Std. Error***: Is the standard deviation of the means of samples taken from a parent population (Porkess 2005). ***Pr(>|z value|)***: Represents the significance level. The value identifies how significant a variable is in contributing or not contributing to rock/debris slides. *Referenced categories for nominal variables:* **Bedrock** categories are in relation to carbonate bedrock.

Table C.8: Rock slide test model:

Variables		Estimate	Odds Ratio	Std. Error	z value	Pr(>|z|)	
		Rock Slide Test Set					
(Intercept)		-0.19	-	0.52	-0.37	7.11E-01	
BEDROCK	Mixed Lithologies	-2.58	0.08	0.67	-3.83	1.28E-04	***
	Igneous	-18.77	0.00	1626.62+	-0.01	9.91E-01	
	Shale	-0.48	0.62	0.55	-0.87	3.86E-01	
LAND COVER	Nonforested	-3.18	0.04	0.77	-4.12	3.82E-05	***
SLOPE		0.06	1.06	0.02	2.83	4.69E-03	**

Notes:
Signif. codes: 0 '***' 0.001 '**' 0.01 '*' 0.05 '.' 0.1 ' ' 1. + identifies variables containing close to zero events making exceptionally large coefficients and standard error values. *Description of table headings:* ***Variables***: Causative factors selected to identify their association with rock/debris slides (ELEV = elevation, CURVPF = profile curvature, and CURVPL = plan curvature). ***Estimate***: Maximum likelihood estimate. These values identify the "most likely" value for the variable given the data that was observed. ***Odds Ratio***: The ratio of the probability of an event to no event occurring (considers all other variables to be zero). ***Z value***: Also known as Wald z statistic is a value that identifies the significance of each coefficient (estimate). Value can be inflated when sample sizes are small (Hosmer and Lemeshow 2000). ***Std. Error***: Is the standard deviation of the means of samples taken from a parent population (Porkess 2005). ***Pr(>|z value|)***: Represents the significance level. The value identifies how significant a variable is in contributing or not contributing to rock/debris slides. *Referenced categories for nominal variables:* **Bedrock** categories are in relation to carbonate bedrock, **Landcover** categories are in relation to forested areas.

Table C.9 Rock slide validation:

Variables		Estimate	Odds Ratio	Std. Error	z value	Pr(>|z|)	
		Rock Slide Validation Set					
(Intercept)		-0.41	-	0.60	-0.69	4.92E-01	
BEDROCK	Mixed Lithologies	-1.97	0.14	0.62	-3.16	1.57E-03	**
	Igneous+	-13.82	0.00	1028.82+	-0.01	9.89E-01	
	Shale	0.37	1.45	0.54	0.69	4.92E-01	
LAND COVER	Nonforested	-3.04	0.05	0.88	-3.46	5.35E-04	***
SLOPE		0.06	1.06	0.02	2.26	2.39E-02	*

Notes:
Signif. codes: 0 '***' 0.001 '**' 0.01 '*' 0.05 '.' 0.1 ' ' 1. + identifies variables containing close to zero events making exceptionally large coefficients and standard error values. *Description of table headings:* ***Variables***: Causative factors selected to identify their association with rock/debris slides (ELEV = elevation, CURVPF = profile curvature, and CURVPL = plan curvature). ***Estimate***: Maximum likelihood estimate. These values identify the "most likely" value for the variable given the data that was observed. ***Odds Ratio***: The ratio of the probability of an event to no event occurring (considers all other variables to be zero). ***Z value***: Also known as Wald z statistic is a value that identifies the significance of each coefficient (estimate). Value can be inflated when sample sizes are small (Hosmer and Lemeshow 2000). ***Std. Error***: Is the standard deviation of the means of samples taken from a parent population (Porkess 2005). ***Pr(>|z value|)***: Represents the significance level. The value identifies how significant a variable is in contributing or not contributing to rock/debris slides. *Referenced categories for nominal variables:* **Bedrock** categories are in relation to carbonate bedrock, **Landcover** categories are in relation to forested areas.